This is a preprint, the final version is subject to change, of the American Mineralogist (MSA)
Cite as Authors (Year) Title. American Mineralogist, in press.
DOI: http://dx.doi.org/10.2138/am-2018-6123

Revision 2: Relationships between unit-cell parameters and composition for rock-forming minerals on Earth, Mars, and other extraterrestrial bodies

SHAUNNA M. MORRISON,[1,2*] ROBERT T. DOWNS,[1] DAVID F. BLAKE,[3] ANIRUDH PRABHU,[4] AHMED ELEISH,[4] DAVID T. VANIMAN,[5] DOUGLAS W. MING,[6] ELIZABETH B. RAMPE,[6] ROBERT M. HAZEN,[2] CHERIE N. ACHILLES,[1] ALLAN H. TREIMAN,[7] ALBERT S. YEN,[8] RICHARD V. MORRIS,[6] THOMAS F. BRISTOW,[3] STEVE J. CHIPERA,[9] PHILIPPE C. SARRAZIN,[10] KIM V. FENDRICH,[11] JOHN MICHAEL MOROOKIAN,[8] JACK D. FARMER,[12] DAVID J. DES MARAIS,[3] AND PATRICIA I. CRAIG[7]

[1]UNIVERSITY OF ARIZONA, 1040 E 4TH ST, TUCSON, AZ, 85721 U.S.A.
[2]GEOPHYSICAL LABORATORY, CARNEGIE INSTITUTION, 5251 BROAD BRANCH RD NW, WASHINGTON, DC, 20015 U.S.A.
[3]NASA AMES RESEARCH CENTER, MOFFETT FIELD, CA 94035, U.S.A.
[4]RENSSELAER POLYTECHNIC INSTITUTE (RPI) 110 EIGHTH STREET, TROY, NY 12180, U.S.A.
[5]PLANETARY SCIENCE INSTITUTE, 1700 E. FORT LOWELL, TUCSON, AZ 85719-2395, U.S.A.
[6]NASA JOHNSON SPACE CENTER, HOUSTON, TX, 77058 U.S.A.
[7]LUNAR AND PLANETARY INSTITUTE, 3600 BAY AREA BLVD, HOUSTON, TX 77058, U.S.A.
[8]JET PROPULSION LABORATORY, CALIFORNIA INSTITUTE OF TECHNOLOGY, 4800 OAK GROVE DRIVE, PASADENA, CA 91109, U.S.A.
[9]CHESAPEAKE ENERGY CORPORATION, 6100 N. WESTERN AVENUE, OKLAHOMA CITY, OK 73118, U.S.A.
[10]SETI INSTITUTE, MOUNTAIN VIEW, CA 94043 U.S.A.
[11]AMERICAN MUSEUM OF NATURAL HISTORY, NEW YORK, NY 10024, U.S.A.
[12]ARIZONA STATE UNIVERSITY, TEMPE, AZ, 85281 U.S.A.

ABSTRACT

Mathematical relationships between unit-cell parameters and chemical composition were developed for selected mineral phases observed with the CheMin X-ray diffractometer onboard the Curiosity rover in Gale crater. This study presents algorithms for estimating the chemical composition of phases based solely on X-ray diffraction data. The mineral systems include plagioclase, alkali feldspar, Mg-Fe-Ca *C*2/*c* clinopyroxene, Mg-Fe-Ca $P2_1/c$ clinopyroxene, Mg-Fe-Ca orthopyroxene, Mg-Fe olivine, magnetite and other selected spinel oxides, and alunite-jarosite. These methods assume compositions of Na-Ca for plagioclase, K-Na for alkali feldspar, Mg-Fe-Ca for pyroxene, and Mg-Fe for olivine; however, some other minor elements may occur and their impact on measured unit-cell parameters is discussed. These crystal-chemical

algorithms can be applied to material of any origin, whether that origin is Earth, Mars, an extraterrestrial body, or a laboratory.

Keywords: X-ray diffraction, crystal chemistry, unit-cell parameters, plagioclase, olivine, pyroxene, magnetite, spinel, jarosite, alunite, Mars, Gale crater, Mars Science Laboratory, CheMin.

INTRODUCTION

The Chemistry and Mineralogy (CheMin) X-ray diffraction (XRD) instrument onboard the Mars Science Laboratory (MSL) rover, Curiosity, is employed by the MSL Science Team to analyze martian rock and sediment samples in Gale crater, Mars (Bish et al. 2013, 2014; Blake et al. 2013; Treiman et al. 2014, 2016; Vaniman et al. 2014; Bristow et al. 2015; Morris et al. 2016; Rampe et al. 2017; Yen et al. 2017; Achilles et al. 2017). XRD data obtained from CheMin allow mineral phase identification and refinement of unit-cell parameters and relative phase abundances. Information regarding phase chemical composition is useful in characterizing the geologic history of a rock unit, region, or planet. We studied the relationships between unit-cell parameters and chemical composition in order to constrain the composition of mineral phases observed in Gale crater. While these crystal-chemical algorithms were created with the purpose of studying Mars, they can be applied to any similar crystalline material regardless of origin.

To develop these crystal-chemical algorithms, we exploited the systematic relationship between atomic radii and unit-cell dimensions. Unit-cell lengths vary with chemical composition due to corresponding changes in atomic radii; therefore, measured unit-cell parameters provide insight into mineral composition and, in many cases, can be used to provide accurate estimates of anion composition. These systematics have been the focus of many mineralogical and XRD studies of synthetic and natural rock-forming minerals (Yoder and Sahama 1957; Bambauer et al.

This is a preprint, the final version is subject to change, of the American Mineralogist (MSA)
Cite as Authors (Year) Title. American Mineralogist, in press.
DOI: http://dx.doi.org/10.2138/am-2018-6123

1967; Louisnathan and Smith 1968; Matsui and Syono 1968; Fisher and Medaris 1969; Jahanbagloo 1969; Nolan 1969; Rutstein and Yund 1969; Turnock et al. 1973; Smith 1974; Schwab and Kustner 1977; Kroll 1983; Kroll and Ribbe 1983; Angel et al. 1990, 1998). Some research, such as the work on olivine by Yoder and Sahama (1957) and Fisher and Medaris (1969), focused on the position of the single most prominent diffraction peak for determining the chemical composition of unidentified phases. The principal reasons for using a single-peak technique are the relative ease of measurement and the difficulty in calculating unit-cell parameters from diffraction data prior to the widespread use of computers and the adoption of full-pattern fitting methods such as Rietveld refinement. Some subsequent studies, such as the work on pyroxenes by Turnock et al. (1973) and Angel et al. (1998), used high-resolution diffraction patterns to estimate chemical composition based entirely on refined cell parameters.

In this study, we present algorithms to estimate the chemical composition of minerals based solely on unit-cell parameters. We developed algorithms for plagioclase, alkali feldspar, Mg-Fe-Ca pyroxene, Fe-Mg olivine, magnetite and related spinel oxides, and alunite-jarosite group phases by least-squares regression of known unit-cell parameters and composition. Additionally, we employed minimization routines for the crystal-chemical relationships of Mg-Fe-Ca pyroxenes. These studies were conducted with mineralogical data from many literature sources, with special attention to previous crystal-chemical studies, and also from the RRUFF Project (Lafuente et al. 2015). These data are publicly available at rruff.info/ima, and are compiled in Appendix 1 and at github.com/shaunnamm/regression-and-minimization. The chemical variation and abundance of phases in this mineralogical database provide a comprehensive list of unit-cell parameters and associated composition, which can be harvested to produce robust chemical

This is a preprint, the final version is subject to change, of the American Mineralogist (MSA)
Cite as Authors (Year) Title. American Mineralogist, in press.
DOI: http://dx.doi.org/10.2138/am-2018-6123

relationships. Their application to refined CheMin unit-cell parameters of martian minerals is reported in Morrison et al. (2017)

CRYSTAL CHEMISTRY

This study incorporates unit-cell parameters and composition of minerals reported in previous studies as well as those documented in the RRUFF Project database (Lafuente et al. 2015) (Appendix 1). The availability of large databases, such as RRUFF, to evaluate compositional systematics has increased the accuracy of estimated phase composition relative to previous studies. The following sections detail these crystal-chemical systematics and the resulting equations offer robust algorithms for estimating mineral composition from X-ray diffraction data. All calculations were performed in R; the R code is provided at github.com/shaunnamm/regression-and-minimization. The models selected in the sections below minimize the residual standard error, σ_{SE}, and contain only significant parameters (p-value > 0.05). Where applicable, the residual standard error is given; the full error analysis procedure is detailed in Appendix 2. In order to limit bias in the models generated by least-squares regression, we averaged the unit-cell parameters of samples with identical compositions. However, the full (not averaged) datasets were used in error determinations. Where applicable, cross-validation was used in order to assess whether these algorithms can be generalized to other datasets, and to recognize any over-fitting. Cross-validation was performed by training the model on 80% of the data and testing on the remaining 20% with 1000 iterations. Errors reported from cross-validation represent the average of the 1000 iterations. The coefficients in the equations listed throughout result in precision to the 4th decimal place for composition (apfu), the 5th decimal place for *a*, *b*, and *c* (Å), and the 3rd decimal place for β (°); more digits can be obtained by specifying the number of desired digits in the R code.

This is a preprint, the final version is subject to change, of the American Mineralogist (MSA)
Cite as Authors (Year) Title. American Mineralogist, in press.
DOI: http://dx.doi.org/10.2138/am-2018-6123

Feldspar

Feldspar, variety plagioclase, is the most abundant mineral detected in twelve of the thirteen Gale crater samples analyzed by CheMin as of June 2016. Alkali feldspar, variety sanidine, is found in significantly lower quantities than plagioclase in all but one of the thirteen CheMin samples. Substitutions of minor elements is relatively common in potassium feldspar and less so in the plagioclase system. In alkali feldspar, minor amounts of other components can be present in a sample without causing the *b* and *c* unit-cell parameters to deviate noticeably from the Na-K trend. For example, alkali feldspars with cell dimensions that correspond to pure Na-K feldspar have been shown to contain Ba and Cs up to 0.02 atoms per formula unit (apfu) (Angel et al. 2013) and Rb up to 0.008 apfu (Dal Negro et al. 1978). In lunar K-feldspar, as much as 0.18 Ba apfu has been detected (Papike et al. 1998). However, Ba in martian meteorites has not been detected above 0.05 apfu and only 0.006% of the ~1000 martian meteorite feldspars contained any measurable Ba (Papike et al. 2009; Santos et al. 2015; Wittmann et al. 2015; Nyquist et al. 2016; Hewins et al. 2017). Additionally, sanidine can incorporate significant Fe^{3+} in the tetrahedral site, up to 0.698 Fe^{3+} apfu (Kuehner and Joswiak 1996; Linthout and Lustenhouwer 1993; Lebedeva et al. 2003). However, when the abundance of Fe^{3+} exceeds 0.1 apfu, the *b* unit-cell parameter increases beyond 13.05 Å and noticeably deviates from the trends shown in the alkali feldspar section below (Best et al. 1968; Lebedeva et al. 2003). Hewins et al. (2017) reported as much as 0.09 Fe^{3+} apfu in martian meteorite feldspar, an abundance that is unlikely to be detectable by examination of unit-cell parameters. In the plagioclase system, Fe^{2+} has been reported in abundance of 0.01-0.02 apfu from localities in Mexico and Japan (rruff.info), with no noticeable deviation from Na-Ca plagioclase unit-cell parameter trends. Matsui and Kimata (1997) synthesized anorthite with 0.196 Mn apfu; the resulting unit-cell parameters are

This is a preprint, the final version is subject to change, of the American Mineralogist (MSA)
Cite as Authors (Year) Title. American Mineralogist, in press.
DOI: http://dx.doi.org/10.2138/am-2018-6123

significantly smaller than those of Na-Ca plagioclase and therefore such a composition can be easily distinguished from a pure Na-Ca phase. Of the martian meteorite feldspars with plagioclase composition (Papike et al. 2009; Santos et al. 2015; Wittmann et al. 2015; Nyquist et al. 2016; Hewins et al. 2017), 97.6% contain less than 2 wt% minor oxides (e.g., Fe_2O_3, K_2O, MgO, MnO, TiO_2, BaO).

Plagioclase

Previous plagioclase crystal-chemical studies reported trends in solid solution composition ($NaAlSi_3O_8$ - $CaAl_2Si_2O_8$) with unit-cell parameters (Bambauer et al. 1967; Smith 1974; Kroll 1983), and examined the relationship between composition and tetrahedral bond lengths to investigate ordering systematics (Angel et al. 1990). Here, we correlate unit-cell parameters and composition of Na-Ca plagioclase. We performed statistical analyses on 49 relatively pure (≤ 0.042 K apfu) plagioclase samples (Table A1a), excluding the high-Ca plagioclase phases in which ordering results in a doubled *c* cell edge. We determined that Na-Ca plagioclase chemical composition can be estimated by a multivariate least-squares regression of the quadratic relationship between Ca- or Na-content and *a*, *b*, *c*, and β (Fig. A3a-d) with a residual standard error of 0.022 and 0.023 apfu for Ca and Na, respectively (Equations 1a-b). Note that only one of the equations below (1a and 1b) is needed to calculate the Ca-Na composition of plagioclase, the other component can be calculated by difference).

$$\text{Ca (apfu)} = -2480.385933a + 152.3540556a^2 + 1505.941326b - 58.71571613b^2 - 11.40375c - 0.003078067\beta^2 - 10.4185945\gamma + 0.057444444\gamma^2 + 1034.7951 \quad (1a)$$

$$\text{Na (apfu)} = 2025.35688a - 124.5278585a^2 - 1255.2328597b + 48.96341472b^2 + 9.244327c + 0.0033346038\beta^2 + 8.63542135\gamma - 0.04765164\gamma^2 - 691.81443 \quad (1b)$$

Equations 1c and 1d result in correlated estimates of Al- and Si-content, respectively.

$$\text{Al (afpu)} = 1 + \text{Ca (apfu)} \quad (1c)$$

$$\text{Si (apfu)} = 3 - \text{Ca (apfu)} \quad (1d)$$

The accuracy of Equations 1a-b is demonstrated by comparing the observed Ca- and Na-content versus calculated Ca- and Na-content (Fig. 1a-b) and calculating the root-mean-square error (RMSE = 0.022 Ca apfu and 0.024 Na apfu; cross-validation RMSE = 0.024 Ca apfu and 0.027 Na apfu). Plagioclase regression data are shown in Table A1a.

Alkali Feldspar

Previous alkali feldspar studies extensively examined and characterized the relationship between composition, site ordering, and unit-cell parameters (Kroll and Ribbe 1983). Kroll and Ribbe (1983) primarily focused on the effects of composition and Al/Si ordering in the tetrahedral sites. In this study, we followed the same principles and similar techniques, while focusing strictly on unit-cell parameters and their direct relationship to composition and fractional order-disorder. In order to characterize fully the composition and ordering of Ca-free alkali feldspars, we constructed a quadrilateral (Fig. 2) similar to that of Kroll and Ribbe (1983). We used well-characterized alkali feldspar end-members (Kroll and Ribbe 1983), low microcline, high sanidine, low albite, and high albite (Table A1b), to assemble the quadrilateral diagram; these end-members were also used to derive the algorithm (Equations 2a-b) for computing composition and ordering (1 = fully ordered; 0 = fully disordered). Note that this model assumes a composition along the Na-K solid solution and does not account for any potential celsian ($BaAl_2Si_2O_8$) component.

$$\begin{bmatrix} -3.76223 & -5.76875 & 90.42789 \\ -5.76875 & 13.37681 & -20.8328 \\ 0 & 0 & 1 \end{bmatrix} \begin{bmatrix} b \\ c \\ 1 \end{bmatrix} = \begin{bmatrix} \text{Na (apfu)} \\ \text{ordering} \\ 1 \end{bmatrix} \quad (2a)$$

This is a preprint, the final version is subject to change, of the American Mineralogist (MSA)
Cite as Authors (Year) Title. American Mineralogist, in press.
DOI: http://dx.doi.org/10.2138/am-2018-6123

$$K\ (apfu) = 1 - Na\ (apfu) \quad (2b)$$

Pyroxene

To date, three distinct pyroxene phases have been detected in Gale crater by CheMin: Augite, ideally $(Ca,Mg,Fe)_2Si_2O_6$, with $C2/c$ symmetry; pigeonite, ideally $(Mg,Fe,Ca)_2Si_2O_6$, with $P2_1/c$ symmetry; and orthopyroxene, ideally $(Mg,Fe)_2Si_2O_6$, with *Pbca* symmetry (Bish et al. 2013, 2014; Blake et al. 2013; Treiman et al. 2014, 2016; Vaniman et al. 2014; Morris et al. 2016; Rampe et al. 2017; Yen et al. 2017; Achilles et al. 2017).

In previous studies of pyroxenes, two approaches were used to correlate X-ray diffraction data with chemical composition. The first approach focused on correlations between lattice spacings and composition (Rutstein and Yund 1969). The second approach used the relationships between unit-cell parameters and composition (Nolan 1969; Rutstein and Yund 1969; Turnock et al. 1973; Angel et al. 1998). Here, we use the latter approach in conjunction with minimization to characterize systematic relationships between unit-cell parameters and Mg-Fe-Ca composition (Fig. A3e-ab). When applied to our dataset, our algorithms yield decreased uncertainty relative to previous studies (Table 1).

Martian high-Ca pyroxenes (Ca mole fraction > 0.2, based on Ca, Fe, Mg and Mn) generally have relatively low abundances of non-quadrilateral components (e.g., Papike et al. 2009) compared to terrestrial high-Ca pyroxenes (e.g., Robinson 1980; Papike 1980). Given that the main focus of the current work is on inferring pyroxene chemistry from XRD data acquired by the Curiosity rover in Gale crater, Mars, we limit our discussion of non-quadrilateral components to martian pyroxenes. Of the 876 high-Ca pyroxene analyses from martian meteorites reported in Papike et al. (2009), Santos et al. (2015), Wittmann et al. (2015), Nyquist et al. (2016), and

This is a preprint, the final version is subject to change, of the American Mineralogist (MSA)
Cite as Authors (Year) Title. American Mineralogist, in press.
DOI: http://dx.doi.org/10.2138/am-2018-6123

Hewins et al. (2017), only 0.2% contain more than 10% non-quadrilateral components (as defined in Cameron and Papike, 1981). None of the 1680 low-Ca pyroxene analyses of martian meteorites (Papike et al. 2009; Santos et al. 2015; Wittmann et al. 2015; Nyquist et al. 2016; Hewins et al. 2017) contain more than 10% non-quadrilateral components and only 1.4% contain more than 5% non-quadrilateral cations. Due to the fact that non-quadrilateral components can have ionic radii (and, consequently, unit-cell parameters) both greater than and less than Mg, Fe, and Ca (Baker and Beckett 1999), it is difficult to determine a unique chemistry based strictly on unit-cell parameters. Therefore, we limit our algorithms below to the Mg-Fe-Ca pyroxene system, with the understanding that there may be small amounts of non-quadrilateral cations that remain undetected by this method. To help the reader determine if their samples lie significantly outside of the Mg-Fe-Ca system, we have determined the maximum chi-squared value (χ^2_{max}) for the *a*, *b*, and β unit-cell parameters in each pyroxene dataset based on Eq. 4a-b, 4d, 5a-b, 5d, and 6a-b below (χ^2_{max}: $C2/c$ = 0.00026; $P2_1/c$ = 0.00043; $Pbca$ = 0.000028) and recommend exercising caution when the χ^2 value of a dataset exceeds ~ $3 \cdot \chi^2_{max}$ because there is a possibility of non-quadrilateral components.

This study incorporated three datasets containing a total 140 pyroxene compositions and corresponding unit-cell parameters (86 $C2/c$, 52 $P2_1/c$, and 41 $Pbca$) (Table A1c-e). Although the compositions of Fe-Mg-Ca pyroxenes are roughly a linear function of select unit-cell parameters, the relationships between composition and cell parameters are more accurately characterized by accounting for non-linearity. In order to determine the best relationship between the unit-cell parameters and composition, we began with the functional form presented in Turnock et al. (1973):

$$\text{Clinopyroxene: } z = c_0 + c_1Mg + c_2Ca + c_3Mg^2 + c_4MgCa + c_5Ca^2 + c_6Mg^3 + c_7Mg^2Ca + c_8MgCa^2 + c_9Ca^3 \quad (3a)$$

This is a preprint, the final version is subject to change, of the American Mineralogist (MSA)
Cite as Authors (Year) Title. American Mineralogist, in press.
DOI: http://dx.doi.org/10.2138/am-2018-6123

228
229 $$\text{Orthopyroxene: } z = c_0 + c_1Mg + c_2Ca + c_3Mg^2 + c_4Ca^2 + ... + c_nMg^n + c_{n+1}Ca^n \quad (3b)$$
230
231
232 Where z is the unit-cell parameter (either *a, b, c,* or β), c_i (i = 0 to 9) are the coefficients, and n is
233 3, 2, and 2 for *a*, *b*, and *c*, respectively (note that Mg and Ca apfu are used in place of the molar
234 compositional parameters, Fe/(Fe+Mg) and Ca/(Ca+Fe+Mg), that were used by Turnock et al.
235 1973; additionally, Eq. 3b is expanded to include Ca whereas Turnock et al. 1973 used Ca-free
236 orthopyroxene).

237 We then tested the accuracy of reproducing the measured unit-cell parameters with Eq. 3a-b
238 and every permutation of variables to determine the most accurate functions of z. The resulting
239 functions are given below (Eq. 4a-d, 5a-d, and 6a-c)

240 Augite - *C*2/*c*:

241 $$a\ (\text{Å}) = -0.106429Mg + 0.074932Ca + 0.016032Mg^2 + 0.1206MgCa + 0.03144Ca^3 –$$
242 $$0.129102MgCa^2 + 9.74681 \quad (4a)$$

243 $$b\ (\text{Å}) = -0.25789Mg – 0.212528Ca + 0.040693Mg^2 + 0.08659Ca^2 + 0.16962MgCa –$$
244 $$0.055575MgCa^2 + 9.16081 \quad (4b)$$

245 $$c\ (\text{Å}) = -0.142494Ca – 0.0421695Mg^2 + 0.107222Ca^2 + 0.109804MgCa +$$
246 $$0.040853Mg^2Ca – 0.107327MgCa^2 + 5.28441 \quad (4c)$$

247 $$\beta\ (°) = 4.405Mg – 3.426Mg^2 – 7.546Ca^2 – 4.2137MgCa + 0.6875Mg^3 + 4.736Ca^3 +$$
248 $$2.2772Mg^2Ca + 1.3864MgCa^2 + 107.599 \quad (4d)$$
249

250 Residual standard error: Eq. 4a = 0.006 Å, 4b = 0.005 Å, 4c = 0.004 Å, 4d = 0.11 Å. RMSE: Eq.
251 4a = 0.005 Å (cross-validation: 0.008 Å), 4b = 0.003 Å (cross-validation: 0.006 Å), 4c = 0.006 Å
252 (cross-validation: 0.009 Å), 4d = 0.05° (cross-validation: 0.19°).

253

254 Pigeonite - $P2_1/c$:

255 $$a\ (\text{Å}) = -0.050902Mg + 0.21487Ca – 0.1471Ca^2 – 0.05754MgCa +$$
256 $$0.04501Mg^2Ca + 9.7121 \quad (5a)$$

This is a preprint, the final version is subject to change, of the American Mineralogist (MSA)
Cite as Authors (Year) Title. American Mineralogist, in press.
DOI: http://dx.doi.org/10.2138/am-2018-6123

$$b\ (\text{Å}) = -0.1751943\text{Mg} + 0.0201938\text{Mg}^2 - 0.03603\text{Ca}^2 + 0.0284\text{Mg}^2\text{Ca} + 9.086603 \quad (5b)$$

$$c\ (\text{Å}) = 0.0910769\text{Ca} - 0.0296873\text{Mg}^2 - 0.17699\text{Ca}^2 + 0.145384\text{MgCa} + 0.007397\text{Mg}^3 - 0.04537\text{Mg}^2\text{Ca} + 5.23027 \quad (5c)$$

$$\beta\ (^\circ) = 0.6804\text{Mg} - 4.2167\text{Ca} - 0.64465\text{Mg}^2 + 7.2514\text{MgCa} + 0.14102\text{Mg}^3 - 2.3217\text{Mg}^2\text{Ca} - 4.187\text{MgCa}^2 + 108.4444 \quad (5d)$$

Residual standard error: Eq. 5a = 0.007 Å, 5b = 0.006 Å, 5c = 0.008 Å, 5d = 0.09°. RMSE: Eq. 5a = 0.006 Å (cross-validation: 0.008 Å), 5b = 0.002 Å (cross-validation: 0.006 Å), 5c = 0.010 Å (cross-validation: 0.014 Å), 5d = 0.04° (cross-validation: 0.10°).

Orthopyroxene - *Pbca*:

$$a\ (\text{Å}) = -0.14978\text{Mg} + 0.7807\text{Ca} + 0.025194\text{Mg}^2 - 4.863\text{Ca}^2 + 18.42965 \quad (6a)$$

$$b\ (\text{Å}) = -0.17051\text{Mg} + 0.01951\text{Mg}^2 + 9.08082 \quad (6b)$$

$$c\ (\text{Å}) = -0.01007\text{Mg} + 0.31524\text{Ca} - 0.00982\text{Mg}^2 - 2.89809\text{Ca}^2 + 5.23733 \quad (6c)$$

Residual standard error: Eq. 6a = 0.013 Å, 6b = 0.008 Å, 6c = 0.005 Å. RMSE: Eq. 6a = 0.012 Å (cross-validation: 0.015 Å), 6b = 0.007 Å (cross-validation: 0.008 Å), 6c = 0.004 Å (cross-validation: 0.006 Å).

Employing Eq. 4a-d, 5a-d, and 6a-c, we performed a minimization of the weighted sum of squared error ($\Sigma\sigma^2$) to estimate pyroxene chemical composition. We used a bounded ($0 \leq$ Mg (apfu) ≤ 2; $0 \leq$ Ca (apfu) ≤ 2) PORT optimization (Gay 1990) with starting parameters of Mg = 2 and Ca = 1. Fe calculated post-minimization and is equal to two minus the sum of Mg and Ca. We began by using all available unit-cell parameters in the minimization routine (Eq. 7a for the clinopyroxenes and 7b for orthopyroxenes).

$$\Sigma\sigma^2 = ((a-a_{calc})/(a_{calc}/\beta_{calc}))^2 + (b-b_{calc})/(b_{calc}/\beta_{calc}))^2 + (c-c_{calc})/(c_{calc}/\beta_{calc}))^2 + (\beta-\beta_{calculated})^2 \quad (7a)$$

$$\Sigma\sigma^2 = ((a-a_{calc})/(a_{calc}/b_{calc}))^2 + (b-b_{calc})^2 + (c-c_{calc})/(c_{calc}/b_{calc}))^2 \quad (7b)$$

We tested every permutation of unit-cell parameter combinations for the minimization (Eq. 7a-b) and found that the lowest error resulted from a combination of *a, b* and β for clinopyroxenes (Eq. 8a) and *a* and *b* for orthopyroxene (Eq. 8b).

$$\Sigma\sigma^2 = ((a–a_{calc})/(a_{calc}/\beta_{calc}))^2 + (b–b_{calc})/(b_{calc}/\beta_{calc}))^2 + (\beta–\beta_{calculated})^2 \quad (8a)$$

$$\Sigma\sigma^2 = ((a–a_{calc})/(a_{calc}/b_{calc}))^2 + (b–b_{calc})^2 \quad (8b)$$

The accuracy of the minimization method is demonstrated by plotting the observed Mg-, Ca-, and Fe-contents versus their calculated values (Fig. 3a-c, 4a-c, and 5a-c). Errors associated with the above method are in Table 1.

Note that Turnock et al. (1973) did not distinguish between $P2_1/c$ and $C2/c$ pyroxenes in their algorithms; we tested this approach by combining all clinopyroxenes and performing the above regressions and minimization. However, the associated error (RMSE: Mg = 0.067 apfu, Ca = 0.090 apfu, Fe = 0.110 apfu) was significantly greater than when $P2_1/c$ and $C2/c$ pyroxenes are treated separately. This difference is likely due to changes in the β trend between space groups (Turnock et al. 1973).

Olivine

As of June 2016, CheMin has detected an olivine phase in three of the thirteen Gale crater samples. Numerous studies have examined the systematics of olivine composition in relation to X-ray diffraction data (Table 2). Some of these studies focused on the correlation between composition and the position of the most intense single diffraction peak, d_{130} (Yoder and Sahama 1957; Fisher and Medaris 1969; Schwab and Kustner 1977). Other studies examined the relationship between composition and unit-cell parameters (Louisnathan and Smith 1968; Matsui and Syono 1968; Jahanbagloo 1969). Following the success of the latter method, our study focused on the crystal-chemical systematics of Fe-Mg olivine unit-cell parameters vs. composition.

We incorporated unit-cell parameters and measured compositional data from 60 olivine samples, including those reported by previous olivine crystal chemistry studies (Table A1f). Our

This is a preprint, the final version is subject to change, of the American Mineralogist (MSA)
Cite as Authors (Year) Title. American Mineralogist, in press.
DOI: http://dx.doi.org/10.2138/am-2018-6123

data were limited to those samples containing only Mg and Fe. Distinguishing Fe-Mg-only olivine from those containing Ca or Mn (Table A1g) is difficult, and sometimes not possible, with unit-cell parameters alone. If Ca exceeds 0.5 apfu, the *b* parameter increases dramatically (> 10.80 Å), confirming that the sample is not in the Fe-Mg or Fe-Mg-Mn system. Likewise, as evident in Fig. 6, if *b* or *V* exceed 10.50 Å or 308 Å^3, respectively, the sample is outside of the Mg-Fe-only system. However, samples within the Mg-Fe-only unit-cell parameter range (*b* = 10.19-10.50 Å; *V* = 289-308 Å^3) can contain up to 0.19 Ca apfu and 1 Mn apfu, according to literature data in Table A1g. In evaluating Gale crater olivine, we can limit our compositional range to that reported in martian meteorites: Mn < 0.038 apfu and Ca < 0.027 apfu (Papike et al. 2009; Hewins et al. 2017).

A linear least-squares regression of Mg- and Fe-content versus *b* in olivine (Fig. A4ac-af) resulted in the expressions 6a-b for estimating the chemical composition of Mg-Fe olivine. Note that only one of the equations below (9a and 9b) is needed to calculate the Fe-Mg composition of olivine, the other component can be calculated by difference). The residual standard error of Mg and Fe is 0.018 and 0.018 apfu, respectively.

$$\text{Mg (apfu)} = -7.15567b + 79.9756 \quad (9a)$$

$$\text{Fe (apfu)} = 7.156854b - 72.98787 \quad (9b)$$

The RMSE of the observed versus calculated Mg- and Fe-content in olivine samples used in this study (Fig. 7a-b) is 0.017 and 0.017 apfu (0.018 and 0.018 apfu in cross-validation), respectively.

Magnetite and selected spinel oxides

As of June 2016, each Gale crater samples analyzed by CheMin contains a spinel phase. In nature, the cubic spinel oxide structure can accommodate a variety of elements, including

This is a preprint, the final version is subject to change, of the American Mineralogist (MSA)
Cite as Authors (Year) Title. American Mineralogist, in press.
DOI: http://dx.doi.org/10.2138/am-2018-6123

transition elements Fe, Ti, Cr, Mn, Co, Cu, Zn, V, and Ni, as well as metals, metalloids, and non-metals such as Mg, Ca, Si, Al, Ge, Sb, and can also exhibit site vacancy (□). Chromite accounts for ~18% of the spinel phases observed in the martian meteorites studied in the 64 references cited in Appendix 4. There are also significant amounts of Al-rich (up to 27.85 wt% Al_2O_3 or 1.01 Al apfu, assuming no site vacancy), Ti-rich (up to 33.8 wt% TiO_2/0.95 Ti apfu), and Mg-rich (up to 9.03 wt% MgO/0.43 Mg apfu) magnetite. Only ~2% have more than 0.50 Al apfu, but ~21% have more than 0.50 Ti apfu, and ~35% have more than 1.00 Cr apfu. Si, V, Mn, Ca, Na, Ni, Co, and Zn have been detected, but in relatively small amounts (<0.05 apfu). In addition to martian meteorite data, the MER Mössbauer spectrometers have also collected information on spinel phases at Gusev crater and Meridiani Planum and found them to be of magnetite ($Fe^{2+}Fe^{3+}{}_2O_4$) or Ti-magnetite composition, with some minor chromite ($Fe^{2+}Cr_2O_4$) (Morris et al. 2006a, 2006b, 2008). Therefore, when evaluating Gale crater samples, we can have some confidence that the spinel phase is likely in the Fe, Fe-Ti or Fe-Cr systems, or a mixture thereof.

While some of spinel compositional space is not relevant to martian samples, it may be to samples of other origins; therefore, we considered it important to characterize the common spinel systems. To characterize the crystal-chemical relationships in spinel phases, we compiled crystallographic and compositional data (Table A1h) and observed that Al, Ti, Mg, Mn, Cr, Ni, Zn, and V were frequently reported as major components of magnetite. In addition to magnetite (Fe_3O_4), other end-member spinel oxides include maghemite ($Fe_{2.67}O_4$), hercynite ($Fe^{2+}Al_2O_4$), ulvöspinel ($Fe^{2+}{}_2TiO_4$), magnesioferrite ($MgFe^{3+}{}_2O_4$), magnesiochromite ($MgCr^{3+}{}_2O_4$), chromite ($Fe^{2+}Cr_2O_4$), trevorite ($NiFe^{3+}{}_2O_4$), franklinite ($ZnFe^{3+}{}_2O_4$), and coulsonite ($Fe^{2+}V^{3+}{}_2O_4$). In Figure 8, the literature trends of Fe versus the *a* unit-cell parameter are given for (Fe,□), (Fe,Al), (Fe,Ti), (Fe,Mg), (Fe,Cr), (Fe,Ni), (Fe,Zn), (Fe,V) (Fe,Al,□), (Fe,Mg,Al), (Fe,Mn,Ti),

This is a preprint, the final version is subject to change, of the American Mineralogist (MSA)
Cite as Authors (Year) Title. American Mineralogist, in press.
DOI: http://dx.doi.org/10.2138/am-2018-6123

(Fe,Mg,Cr), and (Fe,Mg,Ti) phases. Data points with combinations other than those listed were excluded from Figure 8 for clarity and because the complexity of the trends increases significantly beyond three cations. The complexity of Figure 8, a result of variation in cation size and oxidation state of multi-element phases, illustrates that numerous chemical combinations can correlate with a given *a* cell edge in the spinel structure. Note that the (Mg,Fe) data are limited and there is not a linear trend; this complexity likely reflects cation ordering.

In order to interpret the possible composition of spinel oxide phases, we performed linear regressions of Fe-content versus *a* for each of the trends shown in Figure 8 (Equations 10a-m). Error metrics associated with each linear regression can be found in Table 3.

$$\text{(Fe,□): } 4.329809a - 33.4254 = \text{Fe (apfu)} \quad (10a)$$
$$3 - \text{Fe (apfu)} = \text{□ (pfu)}$$

$$\text{(Fe,Al): } 8.230266a - 66.108983 = \text{Fe (apfu)} \quad (10b)$$
$$3 - \text{Fe (apfu)} = \text{Al (apfu)}$$

$$\text{(Fe,Ti): } -6.577146a + 58.16868 = \text{Fe (apfu)} \quad (10c)$$
$$3 - \text{Fe (apfu)} = \text{Ti (apfu)}$$

$$\text{(Fe,Mg): } 74.172617a - 619.86623 = \text{Fe (apfu)} \quad (10d)$$
$$3 - \text{Fe (apfu)} = \text{Mg (apfu)}$$

$$\text{(Fe,Cr): } 97.561a - 816.22 = \text{Fe (apfu)} \quad (10e)$$
$$3 - \text{Fe (apfu)} = \text{Cr (apfu)}$$

$$\text{(Fe,Ni): } 17.802356a - 146.47258 = \text{Fe (apfu)} \quad (10f)$$
$$3 - \text{Fe (apfu)} = \text{Ni (apfu)}$$

$$\text{(Fe,Zn): } -22.6677979a + 193.3425374 = \text{Fe (apfu)} \quad (10g)$$
$$3 - \text{Fe (apfu)} = \text{Zn (apfu)}$$

$$\text{(Fe,V): } -35.714a + 302.89 = \text{Fe (apfu)} \quad (10h)$$
$$3 - \text{Fe (apfu)} = \text{Ni (apfu)}$$

$$\text{(Fe,Al,□): } \begin{bmatrix} 6.521577 & -51.8927 \\ -3.692257 & 31.05033 \end{bmatrix} \begin{bmatrix} a \\ 1 \end{bmatrix} = \begin{bmatrix} \text{Fe (apfu)} \\ \text{Al (apfu)} \end{bmatrix} \quad (10i)$$
$$3 - \text{Fe (apfu)} - \text{Al (apfu)} = \text{□ (pfu)}$$

This is a preprint, the final version is subject to change, of the American Mineralogist (MSA)
Cite as Authors (Year) Title. American Mineralogist, in press.
DOI: http://dx.doi.org/10.2138/am-2018-6123

$$\text{(Fe,Mg,Al): } \begin{bmatrix} 13.506902 & -109.20881 \\ -12.815325 & 104.6199886 \end{bmatrix} \begin{bmatrix} a \\ 1 \end{bmatrix} = \begin{bmatrix} \text{Fe (apfu)} \\ \text{Mg (apfu)} \end{bmatrix} \quad (10j)$$

$$3 - \text{Fe (apfu)} - \text{Mg (apfu)} = \text{Al (apfu)}$$

$$\text{(Fe,Mn,Ti): } \begin{bmatrix} -14.625663 & 126.9668 \\ 14.625663 & -124.9668 \end{bmatrix} \begin{bmatrix} a \\ 1 \end{bmatrix} = \begin{bmatrix} \text{Fe (apfu)}] \\ \text{Mn (apfu)}] \end{bmatrix} \quad (10k)$$

$$3 - \text{Fe (apfu)} - \text{Mn (apfu)} = \text{Ti (apfu)}$$

$$\text{(Fe,Mg,Cr): } \begin{bmatrix} 22.340604 & -186.14709 \\ -22.4088793 & 187.71818 \end{bmatrix} \begin{bmatrix} a \\ 1 \end{bmatrix} = \begin{bmatrix} \text{Fe (apfu)} \\ \text{Mg (apfu)} \end{bmatrix} \quad (10l)$$

$$3 - \text{Fe (apfu)} - \text{Mg (apfu)} = \text{Cr (apfu)}$$

$$\text{(Fe,Mg,Ti): } \begin{bmatrix} 26.893648 & -227.37053 \\ -25.412612 & 216.80734 \end{bmatrix} \begin{bmatrix} a \\ 1 \end{bmatrix} = \begin{bmatrix} \text{Fe (apfu)} \\ \text{Mg (apfu)} \end{bmatrix} \quad (10m)$$

$$3 - \text{Fe (apfu)} - \text{Mg (apfu)} = \text{Ti (apfu)}$$

*Equations based on datasets with only two points do not have an associated value for σ_{SE} because there is no spread in the data. The uncertainty associated with these equations is based solely on the input unit-cell parameters (see Appendix 2 for full error calculation).

Once the amount of Fe is estimated, the relative proportions of Fe^{2+} and Fe^{3+} can be computed by charge balance.

Alunite-Jarosite

Alunite-jarosite group minerals are associated with secondary weathering and alteration of S-bearing deposits. The mineral phases are hexagonal with space group $R\bar{3}m$ and include alunite, $KAl_3(SO_4)_2(OH)_6$; jarosite, $KFe^{3+}{}_3(SO_4)_2(OH)_6$; natroalunite, $NaAl_3(SO_4)_2(OH)_6$; natrojarosite, $NaFe^{3+}{}_3(SO_4)_2(OH)_6$; ammonioalunite, $NH_4Al_3(SO_4)_2(OH)_6$; ammoniojarosite, $NH_4Fe^{3+}{}_3(SO_4)_2(OH)_6$; and hydroniumjarosite, $(H_3O)Fe^{3+}{}_3(SO_4)_2(OH)_6$. Alunite-jarosite minerals have been discovered on Mars and offer clues about the weathering and alteration history of the

This is a preprint, the final version is subject to change, of the American Mineralogist (MSA)
Cite as Authors (Year) Title. American Mineralogist, in press.
DOI: http://dx.doi.org/10.2138/am-2018-6123

martian surface (e.g., Klingelhöfer et al. 2004; Zolotov and Shock 2005; Morris et al. 2006; Golden et al. 2008; Swayze et al. 2008; Mills et al. 2013).

In order to identify which alunite-jarosite phases are present in samples analyzed by CheMin, we constructed an alunite-jarosite quadrilateral (Fig. 9) by examining the relationship between *a* and *c* unit-cell parameters (Table A1i). Due to the lack of orthogonality in the alunite-natroalunite-jarosite-natrojarosite quadrilateral, compositions falling on or within the quadrilateral are calculated with a series of equations (Eq. 11a-e).

$$\text{K (apfu)} = 1.654c - 27.508 \quad (11a)$$

$$\begin{bmatrix} -0.00923 & 7.46919 \\ 0.463717 & -0.966595 \end{bmatrix} \begin{bmatrix} c \\ 1 \end{bmatrix} = \begin{bmatrix} a_{jr} \\ a_{al} \end{bmatrix} \quad (11b)$$

$$\text{Fe (apfu)} = \frac{-3(a - a_{jr})}{a_{al} - a_{jr}} + 3 \quad (11c)$$

$$\text{Na (apfu)} = 1 - \text{K (apfu)} \quad (11d)$$

$$\text{Al (apfu)} = 3 - \text{Fe (apfu)} \quad (11e)$$

Alunite-jarosite group phase regression data are shown in Table A1i.

IMPLICATIONS

The methods provided in this study offer users the opportunity to estimate the chemical composition of select phases based solely on X-ray diffraction data. The mineral systems studied include the important rock-forming mineral groups of Na-Ca plagioclase, Na-K alkali feldspar, Mg-Fe-Ca clinopyroxene, Mg-Fe-Ca orthopyroxene, Mg-Fe olivine, magnetite and selected other spinel-group minerals, and alunite-jarosite phases. These algorithms are applicable to minerals of any origin, whether that origin be a laboratory, Earth, Mars, or any of the various solid objects in our solar system.

ACKNOWLEDGEMENTS

We would like to acknowledge the support of the JPL engineering and Mars Science Laboratory (MSL) operations team. The study benefited from discussions with Mike Baker concerning relationships between the compositions of olivine and pyroxene and their associated unit-cell parameters. We would like to thank the reviewers of this manuscript, Olivier Gagné and Bradley Jolliff, for their insightful and constructive feedback. This research was supported by NASA NNX11AP82A, MSL Investigations, and by the National Science Foundation Graduate Research Fellowship under Grant No. DGE-1143953. Any opinions, findings, or recommendations expressed herein are those of the authors and do not necessarily reflect the views of the National Aeronautics and Space Administration or the National Science Foundation.

REFERENCES CITED

Achilles, C.N., Downs, R.T., Ming, D.W., Rampe, E.B., Morris, R.V., Treiman, A.H., Morrison, S.M., Yen, A.S., Vaniman, D.T., Blake, D.F., Bristow, T.F., Chipera, S.J., Ewing, R.C., Ehlmann, B.L., Crisp, J.A., Gellert, R., Fendrich, K.V., Craig, P.I., Grotzinger, J.P., Des Marais, D.J., Farmer, J.D. Sarrazin, P.C., and Morookian, J.M. (2017) Mineralogy of an Active Eolian Sediment from the Namib Dune, Gale crater, Mars. JGR-Planets, Bagnold Dunes Special Issue (in press).

Angel, R.J., Carpenter, M.A., and Finger, L.W. (1990) Structural variation associated with compositional variation and order-disorder behavior in anorthite-rich feldspars. American Mineralogist, 75, 150-162.

Angel, R.J., McCammon, C., and Woodland, A.B. (1998) Structure, ordering and cation interactions in Ca-free P2(1)/c clinopyroxenes. Physics and Chemistry of Minerals, 25, 249-258.

Angel, R.J., Ross, N.L., Zhao, J., Sochalski-Kolbus, L., Krüger, H., and Schmidt, B.C. (2013) Structural controls on the anisotropy of tetrahedral frameworks: the example of monoclinic feldspars. European Journal of Mineralogy, 25(4), 597-614.

Baker, M.B., and Beckett, J.R. (1999) The origin of abyssal peridotites: a reinterpretation of constraints based on primary bulk compositions. Earth and Planetary Science Letters, 171(1), 49-61.

Bambauer, H.U., Corlett, M., Eberhard, E., and Viswanathan, K. (1967) Diagrams for the determination of plagioclases using X-ray powder methods (Part III of laboratory investigations of plagioclases). Schweizerische Mineralogische und Petrographische Mitteilungen, 47, 333-349.

Best, M.G., Henage, L.F., and Adams, J.A., 1968. Mica peridotite wyomingite and associated pottassic igneous rocks in Northeastern Utah. American Mineralogist, 53(5-6), p.1041.

Bish, D., Blake, D., Vaniman, D., Sarrazin, P., Bristow, T., Achilles, C., Dera, P., Chipera, S., Crisp, J., Downs, R., Farmer, J., Gailhanou, M., Ming, D., Morookian, J.M., Morris, R., Morrison, S., Rampe, E., Treiman, A., and Yen, A. (2014). The first X-ray diffraction measurements on Mars, *IUCrJ* 1, 514-522.

Bish, D.L., Blake, D.F., Vaniman, D.T., Chipera, S.J., Morris, R.V., Ming, D.W., Treiman, A.H., Sarrazin, P., Morrison, S.M., Downs, R.T., Achilles, C.N., Yen, A.S., Bristow, T.F., Crisp, J.A., Morookian, J.M., Farmer, J.D., Rampe, E.B., Stolper, E.M., Spanovich, N., and MSL Science Team (2013) X-ray Diffraction Results from Mars Science Laboratory: Mineralogy of Rocknest at Gale Crater. Science, 27, 341, 1238932.

Blake, D.F., Morris, R.V., Kocurek, G., Morrison, S.M., Downs, R.T., Bish, D.L., Ming, D.W., Edgett, K.S., Rubin, D., Goetz, W., Madsen, M.B., Sullivan, R., Gellert, R., Campbell, I., Treiman, A.H., McLennan, S.M., Yen, A.S., Grotzinger, J., Vaniman, D.T., Chipera, S.J., Achilles, C.N., Rampe, E.B., Sumner, D., Meslin, P-Y., Maurice, S., Forni, O., Gasnault, O., Fisk, M., Schmidt, M., Mahaffy, P., Leshin, L.A., Glavin, D., Steele, A., Freissinet, C., Navarro-González, R., Yingst, R.A., Kah, L.C., Bridges, N., Lewis, K.W., Bristow, T.F., Farmer, J.D., Crisp, J.A., Stolper, E.M., Des Marais, D.J., Sarrazin, P., and MSL Science Team (2013) Curiosity at Gale Crater, Mars: Characterization and Analysis of the Rocknest Sand Shadow. Science, 341, 1239505.

Bristow, T.F., Bish, D.L., Vaniman, D.T., Morris, R.V., Blake, D.F., Grotzinger, J.P., Rampe, E.B., Crisp, J.A., Achilles, C.N., Ming, D.W., Ehlmann, B.L., King, P.L., Bridges, J.C., Eigenbrode, J.L., Sumner, D.Y., Chipera, S.J., Moorokian, J.M., Treiman, A.H., Morrison, S.M., Downs, R.T., Farmer, J.D., Des Marais, D., Sarrazin, P., Floyd, M.M., Mischna, M.A., and McAdam, A. (2015) The origin and implications of clay minerals from Yellowknife Bay, Gale crater, Mars. American Mineralogist, 100, 824-836.

Cameron, M., and Papike, J.J. (1981) Structural and chemical variations in pyroxenes. American Mineralogist, 66(1-2), 1-50.

Dal Negro, A., De Pieri, R., Quareni, S., and Taylor, W.H. (1978) The crystal structures of nine K feldspars from Adamello Massiff (Northern Italy). Acta Crystallographica, B34, 2699-2707.

Fisher, G.W., and Medaris, L.G. (1969) Cell dimensions and X-ray determinative curve for synthetic Mg-Fe olivines. American Mineralogist, 54, 741-753.

Gay, D.M. (1990) Usage summary for selected optimization routines. Computing Science Technical Report 153, AT&T Bell Laboratories, Murray Hill.

Golden, D.C., Ming, D.W., Morris, R.V., and Graff, T.G. (2008) Hydrothermal synthesis of hematite spherules and jarosite - Implications for diagenesis and hematite spherule formation in sulphate outcrops at Meridiani Planum, Mars. American Mineralogist, 93, 1201-1214.

Hewins, R.H., Zanda, B., Humayun, M., Nemchin, A., Lorand, J.P., Pont, S., Deldicque, D., Bellucci, J.J., Beck, P., Leroux, H., and Marinova, M. (2017) Regolith breccia Northwest Africa 7533: Mineralogy and petrology with implications for early Mars. Meteoritics & Planetary Science, 52(1), 89-124.

529 Jahanbagloo, I.C. (1969) X-ray diffraction study of olivine solid solution series. American
530 Mineralogist, 54, 246-250.
531 Klingelhöfer, G., Morris, R.V, Bernhardt, B., Schröder, C., Rodionov, D.S., de Souza, P.A., Yen,
532 A., Gellert, R., Evlanov, E.N., Zubkov, B., and others (2004) Jarosite and hematite at
533 Meridiani Planum from Opportunity's Mössbauer Spectrometer. Science, 306, 1740-5.
534 Kroll, H. (1983) Lattice parameters and determinative methods for plagioclase and ternary
535 feldspars. Reviews in Mineralogy p. 101-119.
536 Kroll, H., and Ribbe, P.J. (1983) Lattice parameters, composition and Al,Si order in alkali
537 feldspars. Reviews in Mineralogy p. 57-100.
538 Kuehner, S.M., and Joswiak, D.J. (1996) Naturally occurring ferric iron sanidine from the
539 Leucite Hills lamproite. American Mineralogist, 81(1-2), 229-237.
540 Lafuente, B., Downs, R.T., Yang, H., and Stone, N. (2015) The power of databases: the RRUFF
541 project. 1-30 p. Highlights in Mineralogical Crystallography.
542 Lebedeva, Y.S., Pushcharovsky, D.Y., Pasero, M., Merlino, S., Kashaev, A.A., Taroev, V.K.,
543 Goettlicher, J., Kroll, H., Pentinghaus, H., Suvorova, L.F., and Wulf-Bernodat, H. (2003)
544 Synthesis and crystal structure of low ferrialuminosilicate sanidine. Crystallography Reports,
545 48(6), 919-924.
546 Linthout, K. and Lustenhouwer, W.J. (1993) Ferrian high sanidine in a lamproite from Cancarix,
547 Spain. Mineralogical magazine, 57(2), 289-299.
548 Louisnathan, S.J., and Smith, J.V. (1968) Cell dimensions of olivine. Mineralogical Magazine,
549 36, 1123-1134.
550 Matsui, T., and Kimata, M. (1997) Crystal chemistry of synthetic Mn-bearing anorthite;
551 incorporation of MnAl 2 Si 2 O 8 end-member into feldspar. European Journal of Mineralogy,
552 9(2), 333-344.
553 Matsui, Y., and Syono, Y. (1968) Unit cell dimensions of some synthetic olivine group solid
554 solutions. Geochemical Journal, 2, 51-59.
555 Mills, S.J., Nestola, F., Kahlenberg, V., Christy, A.G., Hejny, C., and Redhammer, G.J. (2013)
556 Looking for jarosite on Mars: The low-temperature crystal structure of jarosite. American
557 Mineralogist, 98, 1966-1971.
558 Morris, R.V., Klingelhoefer, G., Schröder, C., Rodionov, D.S., Yen, A., Ming, D.W., De Souza,
559 P.A., Fleischer, I., Wdowiak, T., Gellert, R., and Bernhardt, B. (2006) Mössbauer mineralogy
560 of rock, soil, and dust at Gusev crater, Mars: Spirit's journey through weakly altered olivine
561 basalt on the plains and pervasively altered basalt in the Columbia Hills. Journal of
562 Geophysical Research: Planets, 111(E2).
563 Morris, R.V., Klingelhöfer, G., Schröder, C., Fleischer, I., Ming, D.W., Yen, A.S., Gellert, R.,
564 Arvidson, R.E., Rodionov, D.S., Crumpler, L.S., Clark, B.C., Cohen, B.A., McCoy, T.J.,
565 Mittlefehldt, D.W., Schmidt, M.E., de Souza, P.A., and Squyres, S.W. (2008), Iron
566 mineralogy and aqueous alteration from Husband Hill through Home Plate at Gusev Crater,
567 Mars: results from the Mössbauer instrument on the Spirit Mars Exploration Rover, Journal of
568 Geophysical Research: Planets, 113, E12S42.
569 Morris, R.V., Klingelhöfer, G., Schröder, C., Rodionov, D.S., Yen, A., Ming, D.W., de Souza,
570 P.A., Wdowiak, T., Fleischer, I., Gellert, R., and others (2006) Mössbauer mineralogy of
571 rock, soil, and dust at Meridiani Planum, Mars: Opportunity's journey across sulfate-rich
572 outcrop, basaltic sand and dust, and hematite lag deposits. Journal of Geophysical Research:
573 Planets, 111.
574 Morris, R.V., Vaniman, D.T., Blake, D.F., Gellert, R., Chipera, S.J., Rampe, E.B., Ming, D.W.,

575 Morrison, S.M., Downs, R.T., Treiman, A.H., Yen, A.S., Grotzinger, J.P., Achilles, C.N.,
576 Bristow, T.F., Crisp, J.A., Des Marais, D.J., Farmer, J.D., Fendrich, K.V., Frydenvang, J.,
577 Graff, T.G., Morookian, J.M., Stolper, E.M., and Schwenzer, S.P. (2016) Silicic volcanism on
578 Mars evidenced by tridymite in high-SiO_2 sedimentary rock at Gale crater, Proceedings of the
579 National Academy of Sciences, 201607098.
580 Morrison, S.M., Downs, R.T., Blake, D.F., Vaniman, D.T., Ming, D.W., Rampe, E.B., Bristow,
581 T.F., Achilles, C.N., Chipera, S.J., Yen, A.S., Morris, R.V., Treiman, A.H., Hazen, R.M.,
582 Sarrazin, P.C., Gellert, R., Fendrich, K.V., Morookian, J.M., Farmer, J.D., Des Marais, D.J.,
583 and Craig, P.I. (2017) Crystal chemistry of martian minerals from Bradbury Landing through
584 Naukluft Plateau, Gale crater, Mars. American Mineralogist (submitted).
585 Nolan, J. (1969) Physical properties of synthetic and natural pyroxenes in the system diopsite-
586 hedenbergite-acmite. Mineralogical Magazine, 37, 216-229.
587 Nyquist, L.E., Shih, C.Y., McCubbin, F.M., Santos, A.R., Shearer, C.K., Peng, Z.X., Burger,
588 P.V., and Agee, C.B. (2016) Rb-Sr and Sm-Nd isotopic and REE studies of igneous
589 components in the bulk matrix domain of Martian breccia Northwest Africa 7034. Meteoritics
590 & Planetary Science, 51(3), 483-498.
591 Papike, J.J. (1980) Pyroxene mineralogy of the Moon and meteorites. Reviews in Mineralogy 7,
592 495-525.
593 Papike, J.J., Karner, J.M., Shearer, C.K., and Burger, P.V. (2009) Silicate mineralogy of martian
594 meteorites. Geochimica et Cosmochimica Acta, 73, 7443-7485.
595 Papike J.J., Ryder G., Shearer C.K., (1998) Lunar samples, In J.J. Papike, Ed., Reviews in
596 Mineralogy, 36, p. 5.1-5.234.
597 Rampe, E.B. Ming, D.W., Blake, D.F., Vaniman, D.T., Chipera, S.J., Bristow, T.F., Morris,
598 R.V., Yen, A.S., Morrison, S.M., Grotzinger, J.P., Peretyazhko, T., Hurowitz, J.A., Siebach,
599 K., Achilles, C.N., Downs, R.T., Farmer, J.D., Fendrich, K.V., Gellert, R., Morookian, J.M.,
600 Sarrazin, P.C., Treiman, A.H., Berger, J., Fairén, A.G., Forni, O., Kah, L., Eigenbrode, J.,
601 Lanza, N. L., Sutter, B. (2017) Mineralogical trends in mudstones from the Murray formation,
602 Gale crater, Mars. Earth and Planetary Science Letters, 471, 172-185.
603 Robinson, P. (1980) The composition space of terrestrial pyroxenes; internal and external limits.
604 Reviews in Mineralogy, 7, 419-494.
605 Rutstein, M.S., and Yund, R.A. (1969) Unit-cell parameters of synthetic diopside-hedenbergite
606 solid solutions. American Mineralogist, 54, 238-245.
607 Santos, A.R., Agee, C.B., McCubbin, F.M., Shearer, C.K., Burger, P.V., Tartese, R., and Anand,
608 M. (2015) Petrology of igneous clasts in Northwest Africa 7034: Implications for the
609 petrologic diversity of the Martian crust. Geochimica et Cosmochimica Acta, 157, 56-85.
610 Schwab, R.B., and Kustner, D. (1977) Präzisionsgitterkonstantenbestimmung zur festlegung
611 röntgenographischer Bestimmungskurven für synthetische Olivin der Mischkristallreihe
612 Forsterit-Fayalit. Neues Jahrbuch für Mineralogie, Monatshefte, 205-215.
613 Smith, J.V. (1974) Feldspar Minerals, Springer-Verlag, Berlin Heidelberg.
614 Swayze, G.A., Desborough, G.A., Smith, K.S., Lowers, H.A., Hammarstrom, J.M., Diehl, S.F.,
615 Leinz, R.W., and Driscoll, R.H. (2008), Understanding jarosite - From mine waste to Mars.
616 Understanding contaminants associated with mineral deposits, 1328, 8-13.
617 Treiman, A.H., Bish, D.L., Vaniman, D.T., Chipera, S.J., Blake, D.F., Ming, D.W., Morris, R.V.,
618 Bristow, T.F., Morrison, S.M., Baker, M.B., Rampe, E.B., Downs, R.T., Filiberto, J., Glazner,
619 A.F., Gellert, R., Thompson, L.M., Schmidt, M.E., Le Deit, L., Wiens, R.C., McAdam, A.C.,
620 Achilles, C.N., Edgett, K.S., Farmer, J.D., Fendrich, K.V., Grotzinger, J.P., Gupta, S.

621 Morookian, J.M., Newcombe, M.E., Rice, M.S., Spray, J.G., Stolper, E.M., Sumner, D.Y.,
622 Vasavada, A.R., and Yen, A.S. (2016) Mineralogy, provenance, and diagenesis of a potassic
623 basaltic sandstone on Mars: CheMin X-ray diffraction of the Windjana sample (Kimberley
624 area, Gale Crater). Journal of Geophysical Research: Planets, 121, 75-106.
625 Treiman, A.H., Morris, R.V., Agresti, D.G., Graff, T.G., Achilles, C.N., Rampe, E.B., Bristow,
626 T.F., Ming, D.W., Blake, D.F., Bish, D.L., Chipera, S.J., Morrison, S.M., Downs, R.T. (2014)
627 Ferrian saponite from the Santa Monica Mountains (California, U.S.A., Earth):
628 Characterization as an analog for clay minerals on Mars with application to Yellowknife Bay
629 in Gale crater. American Mineralogist, 99, 2234-2250.
630 Turnock, A.C., Lindsley, D.H., and Grover, J.E. (1973) Synthesis and unit cell parameters of Ca-
631 Mg-Fe pyroxenes. American Mineralogist, 58, 50-59.
632 Vaniman, D.T., Bish, D.L., Ming, D.W., Bristow, T.F., Morris, R.V., Blake, D.F., Chipera, S.J.,
633 Morrison, S.M., Treiman, A.H., Rampe, E.B., Rice, M., Achilles, C.N., Grotzinger, J.P.,
634 McLennan, S.M., Williams, J., Bell, J.F. III, Newsom, H.E., Downs, R.T., Maurice, S.,
635 Sarrazin, P., Yen, A.S., Morookian, J.M., Farmer, J.D., Stack, K., Milliken, R.E., Ehlmann,
636 B.L., Sumner, D.Y., Berger, G., Crisp, J.A., Hurowitz, J.A., Anderson, R., Des Marais, D.J.,
637 Stolper, E.M., Edgett, K.S., Gupta, S., Spanovich, N., and MSL Science Team (2014)
638 Mineralogy of a Mudstone at Yellowknife Bay, Gale Crater, Mars. Science, 343, 1-9.
639 Wittmann, A., Korotev, R.L., Jolliff, B.L., Irving, A.J., Moser, D.E., Barker, I., and Rumble, D.
640 (2015) Petrography and composition of Martian regolith breccia meteorite Northwest Africa
641 7475. Meteoritics & Planetary Science, 50(2), 326-352.
642 Yen, A.S., Ming, D.W., Vaniman, D.T., Gellert, R., Blake, D.F., Morris, R.V., Morrison, S.M.,
643 Downs, R.T., Bristow, T.F., Clark, B.C., Chipera, S.J., Farmer, J.D., Grotzinger, J.P., Rampe,
644 E.B., Schimidt, M.E., Sutter, B., Thompson, L.M., Treiman, A.H., and the MSL Science
645 Team (2017) Multiple episodes of aqueous alteration along fractures in mudstone and
646 sandstone in Gale crater, Mars. Earth and Planetary Science Letters, 471, 186-198.
647 Yoder, H.S., Jr., and Sahama, T.G. (1957) Olivine x-ray determinative curve. American
648 Mineralogist, 42, 475-491.
649 Zolotov, M.Y., and Shock, E.L. (2005) Formation of jarosite-bearing deposits through aqueous
650 oxidation of pyrite at Meridiani Planum, Mars. Geophysical Research Letters, 32, L21203.
651
652

This is a preprint, the final version is subject to change, of the American Mineralogist (MSA)
Cite as Authors (Year) Title. American Mineralogist, in press.
DOI: http://dx.doi.org/10.2138/am-2018-6123

TABLES

TABLE 1. Root-mean-square error (RMSE) of estimated Mg-content in pyroxene subsets, based on data from Tables A1c-e. This study's methods compared with selected previous studies.

C*2/*c	**Mg (apfu)**	**Fe (apfu)**	**Ca (apfu)**
This study	0.037	0.049	0.030
Turnock et al. (1973)	0.045	0.079	0.056
Rutstein and Yund (1969) all/Ca=1†	0.221/0.032	0.202/0.032	0.291/NA
P*2$_1$/*c	Mg RMSE (apfu)	Fe RMSE (apfu)	Ca RMSE (apfu)
This study	0.041	0.045	0.026
Turnock et al. (1973)	0.070	0.067	0.045
Angel et al. (1998) all/Ca-free*	0.076/0.036	0.277/0.036	0.235/NA
Pbca			
This study	0.053	0.049	0.021
Turnock et al. (1973)	0.088	0.115	0.043

†The algorithm presented in Rutstein and Yund (1969) is specifically for *C*2/*c* pyroxenes with Ca = 1 apfu. Therefore, we applied it both to our whole dataset (A1c-e) and to a subset with Ca = 1 apfu.

*The algorithm presented in Angel et al. (1998) is specifically for Ca-free *P*2$_1$/*c* pyroxenes. Therefore, we applied it both to our whole dataset (A1c-e) and to a Ca-free subset.

TABLE 2. Root-mean-square error (RMSE) of estimated Mg-content in olivine, based on data from Table A1f. Equation 9a compared with selected previous studies

Study	RMSE (Mg apfu)
Equation 9a, this study	0.017
Yoder and Sahama (1957)	0.064
Louisnathan and Smith (1968)	0.036
Fisher and Medaris (1969)	0.029
Jahanbagloo (1969)	0.062
Schwab and Kustner (1977)	0.024

This is a preprint, the final version is subject to change, of the American Mineralogist (MSA)
Cite as Authors (Year) Title. American Mineralogist, in press.
DOI: http://dx.doi.org/10.2138/am-2018-6123

Table 3. Root-mean-square errors (RMSE), RMSE of cross-validation, and residual standard errors (σ_{SE}) associated with spinel linear models.

Model	Anion	RMSE (apfu)	RMSE (apfu)*	σ_{SE} (apfu)
FeVacancy	Fe	0.038	0.081	0.047
FeAl	Fe	0.012	0.306	0.021
FeTi	Fe	0.029	0.031	0.030
FeMg	Fe	0.031	0.741	0.054
FeNi	Fe	0.016	0.041	0.022
FeZn	Fe	0.027	0.338	0.038
FeAlVacancy	Fe	0.040	0.042	0.042
FeAlVacancy	Al	0.058	0.060	0.059
FeMgAl	Fe	0.035	0.037	0.038
FeMgAl	Mg	0.026	0.027	0.028
FeMnTi	Fe	0.038	0.045	0.042
FeMnTi	Mn	0.038	0.045	0.042
FeMgCr	Fe	0.023	0.023	0.024
FeMgCr	Mg	0.023	0.024	0.025
FeMgTi	Fe	0.036	0.056	0.047
FeMgTi	Mg	0.030	0.046	0.039

*Cross-validation

This is a preprint, the final version is subject to change, of the American Mineralogist (MSA)
Cite as Authors (Year) Title. American Mineralogist, in press.
DOI: http://dx.doi.org/10.2138/am-2018-6123

FIGURES

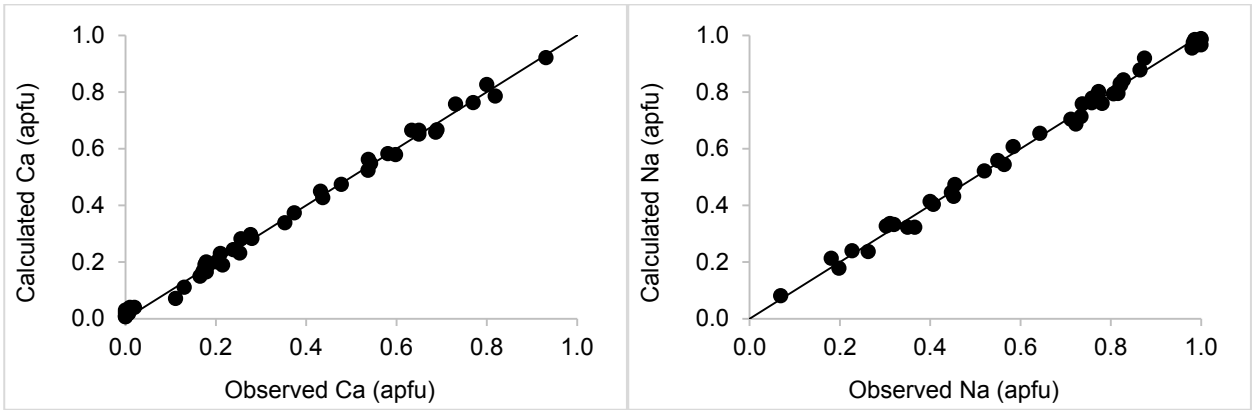

FIGURE 1a-b. Plagioclase Ca- and Na-content: calculated versus observed. RMSE: Ca = 0.022 apfu; Na = 0.023 apfu.

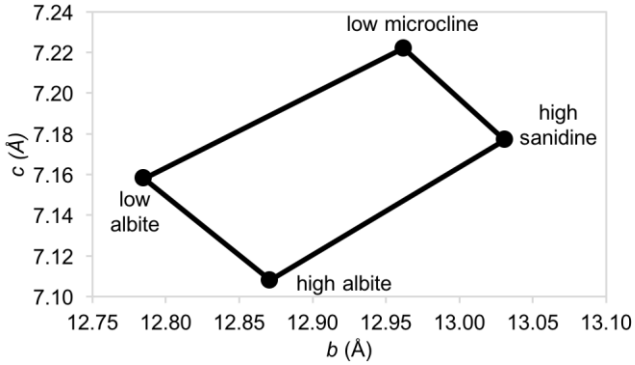

FIGURE 2. Alkali feldspar quadrilateral: composition and Al-Si ordering as a function of *c* and *b* unit-cell parameters. Black circles represent literature end-members. Composition trends from $NaAlSi_3O_8$ at the low albite - high albite edge to $KAlSi_3O_8$ at the low microcline - high sanidine edge. Al-Si ordering trends from completely ordered at the low albite - low microcline edge to completely disordered at the high albite - high sanidine edge.

This is a preprint, the final version is subject to change, of the American Mineralogist (MSA)
Cite as Authors (Year) Title. American Mineralogist, in press.
DOI: http://dx.doi.org/10.2138/am-2018-6123

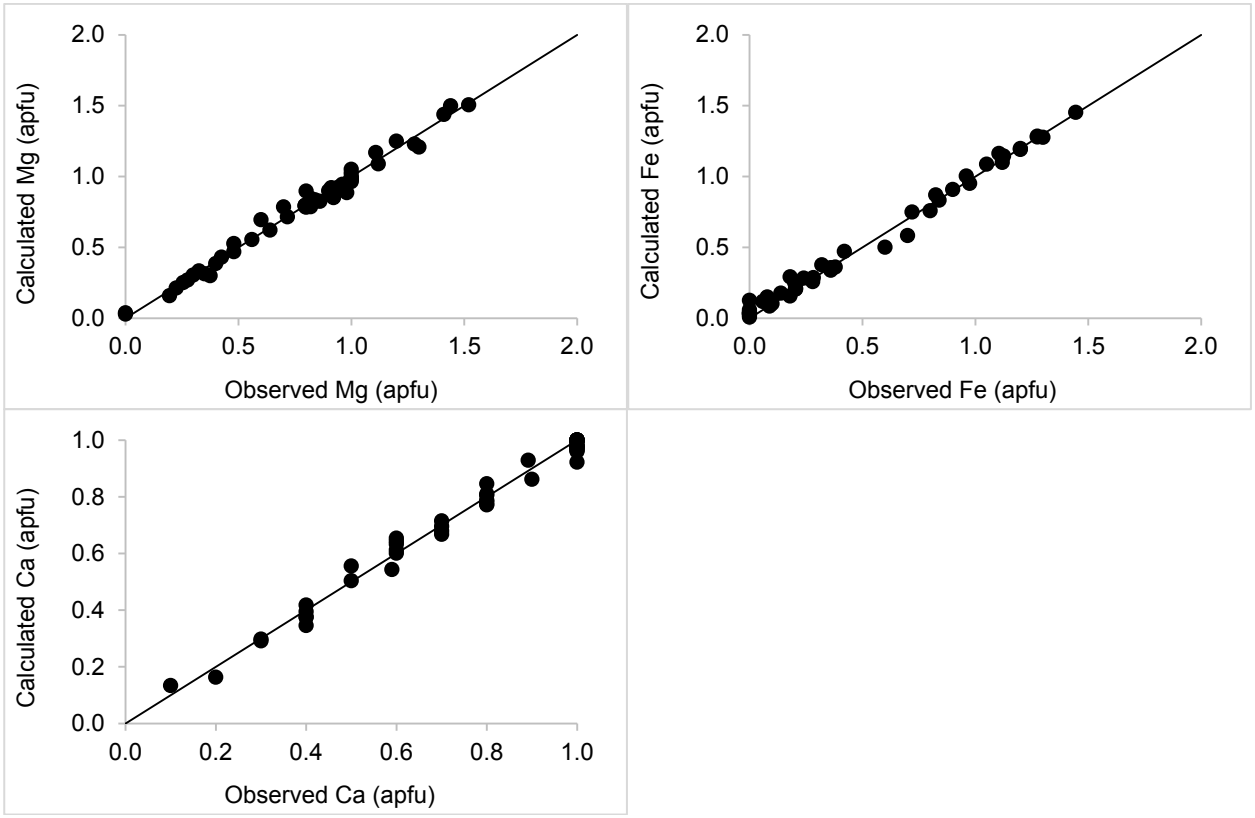

721

722
723
724
725
726

FIGURE 3a-c. Augite Mg-, Fe-, and Ca-content: calculated versus observed. Mg, Fe, and Ca, RMSE = 0.037, 0.049, and 0.030 apfu, respectively.

This is a preprint, the final version is subject to change, of the American Mineralogist (MSA)
Cite as Authors (Year) Title. American Mineralogist, in press.
DOI: http://dx.doi.org/10.2138/am-2018-6123

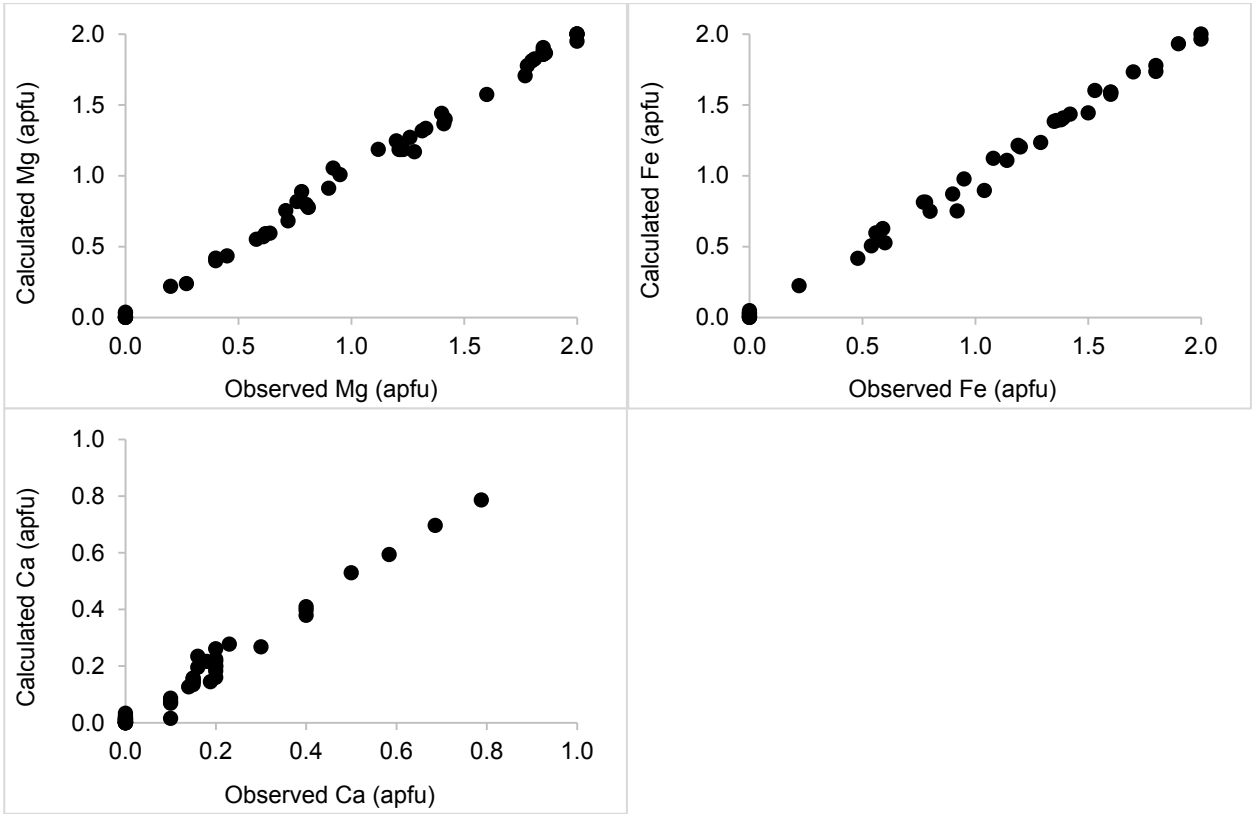

FIGURE 4a-c. Pigeonite Mg-, Fe-, and Ca-content: calculated versus observed. Mg, Fe, and Ca RMSE = 0.041, 0.045, and 0.026 apfu, respectively.

This is a preprint, the final version is subject to change, of the American Mineralogist (MSA)
Cite as Authors (Year) Title. American Mineralogist, in press.
DOI: http://dx.doi.org/10.2138/am-2018-6123

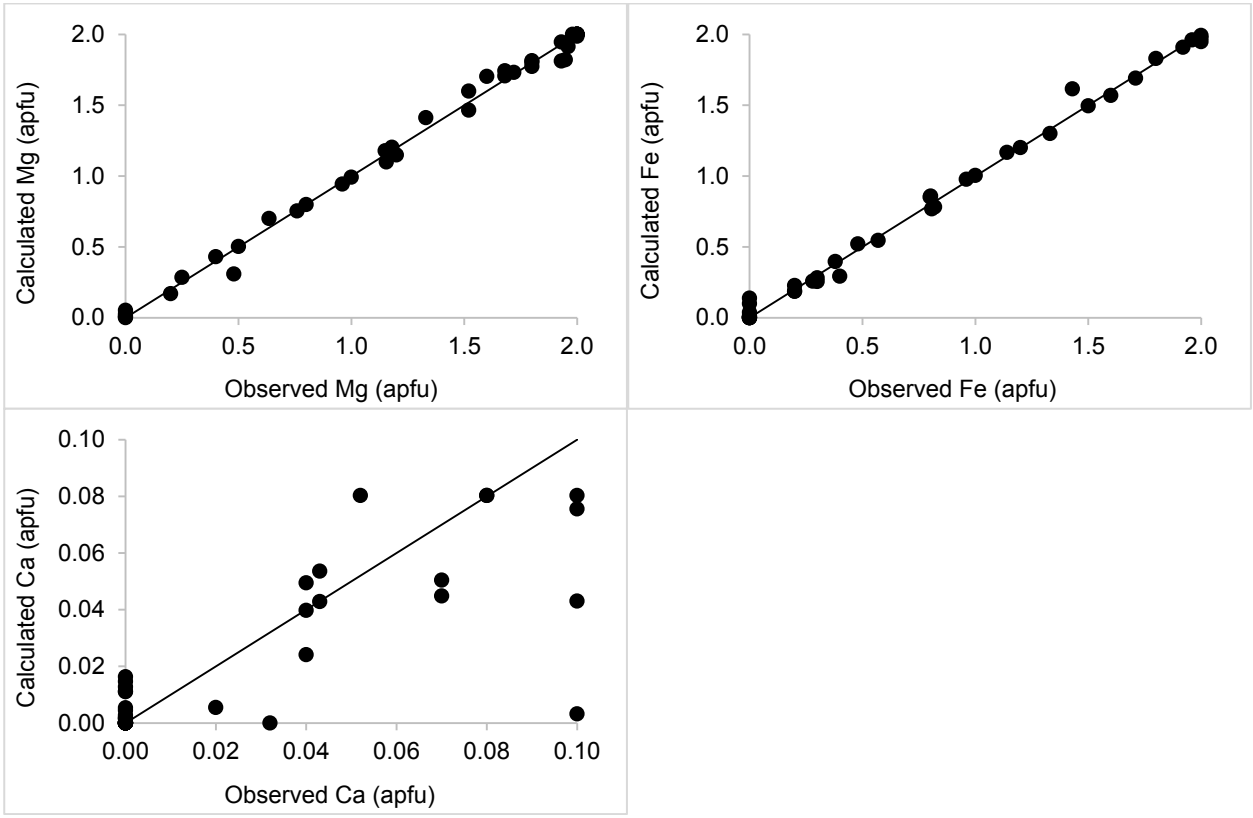

FIGURE 5a-c. Orthopyroxene Mg-, Fe-, and Ca-content: calculated versus observed. Mg, Fe, and Ca RMSE = 0.053, 0.049, and 0.021 apfu, respectively.

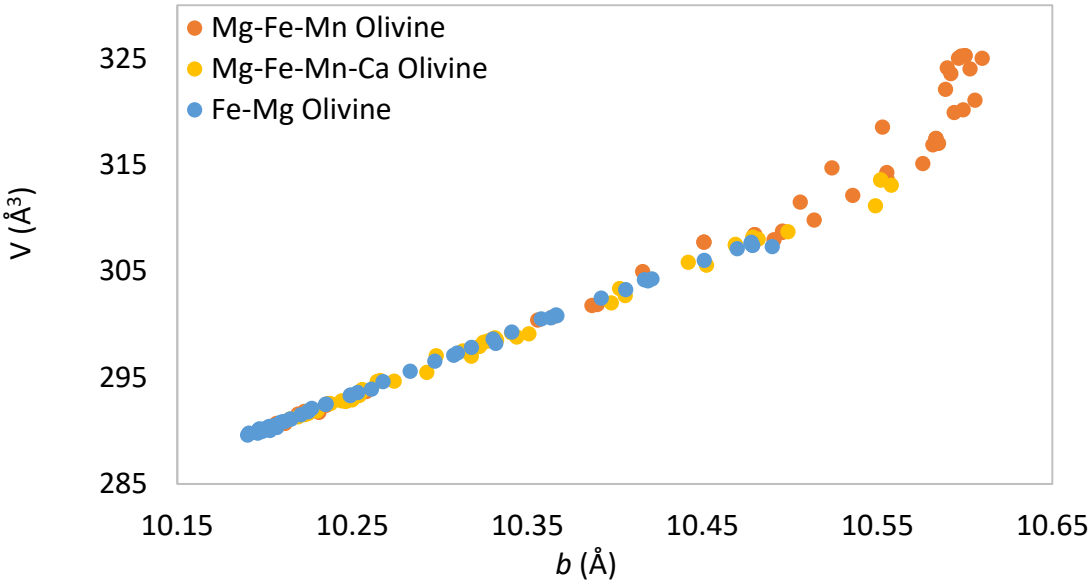

FIGURE 6. Mg-Fe, Mg-Fe-Mn, and Mg-Fe-Mn-Ca (with Ca < 0.5 apfu) olivine *b* unit-cell parameter versus unit-cell volume, *V*.

This is a preprint, the final version is subject to change, of the American Mineralogist (MSA)
Cite as Authors (Year) Title. American Mineralogist, in press.
DOI: http://dx.doi.org/10.2138/am-2018-6123

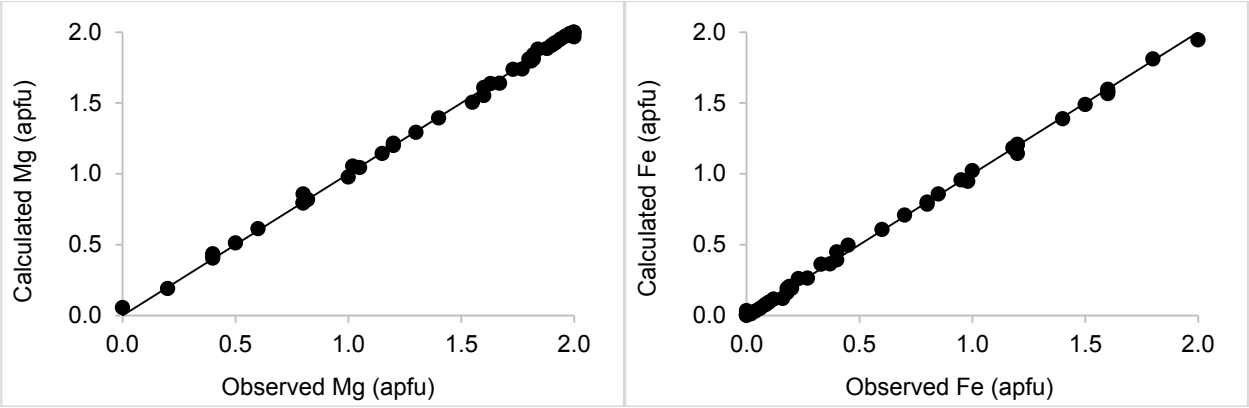

FIGURE 7a-b. Olivine Mg- and Fe-content: calculated versus observed. RMSE = 0.017 Mg apfu and 0.017 Fe apfu.

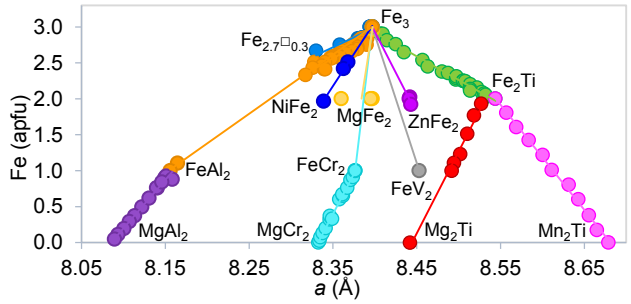

FIGURE 8. Selected spinel oxides (M_3O_4) as a function of Fe-content and *a* unit-cell parameter.

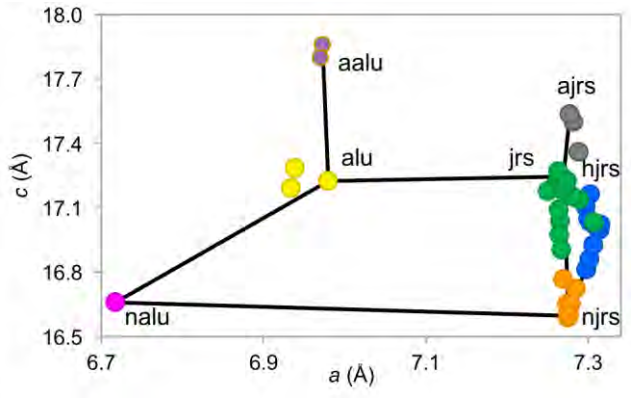

FIGURE 9. Alunite-jarosite phases as a function of *a* unit-cell parameter versus *c* unit-cell parameter. jrs = jarosite, alu = alunite, njrs = natrojarosite, nalu = natroalunite, ajrs = ammoniojarosite, aalu = ammonioalunite, hjrs = hydronuiumjarosite.

This is a preprint, the final version is subject to change, of the American Mineralogist (MSA)
Cite as Authors (Year) Title. American Mineralogist, in press.
DOI: http://dx.doi.org/10.2138/am-2018-6123

Appendices

Appendix 1 - Datasets used in regression analyses

Table A1a. Plagioclase regression data

	Plagioclase-phase							
Chemical Composition	*a* (Å)	*b* (Å)	*c* (Å)	α (°)	β (°)	γ (°)	*V* (Å^3)	Reference
$Na_{0.991}Ca_{0.007}K_{0.002}Al_{1.007}Si_{2.993}O_8$	8.139	12.782	7.157	94.29	116.6	87.69	663.869	[2]
$Na_{0.977}Ca_{0.017}K_{0.006}Al_{1.017}Si_{2.983}O_8$	8.139	12.785	7.158	94.2	116.61	87.76	664.139	[2]
$Na_{0.997}K_{0.003}Al_{1.000}Si_{3.000}O_8$	8.141	12.786	7.159	94.25	116.59	87.69	664.516	[2]
$Na_{0.983}Ca_{0.005}K_{0.012}Al_{1.005}Si_{2.995}O_8$	8.141	12.785	7.159	94.26	116.59	87.69	664.456	[2]
$Na_{0.875}Ca_{0.111}K_{0.014}Al_{1.111}Si_{2.889}O_8$	8.148	12.798	7.156	94.2	116.57	87.85	665.604	[2]
$Na_{0.865}Ca_{0.130}K_{0.005}Al_{1.130}Si_{2.870}O_8$	8.149	12.804	7.142	94.07	116.52	88.45	665.094	[2]
$Na_{0.828}Ca_{0.165}K_{0.007}Al_{1.165}Si_{2.835}O_8$	8.151	12.814	7.138	94.01	116.5	88.63	665.556	[2]
$Na_{0.815}Ca_{0.176}K_{0.009}Al_{1.176}Si_{2.824}O_8$	8.153	12.824	7.134	93.95	116.46	88.84	666.122	[2]
$Na_{0.773}Ca_{0.215}K_{0.012}Al_{1.215}Si_{2.785}O_8$	8.153	12.83	7.134	93.9	116.43	88.94	666.635	[2]
$Na_{0.822}Ca_{0.172}K_{0.006}Al_{1.172}Si_{2.828}O_8$	8.154	12.826	7.137	93.94	116.48	88.74	666.494	[2]
$Na_{0.758}Ca_{0.239}K_{0.003}Al_{1.239}Si_{2.761}O_8$	8.154	12.847	7.12	93.79	116.42	89.45	666.328	[2]
$Na_{0.816}Ca_{0.179}K_{0.005}Al_{1.179}Si_{2.821}O_8$	8.155	12.834	7.13	93.88	116.45	89.07	666.509	[2]
$Na_{0.806}Ca_{0.185}K_{0.009}Al_{1.185}Si_{2.815}O_8$	8.158	12.831	7.137	93.94	116.45	88.8	667.247	[2]
$Na_{0.734}Ca_{0.256}K_{0.010}Al_{1.256}Si_{2.744}O_8$	8.158	12.837	7.124	93.8	116.4	89.26	666.667	[2]
$Na_{0.737}Ca_{0.253}K_{0.010}Al_{1.253}Si_{2.747}O_8$	8.159	12.843	7.127	93.8	116.41	89.28	667.279	[2]
$Na_{0.781}Ca_{0.210}K_{0.009}Al_{1.210}Si_{2.790}O_8$	8.161	12.836	7.131	93.89	116.45	89.01	667.2	[2]
$Na_{0.643}Ca_{0.353}K_{0.004}Al_{1.353}Si_{2.647}O_8$	8.161	12.859	7.116	93.66	116.3	89.71	667.878	[2]
$Na_{0.759}Ca_{0.202}K_{0.039}Al_{1.202}Si_{2.798}O_8$	8.162	12.827	7.137	93.88	116.46	88.85	667.353	[2]
$Na_{0.712}Ca_{0.280}K_{0.008}Al_{1.280}Si_{2.720}O_8$	8.163	12.853	7.124	93.71	116.36	89.38	668.188	[2]
$Na_{0.520}Ca_{0.478}K_{0.002}Al_{1.478}Si_{2.522}O_8$	8.166	12.851	7.113	93.61	116.26	89.64	667.888	[2]
$Na_{0.564}Ca_{0.432}K_{0.004}Al_{1.432}Si_{2.568}O_8$	8.167	12.856	7.113	93.6	116.27	89.71	668.158	[2]
$Na_{0.455}Ca_{0.537}K_{0.008}Al_{1.537}Si_{2.463}O_8$	8.169	12.862	7.108	93.58	116.22	89.81	668.436	[2]
$Na_{0.584}Ca_{0.374}K_{0.042}Al_{1.374}Si_{2.626}O_8$	8.171	12.862	7.119	93.59	116.3	89.68	669.206	[2]
$Na_{0.550}Ca_{0.437}K_{0.013}Al_{1.437}Si_{2.563}O_8$	8.172	12.865	7.116	93.6	116.27	89.66	669.334	[2]
$Na_{0.447}Ca_{0.543}K_{0.010}Al_{1.543}Si_{2.457}O_8$	8.172	12.861	7.107	93.52	116.22	90.03	668.506	[2]
$Na_{0.452}Ca_{0.538}K_{0.010}Al_{1.538}Si_{2.462}O_8$	8.173	12.855	7.11	93.58	116.23	89.79	668.537	[2]
$Na_{0.400}Ca_{0.598}K_{0.002}Al_{1.598}Si_{2.402}O_8$	8.173	12.862	7.107	93.56	116.19	89.98	668.797	[2]
$Na_{0.311}Ca_{0.687}K_{0.002}Al_{1.687}Si_{2.313}O_8$	8.175	12.865	7.102	93.5	116.14	90.31	668.846	[2]
$Na_{0.303}Ca_{0.690}K_{0.007}Al_{1.690}Si_{2.310}O_8$	8.179	12.869	7.102	93.49	116.16	90.36	669.251	[2]
$Na_{0.198}Ca_{0.800}K_{0.002}Al_{1.800}Si_{2.200}O_8$	8.179	12.868	7.093	93.34	116.08	90.8	668.719	[2]
$Na_{0.069}Ca_{0.931}Al_{1.931}Si_{2.069}O_8$	8.179	12.873	7.09	93.21	115.97	91.11	669.261	[2]
$Na_{0.407}Ca_{0.581}K_{0.012}Al_{1.581}Si_{2.419}O_8$	8.18	12.87	7.109	93.52	116.2	90.04	669.928	[2]
$Na_{0.227}Ca_{0.770}K_{0.003}Al_{1.770}Si_{2.230}O_8$	8.18	12.869	7.096	93.38	116.13	90.63	668.905	[2]
$Na_{0.263}Ca_{0.731}K_{0.006}Al_{1.731}Si_{2.269}O_8$	8.181	12.87	7.099	93.41	116.1	90.55	669.509	[2]
$Na_{0.181}Ca_{0.819}Al_{1.819}Si_{2.181}O_8$	8.181	12.871	7.096	93.34	116.1	90.79	669.212	[2]
$Ca_{0.65}Na_{0.32}Si_{2.38}Al_{1.62}O_8$	8.1736	12.874	7.1022	93.46	116.05	90.48	669.65	[9]
$Ca_{0.634}Na_{0.366}Si_{2.348}Al_{1.648}O_8$	8.1747	12.871	7.1014	93.46	116.09	90.51	669.3	[9]
$Ca_{0.650}Na_{0.350}Si_{2.348}Al_{1.648}O_8$	8.1747	12.871	7.1014	93.46	116.09	90.51	669.3	[9]
$Na_{0.986}Al_{1.005}Si_{2.995}O_8$	8.142	12.785	7.159	94.19	116.61	87.68	664.48	[5]

This is a preprint, the final version is subject to change, of the American Mineralogist (MSA)
Cite as Authors (Year) Title. American Mineralogist, in press.
DOI: http://dx.doi.org/10.2138/am-2018-6123

$NaAl_{1.004}Si_{2.994}O_8$	8.142	12.785	7.159	94.19	116.61	87.68	664.48	[5]
$NaAlSi_3O_8$	8.137	12.785	7.1583	94.26	116.6	87.71	664.01	[1]
$NaAlSi_3O_8$	8.1372	12.787	7.1574	94.25	116.61	87.81	664.04	[3]
$NaAlSi_3O_8$	8.133	12.773	7.159	94.23	116.64	87.72	662.92	[6]
$Na_{0.98}Ca_{0.02}Si_{2.98}Al_{1.02}O_8$	8.1459	12.797	7.1578	94.25	116.6	87.8	665.34	[4]
$Na_{0.99}Ca_{0.01}Al_{1.03}Si_{2.97}O_8$	8.135	12.784	7.1594	94.27	116.59	87.72	663.92	[8]
$Na_{0.99}Ca_{0.01}Al_{1.03}Si_{2.97}O_8$	8.1365	12.788	7.1584	94.23	116.58	87.7	664.26	[8]
$NaAlSi_3O_8$	8.1409	12.789	7.1598	94.27	116.59	87.68	664.73	[8]
$Na_{0.821}Ca_{0.179}Al_{1.179}Si_{2.821}O_8$	8.154	12.823	7.139	94.06	116.5	88.59	666.32	[7]
$Na_{0.723}Ca_{0.277}Al_{1.277}Si_{2.723}O_8$	8.169	12.851	7.124	93.63	116.4	89.46	668.39	[7]

[1] Armbruster, T., Burgi, H.B., Kunz, M., Gnos, E., Bronnimann, S., and Lienert, C. (1990) Variation of displacement parameters in structure refinements of low albite. American Mineralogist, 75, 135-140.
[2] Bambauer, H.U., Corlett, M., Eberhard, E., and Viswanathan, K. (1967) Diagrams for the determination of plagioclases using X-ray powder methods (Part III of laboratory investigations of plagioclases). Schweizerische Mineralogische und Petrographische Mitteilungen, 47, 333-349.
[3] Downs, R.T., Hazen, R.M., and Finger, L.W. (1994) The high-pressure crystal chemistry of low albite and the origin of the pressure dependency of Al-Si ordering. American Mineralogist, 79, 1042-1052.
[4] Gualtieri, A.F. (2000) Accuracy of XRPD QPA using the combined Rietveld-RIR method. Journal of Applied Crystallography, 33, 267-278.
[5] Harlow, G., and Brown Jr, G.E. (1980) Low Albite- an X-Ray and Neutron Diffraction Study. American Mineralogist, 65, 986-995.
[6] Meneghinello, E., Alberti, A., and Cruciani, G. (1999) Order-disorder process in the tetrahedral sites of albite. American Mineralogist, 84, 1144-1151.
[7] Phillips, M.W., Colville, A.A., and Ribbe, P.H. (1971) The crystal structures of two oligoclases: A comparison with low and high albite. Zeitschrift fur Kristallographie, 133, 43-65.
[8] RRUFF.info
[9] Wenk, H., Joswig, W., Tagai, T., Korekawa, M., and Smith, B.K. (1980) The average structure of An 62-66 labradorite. American Mineralogist, 65, 81-95.

This is a preprint, the final version is subject to change, of the American Mineralogist (MSA)
Cite as Authors (Year) Title. American Mineralogist, in press.
DOI: http://dx.doi.org/10.2138/am-2018-6123

Table A1b. Alkali feldspar quadrilateral data

Phase	Composition	Ordering	*b*	*c*
high sanidine	$KAlSi_3O_8$	disordered	13.031	7.177
low microcline	$KAlSi_3O_8$	ordered	12.962	7.222
high albite	$NaAlSi_3O_8$	disordered	12.871	7.108
low albite	$NaAlSi_3O_8$	ordered	12.785	7.158

Kroll, H., and Ribbe, P.J. (1983) Lattice parameters, composition and Al,Si order in alkali feldspars. Reviews in Mineralogy p. 57-100.

This is a preprint, the final version is subject to change, of the American Mineralogist (MSA)
Cite as Authors (Year) Title. American Mineralogist, in press.
DOI: http://dx.doi.org/10.2138/am-2018-6123

804 Table A1c. Augite regression data

	Augite (*C*2/*c*)					
Chemical composition	*a* (Å)	*b* (Å)	*c* (Å)	β (°)	*V* (Å^3)	Reference
$Ca_{0.10}Mg_{1.52}Fe_{0.38}Si_2O_6$	9.652	8.872	5.206	108.55	422.6	[7]
$Ca_{0.20}Mg_{1.44}Fe_{0.36}Si_2O_6$	9.655	8.876	5.201	108.46	422.8	[7]
$Ca_{0.59}Mg_{1.41}Si_2O_6$	9.711	8.8935	5.2452	107.278	432.559	[6]
$Ca_{0.40}Mg_{1.28}Fe_{0.32}Si_2O_6$	9.718	8.902	5.239	107.85	431.4	[7]
$Ca_{0.7}Mg_{1.3}Si_2O_6$	9.7264	8.9133	5.2485	106.742	435.728	[6]
$Ca_{0.8}Mg_{1.2}Si_2O_6$	9.7323	8.9152	5.2464	106.357	436.782	[6]
$Ca_{0.892}Mg_{1.108}Si_2O_6$	9.739	8.919	5.25	106.15	438.2	[7]
$Ca_{0.60}Mg_{1.12}Fe_{0.28}Si_2O_6$	9.734	8.921	5.244	106.73	436.1	[7]
$CaMgSi_2O_6$	9.747	8.924	5.252	105.94	439.28	[3]
$CaMgSi_2O_6$	9.748	8.924	5.251	105.79	439.48	[2]
$CaMgSi_2O_6$	9.7483	8.9246	5.2505	105.882	439.355	[4]
$CaMgSi_2O_6$	9.755	8.926	5.241	105.84	439.04	[5]
$CaMgSi_2O_6$	9.7507	8.9264	5.2515	105.837	439.74	[4]
$CaMgSi_2O_6$	9.75	8.927	5.254	105.79	439.99	[5]
$CaMgSi_2O_6$	9.7485	8.931	5.249	105.85	439.6	[7]
$CaMgSi_2O_6$	9.754	8.933	5.252	105.84	440.22	[5]
$CaMg_{0.9116}Fe_{0.0884}Si_2O_6$	9.759	8.934	5.254	105.77	440.86	[2]
$CaMg_{0.921}Fe_{0.079}Si_2O_6$	9.772	8.934	5.253	105.76	441.32	[5]
$Ca_{0.80}Mg_{0.96}Fe_{0.24}Si_2O_6$	9.745	8.935	5.246	106.23	438.6	[7]
$CaMg_{0.90}Fe_{0.10}Si_2O_6$	9.762	8.936	5.249	105.75	441	[7]
$CaMg_{0.921}Fe_{0.079}Si_2O_6$	9.767	8.936	5.246	105.68	440.84	[5]
$CaMg_{0.921}Fe_{0.079}Si_2O_6$	9.775	8.936	5.244	105.74	440.91	[5]
$CaMg_{0.941}Fe_{0.059}Si_2O_6$	9.757	8.937	5.245	105.82	440.05	[5]
$Ca_{0.60}Mg_{0.98}Fe_{0.42}Si_2O_6$	9.745	8.939	5.244	106.69	437.6	[7]
$CaMg_{0.8209}Fe_{0.1791}Si_2O_6$	9.765	8.941	5.250	105.68	441.32	[2]
$Ca_{0.40}Mg_{0.80}Fe_{0.80}Si_2O_6$	9.727	8.942	5.255	108.1	434.4	[7]
$Ca_{0.80}Mg_{0.84}Fe_{0.36}Si_2O_6$	9.757	8.943	5.246	106.05	439.9	[7]
$CaMg_{0.861}Fe_{0.139}Si_2O_6$	9.77	8.943	5.252	105.69	441.75	[5]
$CaMg_{0.796}Fe_{0.204}Si_2O_6$	9.774	8.944	5.249	105.64	441.88	[5]
$CaMg_{0.796}Fe_{0.204}Si_2O_6$	9.772	8.945	5.253	105.65	442.15	[5]
$CaMg_{0.796}Fe_{0.204}Si_2O_6$	9.771	8.946	5.253	105.66	442.08	[5]
$CaMg_{0.80}Fe_{0.20}Si_2O_6$	9.771	8.947	5.25	105.68	442	[7]
$CaMg_{0.82}Fe_{0.18}Si_2O_6$	9.7634	8.9488	5.2504	105.726	441.56	[3]
$CaMg_{0.717}Fe_{0.283}Si_2O_6$	9.782	8.952	5.255	105.6	443.23	[5]
$CaMg_{0.74}Fe_{0.26}Si_2O_6$	9.773	8.9523	5.2524	105.676	442.444	[3]
$Ca_{0.60}Mg_{0.70}Fe_{0.70}Si_2O_6$	9.741	8.953	5.248	106.67	438.5	[7]
$CaMg_{0.7278}Fe_{0.2722}Si_2O_6$	9.780	8.954	5.253	105.59	443.08	[2]
$Ca_1Mg_{0.70}Fe_{0.30}Si_2O_6$	9.7755	8.955	5.251	105.67	443.1	[7]
$Ca_{0.80}Mg_{0.60}Fe_{0.60}Si_2O_6$	9.767	8.956	5.249	105.97	441.4	[7]
$CaMg_{0.717}Fe_{0.283}Si_2O_6$	9.782	8.96	5.243	105.59	442.66	[5]
$CaMg_{0.589}Fe_{0.411}Si_2O_6$	9.789	8.96	5.251	105.49	443.85	[5]
$CaMg_{0.6321}Fe_{0.3679}Si_2O_6$	9.793	8.962	5.254	105.50	444.28	[2]
$CaMg_{0.589}Fe_{0.411}Si_2O_6$	9.794	8.963	5.249	105.48	444	[5]

$CaMg_{0.589}Fe_{0.411}Si_2O_6$	9.794	8.966	5.257	105.47	444.94	[5]
$CaMg_{0.5339}Fe_{0.4661}Si_2O_6$	9.804	8.971	5.253	105.46	445.30	[2]
$CaMg_{0.50}Fe_{0.50}Si_2O_6$	9.7955	8.9725	5.252	105.49	445.4	[7]
$CaFe_{0.523}Mg_{0.477}Si_2O_6$	9.801	8.974	5.248	105.46	444.92	[5]
$CaFe_{0.523}Mg_{0.477}Si_2O_6$	9.802	8.976	5.254	105.4	445.69	[5]
$CaMg_{0.5}Fe_{0.5}Si_2O_6$	9.795	8.979	5.235	105.50	445.34	[3]
$Ca_{0.60}Mg_{0.56}Fe_{0.84}Si_2O_6$	9.752	8.981	5.249	106.63	440.5	[7]
$Ca_{0.80}Mg_{0.48}Fe_{0.72}Si_2O_6$	9.781	8.982	5.244	105.87	443.2	[7]
$Ca_{1.00}Fe_{0.60}Mg_{0.40}Si_2O_6$	9.813	8.982	5.251	105.32	445.5	[7]
$Ca_{0.40}Mg_{0.64}Fe_{0.96}Si_2O_6$	9.731	8.984	5.258	107.82	437.6	[7]
$CaFe_{0.5670}Mg_{0.4330}Si_2O_6$	9.809	8.985	5.249	105.28	446.33	[2]
$CaFe_{0.682}Mg_{0.318}Si_2O_6$	9.816	8.987	5.252	105.07	447.41	[5]
$CaFe_{0.682}Mg_{0.318}Si_2O_6$	9.816	8.991	5.253	105.1	447.61	[5]
$Ca_{1.00}Fe_{0.70}Mg_{0.30}Si_2O_6$	9.821	8.992	5.251	105.18	447.6	[7]
$CaFe_{0.6707}Mg_{0.3293}Si_2O_6$	9.821	8.994	5.247	105.13	447.39	[2]
$CaMg_{0.7}Fe_{0.3}Si_2O_6$	9.814	8.996	5.253	105.33	447.29	[3]
$Ca_{0.40}Mg_{0.48}Fe_{1.12}Si_2O_6$	9.74	8.998	5.251	107.77	438.2	[7]
$Ca_{0.70}Mg_{0.325}Fe_{0.975}Si_2O_6$	9.791	9.001	5.242	106.02	444	[7]
$Ca_{0.80}Mg_{0.30}Fe_{0.90}Si_2O_6$	9.797	9.002	5.243	105.7	445.2	[7]
$Ca_{0.90}Fe_{0.825}Mg_{0.275}Si_2O_6$	9.814	9.002	5.249	105.46	447	[7]
$Ca_{1.00}Fe_{0.75}Mg_{0.25}Si_2O_6$	9.821	9.002	5.251	104.98	448.4	[7]
$CaFe_{0.80}Mg_{0.20}Si_2O_6$	9.832	9.002	5.251	105.02	448.6	[7]
$CaFe_{0.85}Mg_{0.15}Si_2O_6$	9.834	9.01	5.247	104.96	449.15	[5]
$CaFe_{0.7774}Mg_{0.2226}Si_2O_6$	9.826	9.012	5.251	105.01	449.20	[2]
$CaFe_{0.85}Mg_{0.15}Si_2O_6$	9.836	9.014	5.248	104.92	449.6	[7]
$Ca_{0.60}Mg_{0.35}Fe_{1.05}Si_2O_6$	9.767	9.015	5.242	106.44	442.7	[7]
$Ca_{0.40}Mg_{0.40}Fe_{1.20}Si_2O_6$	9.749	9.018	5.247	107.4	440	[7]
$CaFe_{0.8871}Mg_{0.1129}Si_2O_6$	9.832	9.018	5.247	104.88	449.61	[2]
$Ca_{0.50}Mg_{0.375}Fe_{1.125}Si_2O_6$	9.771	9.019	5.244	106.65	442.7	[7]
$Ca_{0.30}Mg_{0.425}Fe_{1.275}Si_2O_6$	9.744	9.021	5.256	108.06	439.2	[7]
$Ca_{1.00}Fe_{1.00}Si_2O_6$	9.84	9.024	5.2495	104.68	450.8	[7]
$CaFeSi_2O_6$	9.847	9.024	5.242	104.77	450.36	[5]
$CaFeSi_2O_6$	9.852	9.025	5.247	104.77	451.16	[5]
$CaFeSi_2O_6$	9.866	9.025	5.225	104.69	450.04	[5]
$CaFeSi_2O_6$	9.857	9.026	5.227	104.7	449.81	[5]
$CaFeSi_2O_6$	9.841	9.027	5.247	104.80	450.69	[2]
$CaFeSi_2O_6$	9.85	9.028	5.23	104.75	449.69	[5]
$Ca_{0.70}Mg_{0.195}Fe_{1.105}Si_2O_6$	9.8	9.03	5.244	105.92	446.3	[7]
$Ca_{0.50}Mg_{0.225}Fe_{1.275}Si_2O_6$	9.772	9.038	5.245	106.75	443.4	[7]
$Ca_{0.80}Fe_{1.20}Si_2O_6$	9.821	9.042	5.242	105.38	448.8	[7]
$Ca_{1.01}Mg_{0.99}Si_2O_6$	9.8672	9.0469	5.2584	104.794	453.84	[1]
$Ca_{0.70}Fe_{1.30}Si_2O_6$	9.8095	9.05	5.238	105.61	447.9	[7]
$Ca_{0.30}Mg_{0.255}Fe_{1.445}Si_2O_6$	9.746	9.055	5.255	107.7	441.8	[7]

[1] Heuer, M., Huber, A.L., Bromiley, G.D., Fehr, K.T., Bente, K. (2005) Characterization of synthetic hedenbergite ($CaFeSi_2O_6$)-petedunnite ($CaZnSi_2O_6$) solid solution series by X-ray single crystal diffraction. Physics and Chemistry of Minerals, 32, 552-563.

This is a preprint, the final version is subject to change, of the American Mineralogist (MSA)
Cite as Authors (Year) Title. American Mineralogist, in press.
DOI: http://dx.doi.org/10.2138/am-2018-6123

[2] Nolan, J. (1969) Physical properties of synthetic and natural pyroxenes in the system diopsite-hedenbergite-acmite. Mineralogical Magazine, 37, 216-229

[3] Raudsepp M, Hawthorne F C, Turnock A C (1990) Evaluation of the Rietveld method for the characterization of fine-grained products of mineral synthesis: the diopside-hedenbergite join. The Canadian Mineralogist 28, 93-109.

[4] Redhammer, G.J. (1998) Mossbauer spectroscopy and Rietveld refinement on synthetic ferri-Tschermak's molecule $CaFe^{3+}(Fe^{3+}Si)O_6$ substituted diopside. European Journal of Mineralogy, 10, 439-452.

[5] Rutstein, M.S., and Yund, R.A. (1969) Unit-cell parameters of synthetic diopside-hedenbergite solid solutions. American Mineralogist, 54, 238-245.

[6] Tribaudino, M., Nestola, F., and Meneghini, C. (2005) Rietveld refinement of clinopyroxene with intermediate Ca-content along the join diopside-enstatite. The Canadian Mineralogist, 43, 1411-1421.

[7] Turnock, A.C., Lindsley, D.H., and Grover, J.E. (1973) Synthesis and unit cell parameters of Ca-Mg-Fe pyroxenes. American Mineralogist, 58, 50-59.

This is a preprint, the final version is subject to change, of the American Mineralogist (MSA)
Cite as Authors (Year) Title. American Mineralogist, in press.
DOI: http://dx.doi.org/10.2138/am-2018-6123

825 Table A1d. Pigeonite regression data

	Pigeonite ($P2_1/c$)					
Chemical composition	a (Å)	b (Å)	c (Å)	β (°)	V (Å^3)	Reference
$Mg_2Si_2O_6$	9.606	8.8131	5.17	108.35	415.429	[9]
$Mg_2Si_2O_6$	9.6076	8.8152	5.1702	108.350	415.61	[1]
$Mg_2Si_2O_6$	9.62	8.825	5.188	108.33	418.095	[6]
$Mg_{1.78}Fe_{0.22}Si_2O_6$	9.6194	8.8396	5.1793	108.438	417.80	[1]
$Mg_{1.85}Ca_{0.15}Si_2O_6$	9.646	8.842	5.201	108.35	421.037	[7]
$Mg_{1.85}Ca_{0.15}Si_2O_6$	9.654	8.845	5.203	108.37	421.642	[10]
$Mg_{1.85}Ca_{0.15}Si_2O_6$	9.651	8.846	5.202	108.38	421.453	[11]
$Mg_{1.85}Ca_{0.15}Si_2O_6$	9.651	8.846	5.202	108.34	421.551	[11]
$Mg_{1.85}Ca_{0.15}Si_2O_6$	9.651	8.846	5.252	108.38	425.504	[4]
$Ca_{0.2}Mg_{1.8}Si_2O_6$	9.6655	8.8534	5.2138	108.349	423.474	[12]
$Ca_{0.23}Mg_{1.77}Si_2O_6$	9.69	8.862	5.229	108.31	426.295	[10]
$Ca_{0.4}Mg_{1.6}Si_2O_6$	9.7042	8.8805	5.2423	108.084	429.455	[12]
$Mg_{1.41}Fe_{0.59}Si_2O_6$	9.6434	8.8852	5.1950	108.548	422.01	[1]
$Mg_{1.26}Fe_{0.54}Ca_{0.20}Si_2O_6$	9.684	8.907	5.227	108.51	427.6	[13]
$Mg_{1.23}Fe_{0.77}Si_2O_6$	9.6519	8.9075	5.2004	108.590	423.77	[1]
$Mg_{1.22}Fe_{0.78}Si_2O_6$	9.6519	8.9075	5.2004	108.59	423.773	[1]
$Mg_{1.28}Fe_{0.56}Ca_{0.16}Si_2O_6$	9.692	8.917	5.239	108.55	429.25	[3]
$Mg_{1.12}Fe_{0.48}Ca_{0.40}Si_2O_6$	9.707	8.919	5.249	108.22	431.6	[13]
$Mg_{0.92}Fe_{0.92}Ca_{0.16}Si_2O_6$	9.689	8.93	5.232	108.53	429.2	[13]
$Mg_{0.95}Fe_{0.95}Ca_{0.10}Si_2O_6$	9.662	8.931	5.218	108.71	426.5	[13]
$Mg_{0.90}Fe_{0.90}Ca_{0.20}Si_2O_6$	9.703	8.947	5.238	108.57	431.1	[13]
$Mg_{0.78}Fe_{1.04}Ca_{0.18}Si_2O_6$	9.706	8.95	5.246	108.59	431.936	[5]
$Mg_{0.81}Fe_{1.19}Si_2O_6$	9.6744	8.9630	5.2157	108.630	428.57	[1]
$Fe_{1.29}Mg_{0.71}Si_2O_6$	9.6761	8.9664	5.2171	108.623	428.93	[1]
$Mg_{0.72}Fe_{1.08}Ca_{0.20}Si_2O_6$	9.712	8.978	5.244	108.49	433.7	[13]
$Mg_{0.72}Fe_{1.08}Ca_{0.20}Si_2O_6$	9.712	8.978	5.244	108.49	433.7	[13]
$Mg_{0.64}Fe_{1.36}Si_2O_6$	9.6846	8.9898	5.2209	108.627	430.73	[1]
$Fe_{1.38}Mg_{0.62}Si_2O_6$	9.6837	8.9905	5.2202	108.604	430.73	[1]
$Fe_{1.39}Mg_{0.61}Si_2O_6$	9.6868	8.9936	5.2218	108.611	431.13	[1]
$Fe_{1.42}Mg_{0.58}Si_2O_6$	9.6856	8.9964	5.2218	108.605	431.22	[1]
$Mg_{0.45}Fe_{1.35}Ca_{0.20}Si_2O_6$	9.732	9.015	5.258	108.38	437.7	[13]
$Fe_{1.60}Mg_{0.40}Si_2O_6$	9.6913	9.0171	5.2263	108.598	432.87	[1]
$Fe_{1.60}Mg_{0.40}Si_2O_6$	9.6931	9.0199	5.2264	108.590	433.10	[1]
$Mg_{0.27}Fe_{1.53}Ca_{0.20}Si_2O_6$	9.74	9.046	5.259	108.2	440.2	[13]
$Fe_{1.80}Mg_{0.20}Si_2O_6$	9.7011	9.0491	5.2321	108.556	435.43	[1]
$Fe_2Si_2O_6$	9.7075	9.0807	5.2347	108.46	437.7	[2]
$Fe_{1.80}Ca_{0.20}Si_2O_6$	9.745	9.083	5.225	107.3	441.5	[13]
$Fe_2Si_2O_6$	9.709	9.087	5.228	108.43	437.6	[13]
$Fe_{1.7}Ca_{0.3}Si_2O_6$	9.779	9.088	5.258	107.39	445.928	[8]
$Fe_{1.90}Ca_{0.10}Si_2O_6$	9.724	9.092	5.226	108.14	439.1	[13]
$Mg_2Si_2O_6$	9.59	8.812	5.159	108.15	414.3	[13]
$(Mg_{1.86}Ca_{0.14})Si_2O_6$	9.65	8.84	5.18	108.45	419.2	[13]
$(Mg_{1.812}Ca_{0.188})\ Si_2O_6$	9.653	8.848	5.202	108.41	421.5	[13]

This is a preprint, the final version is subject to change, of the American Mineralogist (MSA)
Cite as Authors (Year) Title. American Mineralogist, in press.
DOI: http://dx.doi.org/10.2138/am-2018-6123

$(Mg_{1.416}Ca_{0.584})Si_2O_6$	9.714	8.903	5.25	107.27	433.8	[13]
$(Mg_{1.314}Ca_{0.686})Si_2O_6$	9.723	8.908	5.25	106.78	435	[13]
$(Mg_{1.212}Ca_{0.788})Si_2O_6$	9.731	8.916	5.25	106.39	436.5	[13]
$(Mg_{1.40}Fe_{0.60})Si_2O_6$	9.645	8.878	5.193	108.58	421.4	[13]
$(Mg_{1.33}Ca_{0.10}Fe_{0.57})Si_2O_6$	9.662	8.893	5.21	108.61	424.2	[13]
$(Mg_{1.20}Fe_{0.80})Si_2O_6$	9.649	8.9	5.199	108.59	423.2	[13]
$(Fe_{1.20}Mg_{0.80})Si_2O_6$	9.667	8.961	5.216	108.69	428	[13]
$(Fe_{1.14}Ca_{0.10}Mg_{0.76})Si_2O_6$	9.684	8.958	5.227	108.62	429.7	[13]
$(Fe_{1.60}Ca_{0.40})Si_2O_6$	9.765	9.081	5.231	106.69	444.3	[13]
$(Fe_{1.50}Ca_{0.50})Si_2O_6$	9.781	9.072	5.232	106.3	445.6	[13]

[1] Angel, R.J., McCammon, C., and Woodland, A.B. (1998) Structure, ordering and cation interactions in Ca-free *P*2(1)/*c* clinopyroxenes. Physics and Chemistry of Minerals, 25, 249-258.
[2] Hugh-Jones, D.A., Woodland, A.B., and Angel, R.J. (1994) The structure of high-pressure *C*2/*c* ferrosilite and crystal chemistry of high-pressure *C*2/*c* pyroxenes. American Mineralogist, 79, 1032-1041.
[3] Kuno, H. (1953) Unit cell dimensions of clinoenstatite and pigeonite in relation to other common clinopyroxenes. American Journal of Science, 251, 741-752.
[4] Merli, M., and Camara, F. (2003) Topological analysis of the electron density of the clinopyroxene structure by the maximum entropy method: an exploratory study. European Journal of Mineralogy, 15, 903-911.
[5] Morimoto, N., and Guven, N. (1970) Refinement of the Crystal Structure of Pigeonite. American Mineralogist, 55, 1195-1209.
[6] Morimoto, N., Appleman, D.E., and Evans, H.T. (1960) The crystal structures of clinoenstatite and pigeonite. Zeitschrift fur Kristallographie, 114, 120-147.
[7] Nestola, F., Tribaudino, M., and Ballaran, T.B. (2004) High pressure behavior, transformation and crystal structure of synthetic iron-free pigeonite. American Mineralogist, 89, 189-196.
[8] Ohashi, Y., Burnham, C.W., and Finger, L.W. (1975) The Effect of Ca-Fe Substitution Structure Crystal. American Mineralogist, 60, 423-434.
[9] Ohashi, Y. (1984) Polysynthetically-twinned structures of enstatite and wollastonite. Physics and Chemistry of Minerals, 10, 217-229.
[10] Tribaudino, M., and Nestola, F. (2002) Average and local structure in *P*21/*c* clinopyroxenes along the join diopside-enstatite ($CaMgSi_2O_6$-$Mg_2Si_2O_6$). European Journal of Mineralogy 14, 549-555.
[11] Tribaudino, M., Nestola, F., Camara, F., Domeneghetti, M.C. (2002) The high-temperature P21/c-C2/c phase transition in Fe-free pyroxene (Ca0.15Mg1.85Si2O6): Structural and thermodynamic behavior. American Mineralogist, 87, 648-657.
[12] Tribaudino, M., Nestola, F., and Meneghini, C. (2005) Rietveld refinement of clinopyroxene with intermediate Ca-content along the join diopside-enstatite. The Canadian Mineralogist, 43, 1411-1421.
[13] Turnock, A.C., Lindsley, D.H., and Grover, J.E. (1973) Synthesis and unit cell parameters of Ca-Mg-Fe pyroxenes. American Mineralogist, 58, 50.

This is a preprint, the final version is subject to change, of the American Mineralogist (MSA)
Cite as Authors (Year) Title. American Mineralogist, in press.
DOI: http://dx.doi.org/10.2138/am-2018-6123

861 Table A1e. Orthopyroxene regression data

Orthopyroxene-phase					
Chemical composition	*a* (Å)	*b* (Å)	*c* (Å)	*V* (Å^3)	Reference
$Fe_2Si_2O_6$	0	2	0	18.417	[1]
$Fe_2Si_2O_6$	0	2	0	18.418	[2]
$Fe_2Si_2O_6$	0	2	0	18.431	[3]
$Mg_{0.20}Fe_{1.80}Si_2O_6$	0	1.8	0.2	18.402	[3]
$Mg_{0.40}Fe_{1.60}Si_2O_6$	0	1.6	0.4	18.37	[3]
$Mg_{0.50}Fe_{1.50}Si_2O_6$	0	1.5	0.5	18.362	[3]
$Mg_{0.80}Fe_{1.20}Si_2O_6$	0	1.2	0.8	18.321	[3]
$Mg_{1.00}Fe_{1.00}Si_2O_6$	0	1	1	18.31	[3]
$Mg_{1.18}Fe_{0.82}Si_2O_6$	0	0.82	1.18	18.2974	[1]
$Mg_{1.20}Fe_{0.80}Si_2O_6$	0	0.8	1.2	18.289	[3]
$Mg_{1.51}Fe_{0.48}Si_2O_6$	0	0.48	1.52	18.2747	[4]
$Mg_{1.60}Fe_{0.60}Si_2O_6$	0	0.4	1.6	18.251	[3]
$Mg_{1.68}Fe_{0.30}Si_2O_6$	0	0.3	1.68	18.2566	[5]
$Mg_{1.68}Fe_{0.30}Si_2O_6$	0	0.3	1.68	18.2462	[5]
$Mg_{1.72}Fe_{0.28}Si_2O_6$	0	0.28	1.72	18.2539	[5]
$Mg_{1.80}Fe_{0.20}Si_2O_6$	0	0.2	1.8	18.24	[5]
$Mg_{1.80}Fe_{0.20}Si_2O_6$	0	0.2	1.8	18.2496	[5]
$Mg_{1.80}Fe_{0.20}Si_2O_6$	0	0.2	1.8	18.235	[3]
$Mg_2Si_2O_6$	0	0	2	18.21	[6]
$Mg_2Si_2O_6$	0	0	2	18.216	[7]
$Mg_2Si_2O_6$	0	0	2	18.225	[8]
$Mg_2Si_2O_6$	0	0	2	18.233	[9]
$Mg_2Si_2O_6$	0	0	2	18.225	[10]
$Mg_2Si_2O_6$	0	0	2	18.223	[10]
$Mg_2Si_2O_6$	0	0	2	18.223	[3]
$Mg_{1.98}Ca_{0.02}Si_2O_6$	0.02	0	1.98	18.235	[3]
$Mg_{1.331}Fe_{0.636}Ca_{0.032}Si_2O_6$	0.032	1.331	0.636	18.337	[11]
$Fe_{1.96}Ca_{0.04}Si_2O_6$	0.04	1.96	0	18.453	[3]
$Mg_{0.25}Fe_{1.71}Ca_{0.04}Si_2O_6$	0.04	1.71	0.25	18.405	[12]
$Mg_{1.96}Ca_{0.04}Si_2O_6$	0.04	0	1.96	18.262	[13]
$Mg_{1.15}Fe_{0.807}Ca_{0.043}Si_2O_6$	0.043	0.807	1.15	18.316	[14]
$Mg_{1.155}Fe_{0.802}Ca_{0.043}Si_2O_6$	0.043	0.802	1.155	18.32	[14]
$Mg_{1.948}Ca_{0.052}Si_2O_6$	0.052	0	1.948	18.28	[15]
$Mg_{1.93}Ca_{0.07}Si_2O_6$	0.07	0	1.93	18.2588	[16]
$Mg_{1.93}Ca_{0.07}Si_2O_6$	0.07	0	1.93	18.268	[13]
$Fe_{1.92}Ca_{0.08}Si_2O_6$	0.08	1.92	0	18.473	[3]
$Mg_{0.96}Fe_{0.96}Ca_{0.08}Si_2O_6$	0.08	0.96	0.96	18.35	[3]
$Mg_{0.48}Fe_{1.43}Ca_{0.10}Si_2O_6$	0.1	1.43	0.48	18.417	[3]
$Mg_{0.76}Fe_{1.14}Ca_{0.10}Si_2O_6$	0.1	1.14	0.76	18.365	[3]
$Mg_{1.33}Fe_{0.57}Ca_{0.10}Si_2O_6$	0.1	0.57	1.33	18.293	[3]
$Mg_{1.52}Fe_{0.38}Ca_{0.10}Si_2O_6$	0.1	0.38	1.52	18.257	[3]

862 [1] Hugh-Jones, D.A., Chopelas, A., and Angel, R.J. (1997) Tetrahedral compression in
863 (Mg,Fe)SiO3 orthopyroxenes. Physics and Chemistry of Minerals, 24, 301-310.
864 [2] Sueno, S., Cameron, M., and Prewitt, C.T. (1976) Orthoferrosilite: High-temperature
865 crystal chemistry. American Mineralogist, 61, 38-53.
866 [3] Turnock, A.C., Lindsley, D.H., and Grover, J.E. (1973) Synthesis and unit cell
867 parameters of Ca-Mg-Fe pyroxenes. American Mineralogist, 58, 50-59.
868 [4] Yang, H., and Ghose, S. (1995) A transitional structural state and anomalous Fe-Mg
869 order-disorder in Mg-rich orthopyroxene, (Mg0.75Fe0.25)2Si2O6. American
870 Mineralogist, 80, 9-20.
871 [5] RRUFF.info
872 [6] Morimoto, N., and Koto, K. (1969) The crystal structure of orthoenstatite. Zeitschrift
873 fur Kristallographie, 129, 65-83.
874 [7] Hawthorne, F.C., and Ito, J. (1977) Sythensis and crystal-structure refinement of
875 transition-metal orthopyroxenes I: orthoenstatite and (Mg, Mn, Co) orthopyroxene. The
876 Canadian Mineralogist, 15, 321-338.
877 [8] Ohashi, Y. (1984) Polysynthetically-twinned structures of enstatite and wollastonite.
878 Physics and Chemistry of Minerals, 10, 217-229.
879 [9] Hugh-Jones, D.A., and Angel, R.J. (1994) A compressional study of MgSiO,
880 orthoenstatite up to 8.5 GPa. American Mineralogist, 79, 405-410.
881 [10] Huebner, S.J. (1986) Nature of phases synthesized along the join (Mg,Mn)2Si2O6.
882 American Mineralogist, 15, 365-371.
883 [11] Smyth, J.R. (1973) An Orthopyroxene Structure Up to 850°C
884 [12] Burnham, C.W., Ohashi, Y., Hafner, S.S., and Virgo, D. (1971) Cation distribution
885 and atomic thermal vibrations in an iron-rich orthopyroxene. American Mineralogist, 56,
886 850-876.
887 [13] Nestola, F., and Tribaudino, M. (2003) The structure of Pbca orthopyroxenes along
888 the join diopside-enstatite (CaMgSi2O6-Mg2Si2O6). European Journal of Mineralogy,
889 15, 365-371.
890 [14] Domeneghetti, M.C., Molin, G.M., Stimpfl, M., and Tribaudino, M. (1995)
891 Orthopyroxene from the Serra de Mag6 meteorite: Structure refinement and estimation
892 of C2/c pyroxene contributions to apparent Pbca diffraction violations. American
893 Mineralogist, 80, 923-929.
894 [15] Carlson, W.D., Swinnea, J.S., and Miser, D.E. (1988) Stability of orthoenstatite at
895 high temperature and low pressure. American Mineralogist, 73, 1255-1263.
896 [16] Nestola, F., Gatta, G.D., and Ballaran, T.B. (2006) The effect of Ca substitution on
897 the elastic and structural behavior of orthoenstatite. American Mineralogist, 91, 809-
898 815.

This is a preprint, the final version is subject to change, of the American Mineralogist (MSA)
Cite as Authors (Year) Title. American Mineralogist, in press.
DOI: http://dx.doi.org/10.2138/am-2018-6123

899 Table A1f. Olivine regression data

	Olivine-phase (Fe-Mg only)				
Chemical composition	*a* (Å)	*b* (Å)	*c* (Å)	*V* (Å^3)	Reference
Mg_2SiO_4	4.7534	10.1902	5.9783	289.577	[9]
Mg_2SiO_4	4.753	10.191	5.982	289.755	[7]
Mg_2SiO_4	4.753	10.196	5.979	289.76	[6]
Mg_2SiO_4	4.754	10.1971	5.9806	289.92	[21]
Mg_2SiO_4	4.7549	10.1985	5.9792	289.948	[4]
Mg_2SiO_4	4.755	10.196	5.9809	289.97	[24]
Mg_2SiO_4	4.7534	10.1989	5.9813	289.97	[13]
Mg_2SiO_4	4.751	10.203	5.983	290.023	[23]
Mg_2SiO_4	4.7558	10.1965	5.9817	290.068	[20]
Mg_2SiO_4	4.7545	10.2	5.9814	290.08	[14]
Mg_2SiO_4	4.7553	10.1977	5.982	290.09	[15]
Mg_2SiO_4	4.757	10.197	5.982	290.17	[24]
Mg_2SiO_4	4.75534	10.20141	5.98348	290.266	[25]
Mg_2SiO_4	4.756	10.207	5.98	290.296	[22]
Mg_2SiO_4	4.7533	10.2063	5.9841	290.31	[5]
Mg_2SiO_4	4.7536	10.2066	5.9845	290.36	[18]
$Mg_{1.997}Si_{0.995}O_4$	4.7552	10.1985	5.9822	290.112	[12]
$Mg_{1.98}Fe_{0.02}SiO_4$	4.7555	10.1999	5.9816	290.14	[21]
$Mg_{1.96}Fe_{0.04}SiO_4$	4.7563	10.2026	5.9842	290.39	[21]
$Mg_{1.94}Fe_{0.06}SiO_4$	4.7571	10.2053	5.9831	290.47	[21]
$Mg_{1.92}Fe_{0.08}SiO_4$	4.7578	10.2085	5.9857	290.72	[21]
$Mg_{1.91}Fe_{0.09}SiO_4$	4.7584	10.2099	5.9863	290.83	[21]
$Mg_{1.9}Fe_{0.1}SiO_4$	4.758	10.2115	5.9865	290.86	[21]
$Mg_{1.88}Fe_{0.12}SiO_4$	4.759	10.2145	5.988	291.08	[21]
$Mg_{1.84}Fe_{0.16}SiO_4$	4.7579	10.2151	5.989	291.08	[17]
$Mg_{1.82}Fe_{0.18}SiO_4$	4.7611	10.2207	5.99	291.49	[1]
$Mg_{1.82}Fe_{0.18}Si_1O_4$	4.7615	10.2248	5.9932	291.781	[20]
$Fe_{0.19}Mg_{1.81}SiO_4$	4.7641	10.2269	5.9952	292.098	[16]
$Mg_{1.8}Fe_{0.2}SiO_4$	4.762	10.225	5.994	291.857	[3]
$Mg_{1.77}Fe_{0.23}SiO_4$	4.7645	10.23467	5.99727	292.45	[11]
$Mg_{1.73}Fe_{0.27}SiO_4$	4.7655	10.2351	5.997	292.5	[21]
$Mg_{1.67}Fe_{0.33}SiO_4$	4.7673	10.2488	6.003	293.301	[20]
$Mg_{1.63}Fe_{0.37}SiO_4$	4.7687	10.2491	6.0023	293.36	[21]
$Mg_{1.6}Fe_{0.4}SiO_4$	4.7698	10.2531	6.003	293.58	[21]
$Mg_{1.6}Fe_{0.4}SiO_4$	4.769	10.261	6.006	293.9	[6]
$Mg_{1.55}Fe_{0.45}SiO_4$	4.7733	10.2676	6.0112	294.611	[10]
$Mg_{1.4}Fe_{0.6}SiO_4$	4.7779	10.2831	6.0161	295.58	[21]
$Mg_{1.3}Fe_{0.7}SiO_4$	4.7818	10.2972	6.0223	296.53	[21]
$Mg_{1.2}Fe_{0.8}SiO_4$	4.784	10.308	6.024	297.09	[6]
$Mg_{1.2}Fe_{0.8}SiO_4$	4.7849	10.3101	6.0263	297.29	[21]
$Mg_{1.15}Fe_{0.85}SiO_4$	4.7871	10.3181	6.0297	297.83	[21]
$Mg_{1.05}Fe_{0.95}SiO_4$	4.786	10.332	6.032	298.2	[19]
$Mg_{1.02}Fe_{0.98}SiO_4$	4.7901	10.3305	6.0343	298.6	[1]

$Fe_{1.0}Mg_{1.0}SiO_4$	4.7929	10.3412	6.038	299.27	[21]
$Fe_{1.18}Mg_{0.82}SiO_4$	4.7974	10.3635	6.0463	300.61	[21]
$Fe_{1.2}Mg_{0.8}SiO_4$	4.797	10.358	6.048	300.5	[6]
$Fe_{1.2}Mg_{0.8}SiO_4$	4.798	10.367	6.047	300.8	[6]
$Fe_{1.2}Mg_{0.8}SiO_4$	4.7986	10.3665	6.0482	300.87	[21]
$Fe_{1.4}Mg_{0.6}SiO_4$	4.8043	10.3923	6.0577	302.45	[21]
$Fe_{1.5}Mg_{0.5}SiO_4$	4.8074	10.4063	6.0618	303.25	[21]
$Fe_{1.6}Mg_{0.4}SiO_4$	4.81	10.419	6.068	304.08	[6]
$Fe_{1.6}Mg_{0.4}SiO_4$	4.813	10.417	6.067	304.18	[6]
$Fe_{1.6}Mg_{0.4}SiO_4$	4.8111	10.4213	6.0684	304.26	[21]
$Fe_{1.8}Mg_{0.2}SiO_4$	4.8169	10.4512	6.0783	306	[21]
Fe_2SiO_4	4.819	10.47	6.086	307.1	[6]
Fe_2SiO_4	4.815	10.49	6.085	307.3	[6]
Fe_2SiO_4	4.8195	10.4788	6.0873	307.42	[8]
Fe_2SiO_4	4.8195	10.4788	6.0873	307.424	[9]
Fe_2SiO_4	4.8211	10.4779	6.0889	307.58	[21]
Fe_2SiO_4	4.821	10.478	6.092	307.7	[2]

[1] Akamatsu, T., Kumazawa, M., Aikawa, N., and Takei, H. (1993) Pressure Effect on the Divalent Cation Distribution in Nonideal Solid Solution of Forsterite and Fayalite. Physics and Chemistry of Minerals, 19, 431-444.
[2] Annersten, H., Ericsson, T., and Filippidis, A. (1982) Cation ordering in Ni-Fe olivines. American Mineralogist, 67, 1212-1217.
[3] Birle, J.D., Gibbs, G.V., Moore, P.B., and Smith, J.V. (1968) Crystal structures of natural olivines. American Mineralogist, 53, 807-824.
[4] Bostrom, D. (1987) Single-crystal X-ray diffraction studies of synthetic Ni-Mg olivine solid solutions. American Mineralogist, 72, 965-972.
[5] Cernik, R.J., Murray, P.K., Pattison, P., and Fitch, A.N. (1990) A two-circle powder diffractometer for synchrotron radiation with a closed loop encoder feedback system. Journal of Applied Crystallography, 23, 292-296.
[6] Fisher G W, Medaris L G (1969) Cell dimensions and X-ray determinative curve for synthetic Mg-Fe olivines. American Mineralogist, 54, 741-753.
[7] Frances, C.A. (1985) New data on the forsterite-tephroite series. American Mineralogist, 70, 568-575.
[8] Fujino, K., Sasaki, S., Takeuchi, Y., and Sadanaga, R. (1981) X-ray determination of electron distributions in forsterite, fayalite and tephroite. Acta Crystallographica B, 37, 513-518.
[9] Fujino, K., Sasaki, S., Takeuchi, Y., and Sadanaga, R. (1981) X-ray determination of electron distributions in forsterite, fayalite and tephroite. Acta Crystallographica, B37, 513-518.
[10] Heinemann, R., Kroll, H., Kirfel, A., and Barbier, B. (2007) Order and anti-order in olivine III: variation of the cation distribution in the Fe,Mg olivine solid solution series with temperature and composition. European Journal of Mineralogy, 19, 15-27.
[11] Heuer, M. (2001) The determination of site occupancies using a new strategy in Rietveld refinements. Journal of applied crystallography, 34, 271-279.

[12] Hushur, A., Manghnani, M.H., Smyth, J.R., Nestola F., and Frost, D.J. (2009) Crystal chemistry of hydrous forsterite and its vibrational properties up to 41 GPa. American Mineralogist, 94, 751-760.
[13] Lager, G.A., Ross, F.K., Rotella, F.J., and Jorgensen, J.D. (1981) Neutron powder diffraction of Forsterite, Mg2SiO4: a comparison with single-crystal investigations. Journal of applied crystallography, 14, 137-139.
[14] Louisnathan, S.J., and Smith, J.V. (1968) Cell dimensions of olivine. Mineralogical Magazine, 36, 1123-1134.
[15] Matsui, Y., and Syono, Y. (1968) Unit cell dimensions of some synthetic olivine group solid solutions. Geochemical Journal, 2, 51-59.
[16] McCormick, T.C., Smyth, J.R., and Lofgren, G.E. (1987) Site occupancies of minor elements in synthetic olivines as determined by channeling-enhanced X-ray emission. Physics and Chemistry of Minerals, 14, 368-372.
[17] Merli, M., Oberti, R., Caucia, F., and Ungaretti, L. (2001) Determination of site population in olivine: Warnings on X-ray data treatment and refinement. American Mineralogist, 86, 55-65.
[18] Müller-Sommer, M., Hock, R., and Kirfel, A. (1997) Rietveld refinement study of the cation distribution in (Co, Mg)-olivine solid solution. Physics and Chemistry of Minerals, 24, 17-23.
[19] Nord, A.G., Annersten, H., and Filippidis, A. (1982) The cation distribution in synthetic Mg-Fe-Ni olivines. American Mineralogist, 67, 1206-1211.
[20] RRUFF.info
[21] Schwab, R.G., and Kustner, D. (1977) Precise determination of lattice constants to establish X-ray determinative curves for synthetic olivines of the solid solution series forsterite-fayalite. Neues Jahrbuch für Mineralogie, Monatshefte, 5, 205-215.
[22] Smyth, J.R., and Hazen, R.M. (1973) The crystal structures of forsterite and hortonolite at several temperatures up to 900 C. American Mineralogist, 58, 588-593.
[23] Urusov, V.S., Lapina, I.V., Kabala, Yu.K., and Kravchuk, I.F. (1984) Isomorphism in the forsterite-tephrolite series. Geokhimiya, 7, 1047-1055.
[24] van der Wal, R.J., Vos, A., and Kirfel, A. (1987) Conflicting results for the deformation properties of Forsterite, Mg2SiO4. Acta Crystallographica B, 43, 132-143.
[25] Yamazaki, S., and Toraya, H. (1999) Rietveld refinement of site-occupancy parameters of Mg2-xMnxSiO4 using a new weight function in least-squares fitting. Journal of Applied Crystallography, 32, 51-59.

This is a preprint, the final version is subject to change, of the American Mineralogist (MSA)
Cite as Authors (Year) Title. American Mineralogist, in press.
DOI: http://dx.doi.org/10.2138/am-2018-6123

973

974 Table A1g. Olivine with Mn and Ca

Olivine phase (with Ca and/or Mn)									
Ca	Fe	Mg	Mn	*a* (Å)	*b* (Å)	*a/b*	*c* (Å)	*V* (Å^3)	ref
0.01	0.35	1.64	0	4.771	10.274	0.464	6.011	294.643	[19]
0.01	0.61	1.38	0	4.785	10.298	0.465	6.028	297.035	[19]
0.045	0	1.955	0	4.7575	10.2144	0.466	5.99	291.08	[20]
0.045	0	1.955	0	4.7581	10.223	0.465	5.9929	291.51	[20]
0.045	0	1.955	0	4.7585	10.2248	0.465	5.9933	291.61	[20]
0.091	0	1.909	0	4.7596	10.2463	0.465	6.0027	292.74	[20]
0.091	0	1.909	0	4.7606	10.2499	0.464	6.0023	292.89	[20]
0.137	0	1.863	0	4.7664	10.2926	0.463	6.023	295.48	[20]
0.18	0	1.82	0	4.7694	10.318	0.462	6.0353	297	[20]
0.492	1.508	0	0	4.854	10.83	0.448	6.24	328.029	[21]
0.748	1.252	0	0	4.87	11.078	0.440	6.385	344.47	[21]
0.782	0	1.218	0	4.8139	10.9131	0.441	6.2921	330.56	[20]
0.836	0	1.164	0	4.8152	10.9599	0.439	6.3092	332.96	[20]
0.89	0	1.11	0	4.818	11.0074	0.438	6.3327	335.84	[20]
0.935	0	1.065	0	4.8202	11.0506	0.436	6.3519	338.34	[20]
0.945	0	1.055	0	4.8201	11.053	0.436	6.3552	338.59	[20]
0.99	0	1.01	0	4.8209	11.0911	0.435	6.3726	340.74	[20]
0.998	1.002	0	0	4.91	11.126	0.441	6.457	352.737	[21]
1	0	1	0	4.815	11.08	0.435	6.37	339.841	[22]
1	0	1	0	4.821	11.105	0.434	6.381	341.621	[23]
1	0.07	0.93	0	4.825	11.111	0.434	6.383	342.196	[24]
1	0.12	0.88	0	4.8281	11.1098	0.435	6.3894	342.722	[25]
1	0.69	0.31	0	4.875	11.164	0.437	6.447	350.875	[26]
1	0.77	0.22	0	4.877	11.166	0.437	6.448	351.136	[26]
1.104	0.896	0	0	4.922	11.202	0.439	6.489	357.779	[21]
1.217	0.783	0	0	4.906	11.206	0.438	6.485	356.523	[21]
2	0	0	0	5.07389	11.21128	0.453	6.7534	384.166	[27]
2	0	0	0	5.081	11.224	0.453	6.778	386.544	[28]
0	0.172	1.826	0.002	4.7605	10.2116	0.466	5.9894	290.68	[1]
0	0.19	1.808	0.002	4.7613	10.219	0.466	5.9921	291.55	[1]
0	0.216	1.782	0.002	4.7628	10.2227	0.466	5.9933	291.81	[1]
0.002	0.194	1.802	0.002	4.7599	10.2299	0.465	5.9933	291.85	[1]
0.002	0.226	1.77	0.002	4.7619	10.2248	0.466	5.9943	291.85	[1]
1.021	0.086	0.896	0.003	4.829	11.116	0.434	6.393	343.171	[2]
0	0.092	1.904	0.004	4.757	10.2067	0.466	5.987	290.68	[1]

This is a preprint, the final version is subject to change, of the American Mineralogist (MSA)
Cite as Authors (Year) Title. American Mineralogist, in press.
DOI: http://dx.doi.org/10.2138/am-2018-6123

0.01	0.23	1.756	0.004	4.7636	10.2376	0.465	5.9989	292.55	[1]
0	0.238	1.756	0.006	4.7631	10.2351	0.465	5.9975	292.38	[1]
0.002	0.25	1.742	0.006	4.7646	10.236	0.465	5.9983	292.54	[1]
0.002	0.482	1.51	0.006	4.7723	10.2643	0.465	6.0147	294.62	[1]
0.008	0.47	1.516	0.006	4.774	10.266	0.465	6.0133	294.71	[1]
0.01	0.378	1.606	0.006	4.7698	10.2558	0.465	6.007	293.85	[1]
0.004	0.914	1.07	0.012	4.7832	10.3227	0.463	6.0337	297.92	[1]
0.004	0.912	1.07	0.012	4.785	10.325	0.463	6.038	298.308	[3]
0.005	0.399	1.583	0.012	4.7696	10.255	0.465	6.0053	293.733	[4]
0.005	0.399	1.583	0.012	4.7687	10.2555	0.465	6.0066	293.755	[4]
0.005	0.399	1.583	0.012	4.7688	10.256	0.465	6.0065	293.771	[4]
0.005	0.399	1.584	0.012	4.7701	10.2556	0.465	6.006	293.815	[4]
0	0.956	1.03	0.014	4.786	10.3304	0.463	6.04	298.62	[1]
0.01	0.778	1.198	0.014	4.7839	10.3133	0.464	6.0295	297.49	[1]
0.012	0.756	1.218	0.014	4.7787	10.3168	0.463	6.0315	297.36	[1]
0.012	0.928	1.046	0.014	4.7849	10.3275	0.463	6.0391	298.43	[1]
0.002	1.434	0.544	0.02	4.8002	10.4028	0.461	6.0748	303.36	[1]
0.02	0.98	0.98	0.02	4.787	10.341	0.463	6.044	299.192	[3]
0.004	1.704	0.266	0.026	4.8099	10.442	0.461	6.0892	305.83	[1]
0.012	1.96	0	0.028	4.8176	10.482	0.460	6.0995	308.01	[1]
0.006	0.825	1.139	0.03	4.7871	10.3325	0.463	6.0347	298.493	[4]
0.006	0.825	1.139	0.03	4.7891	10.3321	0.464	6.0346	298.601	[4]
0.006	0.825	1.139	0.03	4.7911	10.3316	0.464	6.035	298.731	[4]
0.01	1.778	0.182	0.03	4.8122	10.4524	0.460	6.0945	305.55	[1]
0.99	0.12	0.85	0.03	4.8295	11.1083	0.435	6.3872	342.658	[2]
0	1.134	0.824	0.042	4.7912	10.3642	0.462	6.055	300.67	[1]
0.004	1.936	0	0.06	4.8177	10.4789	0.460	6.1046	308.19	[1]
0.004	1.844	0.078	0.074	4.816	10.469	0.460	6.099	307.504	[3]
0.001	0.002	1.918	0.079	4.757	10.219	0.466	5.993	291.3	[5]
0	0	1.9	0.1	4.753	10.231	0.465	5.999	291.719	[6]
0	1.89	0	0.11	4.8233	10.4959	0.460	6.0966	308.64	[2]
0.002	1.806	0.074	0.118	4.8161	10.4689	0.460	6.0974	307.43	[1]
0	1.87	0	0.13	4.8245	10.4959	0.460	6.0974	308.757	[2]
0	1.1	0.75	0.15	4.798	10.387	0.462	6.055	301.762	[7]
0	1.1	0.75	0.15	4.798	10.39	0.462	6.055	301.849	[8]
0.001	0.004	1.832	0.163	4.761	10.254	0.464	6.007	293.3	[5]
0.001	0.003	1.832	0.164	4.76	10.244	0.465	6.006	292.8	[5]
0	0	1.8	0.2	4.761	10.258	0.464	6.013	293.665	[6]
0	1.78	0	0.22	4.826	10.514	0.459	6.105	309.8	[9]

0	0	1.6	0.4	4.773	10.317	0.463	6.043	297.576	[6]
0.001	0	1.548	0.451	4.775	10.344	0.462	6.049	298.8	[5]
0.003	0.001	1.543	0.453	4.773	10.351	0.461	6.055	299.1	[5]
0	1.52	0	0.48	4.8378	10.536	0.459	6.1234	312.116	[10]
0.001	1.319	0.052	0.545	4.831	10.558	0.458	6.137	313.075	[11]
0.001	1.297	0.057	0.567	4.844	10.552	0.459	6.135	313.563	[11]
0.002	1.225	0.089	0.596	4.828	10.549	0.458	6.109	311.135	[11]
0	0	1.4	0.6	4.781	10.356	0.462	6.067	300.39	[6]
0	1.4	0	0.6	4.84857	10.55545	0.459	6.14054	314.266	[12]
0	1.38	0	0.62	4.84	10.556	0.459	6.135	313.5	[9]
0.004	0.002	1.368	0.626	4.778	10.398	0.460	6.078	302	[5]
0.003	0.002	1.356	0.64	4.782	10.406	0.460	6.083	302.7	[5]
0.001	1.112	0.078	0.728	4.842	10.552	0.459	6.136	313.558	[11]
0	0	1.2	0.8	4.798	10.416	0.461	6.102	304.953	[6]
0	1.1	0	0.9	4.852	10.576	0.459	6.142	315.1	[9]
0.006	0.002	1.028	0.964	4.799	10.499	0.457	6.127	308.7	[5]
0	0	1.03	0.97	4.794	10.491	0.457	6.123	307.949	[13]
0	1.01	0	0.99	4.8578	10.5818	0.459	6.1641	316.861	[10]
0	0	1	1	4.80757	10.451	0.460	6.12446	307.717	[14]
0	0	1	1	4.80757	10.451	0.460	6.12446	307.717	[14]
0	0	1	1	4.797	10.48	0.458	6.135	308.422	[6]
0	0	1	1	4.797	10.48	0.458	6.135	308.422	[6]
0	1	0	1	4.86184	10.58358	0.459	6.1695	317.456	[12]
0	1	0	1	4.86184	10.58358	0.459	6.1695	317.456	[12]
0	0.94	0	1.06	4.856	10.585	0.459	6.168	317	[9]
0	0	0.8	1.2	4.813	10.506	0.458	6.16	311.483	[6]
0	0	0.6	1.4	4.83927	10.52411	0.460	6.17903	314.692	[14]
0	0.6	0	1.4	4.871	10.594	0.460	6.2	319.9	[9]
0	0.6	0	1.4	4.8789	10.60587	0.460	6.20468	321.061	[12]
0	0.584	0	1.416	4.8734	10.5991	0.460	6.1982	320.16	[10]
0	0	0.2	1.8	4.862	10.553	0.461	6.208	318.524	[6]
0	0.18	0	1.82	4.896	10.603	0.462	6.241	324	[9]
0	0	0.17	1.83	4.879	10.589	0.461	6.234	322.072	[13]
0	0	0.015	1.993	4.893	10.592	0.462	6.243	323.55	[15]
0	0	0	2	4.8968	10.59	0.462	6.25	324.1	[16]
0	0	0	2	4.894	10.61	0.461	6.259	325.001	[6]
0	0	0	2	4.9023	10.5964	0.463	6.2567	325.015	[17]
0	0	0	2	4.9042	10.597	0.463	6.2545	325.045	[18]
0	0	0	2	4.906	10.598	0.463	6.255	325.2	[5]

0	0	0	2	4.90338	10.60016	0.463	6.25753	325.245	[14]
0	0	0	2	4.90338	10.60016	0.463	6.25753	325.246	[14]

[1] Louisnathan, S.J., and Smith, J.V. (1968) Cell dimensions of olivine. Mineralogical Magazine, 36, 1123-1134.
[2] RRUFF.info
[3] Birle, J.D., Gibbs, G.V., Moore, P.B., and Smith, J.V. (1968) Crystal structures of natural olivines. American Mineralogist, 53, 807-824.
[4] Ottonello, G., Princivalle, F., and Della Giusta, A., 1990. Temperature, composition, and fO2 effects on intersite distribution of Mg and Fe2+ in olivines. Physics and Chemistry of Minerals, 17(4), 301-312.
[5] Frances, C.A. (1985) New data on the forsterite-tephroite series. American Mineralogist, 70, 568-575.
[6] Urusov, V.S., Lapina, I.V., Kabala, Yu.K., and Kravchuk, I.F. (1984) Isomorphism in the forsterite-tephrolite series. Geokhimiya, 7, 1047-1055.
[7] Smyth, J.R., and Hazen, R.M. (1973) The crystal structures of forsterite and hortonolite at several temperatures up to 900 C. American Mineralogist, 58, 588-593.
[8] Hazen, R.M., 1977. Effects of temperature and pressure on the crystal structure of ferromagnesian olivine. American Mineralogist, 62(3-4), 286-295.
[9] Annersten, H., Adetunji, J., and Filippidis, A., 1984. Cation ordering in Fe-Mn silicate olivines. American Mineralogist, 69(11-12), 1110-1115.
[10] Ballet, O., Fuess, H., and Fritzsche, T., 1987. Magnetic structure and cation distribution in (Fe, Mn) 2 SiO 4 (olivine) by neutron diffraction. Physics and chemistry of minerals, 15(1), 54-58.
[11] Mossman, D.J., and Pawson, D.J., 1976. X-ray and optical characterization of the forsterite-fayalite-tephroite series with comments on knebelite from Bluebell Mine, British Columbia. The Canadian Mineralogist, 14(4), 479-486.
[12] Redfern, S.A., Knight, K.S., Henderson, C.M.B., and Wood, B.J., 1998. Fe-Mn cation ordering in fayalite-tephroite (FexMn1− x) 2SiO4 olivines: a neutron diffraction study. Mineralogical Magazine, 62(5), 607-615.
[13] Francis, C.A., and Ribbe, P.H., 1980. The forsterite-tephroite series: I. Crystal structure refinements. American Mineralogist, 65(11-12), 1263-1269.
[14] Matsui, Y., and Syono, Y. (1968) Unit cell dimensions of some synthetic olivine group solid solutions. Geochemical Journal, 2, 51-59.
[15] Lucchetti, G., 1991. Tephroite from the Val Graveglia metacherts (Liguria, Italy): mineral data and reactions for Mn-silicates and Mn-Ca-carbonates. European Journal of Mineralogy, 63-68.
[16] Sharp, Z.D., Hazen, R.M., and Finger, L.W., 1987. High-pressure crystal chemistry of monticellite, CaMgSiO 4. American Mineralogist, 72(7-8), 748-755.
[17] Fujino, K., Sasaki, S., Takeuchi, Y., and Sadanaga, R. (1981) X-ray determination of electron distributions in forsterite, fayalite and tephroite. Acta Crystallographica B, 37, 513-518.
[18] Takei, H., 1976. Czochralski growth of Mn2SiO4 (tephroite) single crystal and its properties. Journal of Crystal Growth, 34(1), 125-131.

[19] Brown, G.E., and Prewitt, C.T., 1973. High-temperature crystal chemistry of hortonolite. Am. Mineral, 58, 577-587.
[20] WeRNrnl, R.D., and Lurn, W.C., 1973. Two-Phase Data for the Join Monticellite (GaMgSiO.)-Forsterite (MgSiO,): Experimental Results and Numerical Analysis. American Mineralogist, 58, 998-1008.
[21] Wyderko, M., and Mazanek, E., 1968. The mineralogical characteristics of calcium-iron olivines. Mineral. Mag, 36, 955-961.
[22] Brown, G.B., and West, J., 1928. X. The structure of monticellite (MgCaSiO4). Zeitschrift für Kristallographie-Crystalline Materials, 66(1-6), 154-161.
[23] Bradley, R.S., Engel, P., and Munro, D.C., 1966. Subsolidus Solubility Between R2·· SiO4 and LiR·· PO 4: A Hydrothermal Investigation. Min. Mag, 35, 742-755.
[24] Lncnn, G.A., and eNo, E.P., 1978. High-temperature structural study of six olivines. American Mineralogist, 63, 365-377.
[25] Pilati, T., Demartin, F., and Gramaccioli, C.M., 1995. Thermal parameters for minerals of the olivine group: their implication on vibrational spectra, thermodynamic functions and transferable force fields. Acta Crystallographica Section B: Structural Science, 51(5), 721-733.
[26] Folco, L., and Mellini, M., 1997. Crystal chemistry of meteoritic kirschsteinite. European Journal of Mineralogy, 9(5), 969-973.
[27] Gobechiya, E.R., Yamnova, N.A., Zadov, A.E., and Gazeev, V.M. (2008. Calcio-olivine γ-Ca 2 SiO 4: I. Rietveld refinement of the crystal structure. Crystallography Reports, 53(3), 404-408.
[28] Udagawa, S., Urabe, K., Natsume, M., and Yano, T., 1980. Refinement of the crystal structure of γ-Ca2SiO4. Cement and Concrete Research, 10(2), 139-144.

This is a preprint, the final version is subject to change, of the American Mineralogist (MSA)
Cite as Authors (Year) Title. American Mineralogist, in press.
DOI: http://dx.doi.org/10.2138/am-2018-6123

1042 Table A1h. Spinel regression data

Mineral	Spinel-phase Chemical composition	*a* (Å)	*V* (Å^3)	Reference
	Fe + □			
Maghemite	$Fe_{2.667}O_4$	8.33	578.01	[9]
Magnetite	$Fe^{2+}_{0.26}Fe^{3+}_{2.49}O_4$	8.3583	583.921	[10]
Magnetite	$Fe^{2+}_{0.52}Fe^{3+}_{2.32}O_4$	8.3799	588.459	[10]
Magnetite	$Fe^{2+}_{0.48}Fe^{3+}_{2.35}O_4$	8.3806	588.607	[10]
Magnetite	$Fe^{2+}_{0.50}Fe^{3+}_{2.33}O_4$	8.3833	589.176	[10]
Magnetite	$Fe^{2+}_{0.57}Fe^{3+}_{2.28}O_4$	8.3846	589.45	[10]
Magnetite	$Fe^{2+}_{0.56}Fe^{3+}_{2.29}O_4$	8.3852	589.577	[10]
Magnetite	Fe_3O_4	8.394	591.435	[15]
Magnetite	Fe_3O_4	8.3941	591.456	[3]
Magnetite	Fe_3O_4	8.395	591.646	[6]
Magnetite	Fe_3O_4	8.3958	591.815	[13]
Magnetite	Fe_3O_4	8.3967	592.006	[1]
Magnetite	Fe_3O_4	8.3969	592.048	[4]
Magnetite	Fe_3O_4	8.397	592.069	[8]
	Fe + Al			
Magnetite	Fe_3O_4	8.397	592.069	[8]
Hercynite	$(Al_{1.897}\ Fe_{1.103})\ O_4$	8.1646	544.258	[16]
Hercynite	$Fe\ Al_2\ O_4$	8.15579	542.498	[28]
	Fe + Al + □			
Magnetite	$Fe^{2+}_{0.70}Fe^{3+}_{2.15}Al_{0.05}O_4$	8.3887	590.315	[10]
Magnetite	$Fe^{2+}_{0.64}Fe^{3+}_{2.20}Al_{0.04}O_4$	8.3844	589.408	[10]
Magnetite	$Fe^{2+}_{0.77}Fe^{3+}_{2.07}Al_{0.08}O_4$	8.391	590.801	[10]
Magnetite	$Fe^{2+}_{0.61}Fe^{3+}_{2.21}Al_{0.05}O_4$	8.3824	588.986	[10]
Magnetite	$Fe^{2+}_{0.62}Fe^{3+}_{2.20}Al_{0.05}O_4$	8.387	589.956	[10]
Magnetite	$Fe^{2+}_{0.70}Fe^{3+}_{2.12}Al_{0.07}O_4$	8.3877	590.104	[10]
Magnetite	$Fe^{2+}_{0.65}Fe^{3+}_{2.16}Al_{0.08}O_4$	8.3833	589.176	[10]
Magnetite	$Fe^{2+}_{0.67}Fe^{3+}_{2.11}Al_{0.11}O_4$	8.3795	588.375	[10]
Magnetite	$Fe^{2+}_{0.68}Fe^{3+}_{2.09}Al_{0.12}O_4$	8.3842	589.366	[10]
Magnetite	$Fe^{2+}_{0.47}Fe^{3+}_{2.29}Al_{0.07}O_4$	8.3742	587.259	[10]
Magnetite	$Fe^{2+}_{0.70}Fe^{3+}_{2.05}Al_{0.15}O_4$	8.3904	590.674	[10]
Magnetite	$Fe^{2+}_{0.51}Fe^{3+}_{2.23}Al_{0.10}O_4$	8.3732	587.049	[10]
Magnetite	$Fe^{2+}_{0.64}Fe^{3+}_{2.08}Al_{0.16}O_4$	8.3776	587.975	[10]
Magnetite	$Fe^{2+}_{0.50}Fe^{3+}_{2.22}Al_{0.12}O_4$	8.3794	588.354	[10]
Magnetite	$Fe^{2+}_{0.18}Fe^{3+}_{2.51}Al_{0.03}O_4$	8.3628	584.864	[10]
Magnetite	$Fe^{2+}_{0.55}Fe^{3+}_{2.14}Al_{0.16}O_4$	8.3717	586.734	[10]
Magnetite	$Fe^{2+}_{0.62}Fe^{3+}_{2.07}Al_{0.19}O_4$	8.379	588.27	[10]
Magnetite	$Fe^{2+}_{0.19}Fe^{3+}_{2.48}Al_{0.05}O_4$	8.3612	584.529	[10]
Magnetite	$Fe^{2+}_{0.54}Fe^{3+}_{2.12}Al_{0.19}O_4$	8.3728	586.965	[10]
Magnetite	$Fe^{2+}_{0.44}Fe^{3+}_{2.19}Al_{0.18}O_4$	8.3581	583.879	[10]
Magnetite	$Fe^{2+}_{0.59}Fe^{3+}_{2.04}Al_{0.23}O_4$	8.3651	585.347	[10]
Magnetite	$Fe^{2+}_{0.19}Fe^{3+}_{2.42}Al_{0.12}O_4$	8.355	583.229	[10]
Magnetite	$Fe^{2+}_{0.43}Fe^{3+}_{2.17}Al_{0.21}O_4$	8.3562	583.481	[10]

This is a preprint, the final version is subject to change, of the American Mineralogist (MSA)
Cite as Authors (Year) Title. American Mineralogist, in press.
DOI: http://dx.doi.org/10.2138/am-2018-6123

Magnetite	$Fe^{2+}_{0.46}Fe^{3+}_{2.13}Al_{0.24}O_4$	8.3496	582.099	[10]
Magnetite	$Fe^{2+}_{0.48}Fe^{3+}_{2.10}Al_{0.25}O_4$	8.3546	583.146	[10]
Magnetite	$Fe^{2+}_{0.44}Fe^{3+}_{2.14}Al_{0.23}O_4$	8.3588	584.025	[10]
Magnetite	$Fe^{2+}_{0.24}Fe^{3+}_{2.33}Al_{0.18}O_4$	8.3471	581.576	[10]
Magnetite	$Fe^{2+}_{0.36}Fe^{3+}_{2.21}Al_{0.22}O_4$	8.3493	582.036	[10]
Magnetite	$Fe^{2+}_{0.46}Fe^{3+}_{2.10}Al_{0.26}O_4$	8.3481	581.786	[10]
Magnetite	$Fe^{2+}_{0.16}Fe^{3+}_{2.35}Al_{0.21}O_4$	8.3278	577.552	[10]
Magnetite	$Fe^{2+}_{0.31}Fe^{3+}_{2.20}Al_{0.26}O_4$	8.3406	580.219	[10]
Magnetite	$Fe^{2+}_{0.26}Fe^{3+}_{2.20}Al_{0.29}O_4$	8.3369	579.447	[10]
Magnetite	$Fe^{2+}_{0.08}Fe^{3+}_{2.35}Al_{0.27}O_4$	8.326	577.177	[10]
Magnetite	$Fe^{2+}_{0.29}Fe^{3+}_{2.12}Al_{0.36}O_4$	8.3395	579.989	[10]
Magnetite	$Fe^{2+}_{0.27}Fe^{3+}_{2.14}Al_{0.35}O_4$	8.3409	580.282	[10]
Magnetite	$Fe^{2+}_{0.10}Fe^{3+}_{2.23}Al_{0.37}O_4$	8.3174	575.391	[10]
	Fe + Ti			
Magnetite	$Fe_{2.904}Ti_{0.096}O_4$	8.4067	594.123	[1]
Magnetite	$Fe_{2.902}Ti_{0.098}O_4$	8.4095	594.717	[1]
Magnetite	$Fe_{2.814}Ti_{0.186}O_4$	8.4145	595.779	[1]
Magnetite	$Fe_{2.758}Ti_{0.242}O_4$	8.425	598.012	[1]
Magnetite	$Fe_{2.646}Ti_{0.354}O_4$	8.4348	600.101	[1]
Magnetite	$Fe_{2.538}Ti_{0.462}O_4$	8.4569	604.83	[1]
Ulvospinel	$Fe_{2.0}Ti_{1.0}O_4$	8.5297	620.585	[14]
Ulvospinel	$Fe_{2.169}Ti_{0.831}O_4$	8.5131	616.969	[14]
Ulvospinel	$Fe_{2.266}Ti_{0.734}O_4$	8.4969	613.453	[14]
Ulvospinel	$Fe_{2.376}Ti_{0.624}O_4$	8.4802	609.843	[14]
Ulvospinel	$Fe_{2.449}Ti_{0.551}O_4$	8.4632	606.183	[14]
Ulvospinel	$Fe_{2.356}Ti_{0.644}O_4$	8.4875	611.42	[1]
Ulvospinel	$Fe_{2.287}Ti_{0.713}O_4$	8.4972	613.518	[1]
Ulvospinel	$Fe_{2.31}Ti_{0.69}O_4$	8.4975	613.583	[1]
Ulvospinel	$Fe_{2.248}Ti_{0.752}O_4$	8.5052	615.253	[1]
Ulvospinel	$Fe_{2.247}Ti_{0.751}O_4$	8.5059	615.405	[1]
Ulvospinel	$Fe_{2.244}Ti_{0.756}O_4$	8.5079	615.839	[1]
Ulvospinel	$Fe_{2.2}Ti_{0.8}O_4$	8.5139	617.143	[1]
Ulvospinel	$Fe_{2.155}Ti_{0.845}O_4$	8.522	618.906	[1]
Ulvospinel	$Fe_{2.092}Ti_{0.908}O_4$	8.5274	620.083	[1]
Ulvospinel	$Fe_{2.07}Ti_{0.93}O_4$	8.5307	620.803	[1]
Ulvospinel	$Fe_{2.055}Ti_{0.945}O_4$	8.5322	621.131	[1]
Ulvospinel	$Fe_{2.134}Ti_{0.866}O_4$	8.5139	617.143	[5]
Ulvospinel	$Fe_{2.111}Ti_{0.889}O_4$	8.5139	617.143	[5]
Ulvospinel	$TiFe_2O_4$	8.5439	623.69	[11]
	Fe + Mg			
Magnetite	$Fe_3\ O_4$	8.397	592.069	[8]
Magnetite	$(Fe_{2.961}\ Mg_{.039})\ O_4$	8.3975	592.175	[4]
Magnesioferrite	$(Fe_2\ Mg)\ O_4$	8.39704	592.078	[26]
Magnesioferrite	$(Fe_2\ Mg)\ O_4$	8.39514	591.676	[26]
Magnesioferrite	$(Fe_2\ Mg)\ O_4$	8.36	584.277	[27]
	Fe + Cr			

This is a preprint, the final version is subject to change, of the American Mineralogist (MSA)
Cite as Authors (Year) Title. American Mineralogist, in press.
DOI: http://dx.doi.org/10.2138/am-2018-6123

Magnetite	$Fe_3 O_4$	8.397	592.069	[8]
Chromite	$Fe Cr_2 O_4$	8.3765	587.743	[7]
	Fe + Ni			
Magnetite	$Fe_3 O_4$	8.397	592.069	[8]
Magnetite	$(Fe^{2+}_{0.51}Ni_{0.48}Co_{0.01})Fe^{3+}_2O_4$	8.368	585.956	[23]
Trevorite	$Fe_{2.42} Ni_{.52} Cr_{.03} Al_{.01} Co_{.02} O_4$	8.3626	584.822	[24]
Trevorite	$(Ni_{0.963}Mn_{0.001}Mg_{0.002}Co_{0.013})(Fe^{3+}_{1.964}Si_{0.014}Cr_{0.012}Al_{0.010})O_4$	8.339	579.885	[25]
	Fe + Zn			
Magnetite	$Fe_3 O_4$	8.397	592.069	[8]
Franklinite	$Fe_{2.024} Zn_{.976} O_4$	8.4418	601.596	[20]
Franklinite	$Zn Fe_2 O_4$	8.4412	601.468	[21]
Franklinite	$(Zn_{1.08} Fe_{1.92}) O_4$	8.443	601.853	[22]
	Fe + V			
Magnetite	$Fe_3 O_4$	8.397	592.069	[8]
Coulsonite	$Fe V_2 O_4$	8.453	603.994	[19]
	Fe + Ti + Mg			
Ulvospinel	$Mg_{0.135}Fe_{1.929}Ti_{0.94}O_4$	8.5271	620.018	[2]
Ulvospinel	$Mg_{0.29}Fe_{1.768}Ti_{0.94}O_4$	8.5184	618.122	[2]
Ulvospinel	$Mg_{0.531}Fe_{1.511}Ti_{0.96}O_4$	8.5104	616.382	[2]
Ulvospinel	$Mg_{0.79}Fe_{1.228}Ti_{0.98}O_4$	8.5021	614.58	[2]
Ulvospinel	$Mg_{0.918}Fe_{1.106}Ti_{0.98}O_4$	8.4946	612.955	[2]
	Fe + Mg + Al			
Hercynite	$(Al_{1.926} Mg_{.177} Fe_{.897)} O_4$	8.1494	541.224	[16]
Hercynite	$(Al_{1.938} Mg_{.303} Fe_{.759}) O_4$	8.1406	539.472	[16]
Hercynite	$Al_{1.94} Fe_{.76} Mg_{.3} O_4$	8.1396	539.274	[17]
Hercynite	$Fe_{.924} Al_{1.948} Mg_{.116} O_4$	8.1511	541.563	[18]
Hercynite	$(Al_{1.962} Mg_{.544} Fe_{.494}) O_4$	8.1221	535.803	[16]
Hercynite	$Fe_{.878} Al_{1.964} Mg_{.138} O_4$	8.1584	543.019	[18]
Hercynite	$(Al_{1.964} Mg_{.419} Fe_{.617}) O_4$	8.1306	537.487	[16]
Hercynite	$Fe_{.84} Al_{1.966} Mg_{.19} O_4$	8.146	540.547	[18]
Hercynite	$(Al_{1.981} Mg_{.648} Fe_{.371}) O_4$	8.1134	534.083	[16]
Hercynite	$(Al_{1.982} Mg_{.726} Fe_{.292}) O_4$	8.1071	532.84	[16]
Hercynite	$(Al_{1.99} Mg_{.816} Fe_{.194}) O_4$	8.1006	531.559	[16]
Hercynite	$Al_{1.999} Mg_{.89} Fe_{.111} O_4$	8.0937	530.202	[16]
Hercynite	$Al_{1.999} Mg_{.955} Fe_{.046} O_4$	8.0895	529.377	[16]
	Mn + Ti + Fe			
Ulvospinel	$Ti(Fe_{0.804}Mn_{1.196})O_4$	8.6315	643.071	[11]

This is a preprint, the final version is subject to change, of the American Mineralogist (MSA)
Cite as Authors (Year) Title. American Mineralogist, in press.
DOI: http://dx.doi.org/10.2138/am-2018-6123

Ulvospinel	$Ti(Fe_{0.6}Mn_{1.4})O_4$	8.6429	645.622	[11]
Ulvospinel	$Ti(Fe_{0.378}Mn_{1.622})O_4$	8.6556	648.472	[11]
Ulvospinel	$Ti(Fe_{0.174}Mn_{1.826})O_4$	8.6651	650.61	[11]
Ulvospinel	$TiMn_2O_4$	8.6789	653.723	[11]
Ulvospinel	$Ti(Fe_{1.804}Mn_{0.196})O_4$	8.557	626.563	[11]
Ulvospinel	$Ti(Fe_{1.604}Mn_{0.396})O_4$	8.5688	629.158	[11]
Ulvospinel	$Ti(Fe_{1.424}Mn_{0.576})O_4$	8.5837	632.446	[11]
Ulvospinel	$Ti(Fe_{1.218}Mn_{0.782})O_4$	8.6004	636.145	[11]
Ulvospinel	$TiFe_2O_4$	8.5439	623.69	[11]
Ulvospinel	$Ti(Fe_{1.008}Mn_{0.992})O_4$	8.6112	638.544	[11]
	Fe + Cr + Mg			
Chromite	$(Fe_{0.6}Mg_{0.4})Cr_2O_4$	8.3577	583.795	[7]
Chromite	$(Fe_{0.65}Mg_{0.35})Cr_2O_4$	8.362	584.696	[7]
Chromite	$(Fe_{0.67}Mg_{0.33})Cr_2O_4$	8.3613	584.55	[7]
Chromite	$(Fe_{0.76}Mg_{0.24})Cr_2O_4$	8.3672	585.788	[7]
Chromite	$(Fe_{0.87}Mg_{0.13})Cr_2O_4$	8.371	586.586	[7]
Chromite	$(Fe_{0.91}Mg_{0.09})Cr_2O_4$	8.3739	587.196	[7]
Chromite	$FeCr_2O_4$	8.3765	587.743	[7]
Magnesiochromite	$MgCr_2O_4$	8.3327	578.572	[12}
Magnesiochromite	$Mg_{0.984}Fe_{0.024}Cr_{1.992}O_4$	8.334	578.843	[7]
Magnesiochromite	$Mg_{0.932}Fe_{0.072}Cr_{1.996}O_4$	8.3352	579.093	[7]
Magnesiochromite	$(Mg_{0.87}Fe_{0.13})Cr_2O_4$	8.3379	579.656	[7]
Magnesiochromite	$(Mg_{0.8}Fe_{0.2})Cr_2O_4$	8.3415	580.407	[7]
Magnesiochromite	$(Mg_{0.68}Fe_{0.32})Cr_2O_4$	8.3462	581.388	[7]
Magnesiochromite	$(Mg_{0.63}Fe_{0.37})Cr_2O_4$	8.3465	581.451	[7]
Magnesiochromite	$(Mg_{0.67}Fe_{0.33})Cr_2O_4$	8.349	581.974	[7]

[1] Bosi, F., Halenius, U., and Skogby, H. (2009) Crystal chemistry of the magnetite-ulvospinel series. American Mineralogist, 94, 181-189.
[2] Bosi, F., Halenius, U., and Skogby, H. (2014) Crystal chemistry of the ulvospinel-qandilite series. American Mineralogist, 99, 847-851.
[3] Fleet, M.E. (1981) The structure of magnetite, Acta Crystallographica, B37, 917-920.
[4] Fleet, M.E. (1984) The structure of magnetite: two annealed natural magnetites, Fe3.005O4 and Fe2.96Mg0.04O4, Acta Crystallographica, C40, 1491-1493.
[5] Gatta, G.D., Bosi, F., McIntyre, G.J., and Halenius, U. (2014) Static positional disorder in ulvospinel: A single-crystal neutron diffraction study. American Mineralogist, 99, 255-260.
[6] Gatta, G.D., Kantor, I., Ballaran, T.B., Dubrovinsky, L., and McCammon, C. (2007) Effect of non-hydrostatic conditions on the elastic behaviour of magnetite: an in situ single-crystal X-ray diffraction study. Physics and Chemistry of Minerals, 34, 627-635.
[7] Lenaz, D., Skogby, H., Princivalle, F., and Halenius, U. (2004) Structural changes and valence states in the MgCr2O4-FeCr2O4 solid solution series. Physics and Chemistry of Minerals, 31, 633-642.
[8] O'Neill, H.St.C., and Dollase, W.A. (1994) Crystal structures and cation distributions in simple spinels from powder XRD structural refinements: MgCr2O4, ZnCr2O4, Fe3O4 and the temperature dependence of the cation distribution in ZnAl2O4. Physics and Chemistry of Minerals, 20, 541-555.

[9] Pecharroman, C., Gonzalez-Carreno, T., and Iglesias, J.E. (1995) The infrared dielectric properties of maghemite, gamma-Fe2O3, from reflectance measurement on pressed powders. Physics and Chemistry of Minerals, 22, 21-29.
[10] Schwertmann, U., and Murad, E. (1990) The influence of aluminum on iron oxides: XIV. Al-substituted magnetite synthesized at ambient temperatures. Clay and Clay Minerals, 38, 196-202.
[11] Sedler, I.K., Feenstra, A., and Peters, T. (1994) An X-ray powder diffraction study of synthetic (Fe,Mn)2TiO4 spinel. European Journal of Mineralogy, 6, 873-885.
[12] Tabira, Y., and Withers, R.L. (1999) Cation ordering in NiAl2O4 spinel by a 111 systematic row CBED technique. Physics and Chemistry of Minerals, 27, 112-118.
[13] Wechsler B A, Lindsley D H, Prewitt C T (1984) Crystal structure and cation distribution in titanomagnetites (Fe3-xTixO4). American Mineralogist, 69, 754-770.
[14] Yamanaka, T., Kyono, A., Nakamoto, Y., Meng, Y., Kharlamova, S., Struzhkin, V.V., and Mao, H. (2013) High-pressure phase transitions of Fe3-xTixO4 solid solution up to 60 GPa correlated with electronic spin transition. American Mineralogist, 98, 736-744.
[15] Yamanaka, T., Shimazu, H., and Ota, K. (2001) Electric conductivity of Fe2SiO4-Fe3O4 spinel solid solutions. Physics and Chemistry of Minerals, 28, 110-118.
[16] Andreozzi, G B, and Lucchesi, S. (2002) Intersite distribution of Fe2+ and Mg in the spinel (sensu stricto)-hercynite series by single-crystal X-ray diffraction, American Mineralogist, 87, 1113-1120
[17] Lavina B, Princivalle F, Della Giusta A (2005) Controlled time-temperature oxidation reaction in a synthetic Mg-hercynite, Physics and Chemistry of Minerals, 32, 83-88.
[18] Lavina B, Cesare B, Álvarez-Valero A M, Uchida H, Downs R T, Koneva A, Dera P (2009) Closure temperatures of intracrystalline ordering in anatectic and metamorphic hercynite, $Fe^{2+}Al_2O_4$. American Mineralogist 94, 657-665.
[19] Reuter B, Riedel E, Hug P, Arndt D, Geisler U, Behnke J (1969) Zur kristallchemie der vanadin(III)-spinelle. Zeitschrift für Anorganische und Allgemeine Chemie 369, 306-312.
[20] Pavese A, Levy D, Hoser A (2000) Cation distribution in synthetic zinc ferrite (Zn0.97Fe2.02O4) from in situ high temperature neutron powder diffraction, American Mineralogist, 85, 1497-1502.
[21] Levy D, Pavese A, Hanfland M (2000) Phase transition of synthetic zinc ferrite spinel (ZnFe2O4) at high pressure, from synchrotron X-ray powder diffraction, Physics and Chemistry of Minerals, 27, 638-644.
[22] Moran E, Blesa M C, Medina M E, Tornero J D, Menendez N, Amado U (2002) Nonstoichiometric spinel ferrites obtained from α-NaFeO2 via molten media reactions. Inorganic Chemistry 41, 5961-5967.
[23] RRUFF.info
[24] O'Driscoll B, Clay P L, Cawthorn P L, Lenaz D, Adetunji J, Kronz A (2014) Trevorite: Ni-rich spinel formed by metasomatism and desulfurization processes at Bon Accord, South Africa?. Mineralogical Magazine 78, 145-163.
[25] de Waal S A (1972) Mineralogical notes: nickel minerals from Barberton, South Africa: V. trevorite, redescribed. American Mineralogist 57, 1524-1527.

This is a preprint, the final version is subject to change, of the American Mineralogist (MSA)
Cite as Authors (Year) Title. American Mineralogist, in press.
DOI: http://dx.doi.org/10.2138/am-2018-6123

[26] Antao S M, Hassan I, Parise J B (2005) Cation ordering in magnesioferrite, MgFe2O4 to 982°C using in situ synchrotron X-ray powder diffraction. American Mineralogist 90, 219-228
[27] Nakatsuka A, Ueno H, Nakayama N, Mizota T, Maekawa H (2004) Single-crystal X-ray diffraction study of cation distribution in MgAl2O4 - MgFe2O4 spinel solid solution. Physics and Chemistry of Minerals 31, 278-287
[28] Hill R J (1984) X-ray powder diffraction profile refinement of synthetic hercynite inversion parameter = .163, American Mineralogist, 69, 937-942.

Table A1i. Jarosite-Alunite regression data

mineral name	chemical composition	*a*(Å)	*b*(Å)	*c*(Å)	*V*(Å^3)	R
Alunite	$(K_{0.94}Na_{0.06})Al_3(SO_4)_2(OH)_6$	6.979	6.979	17.284	729.057	
Alunite	$S_2Al_{2.967}O_{14.063}K_{0.805}Na_{0.132}H_6$	6.9741	6.9741	17.19	724.074	
Alunite	$KAl_3(SO_4)_2(OH)_6$	7.02	7.02	17.223	735.045	
Jarosite	$(K_{0.88}Sr_{0.12})(Fe^{3+}_{0.96}Al_{0.04})_3((S_{0.94}P_{0.06})O_4)_2(OH)_6$	7.3013	7.3013	17.211	794.579	
Jarosite	$K_{0.51}H_{6.49}Fe_3S_2O_{14}$	7.33009	7.33009	17.1374	797.433	
Jarosite	$K_{0.6}H_{6.4}Fe_3S_2O_{14}$	7.3207	7.3207	17.1517	796.055	
Jarosite	$K_{0.7}H_{6.3}Fe_3S_2O_{14}$	7.3112	7.3112	17.1792	795.263	
Jarosite	$K_{0.86}H_{6.14}Fe_3S_2O_{14}$	7.307	7.307	17.1916	794.923	
Jarosite	$K_{0.95}H_{6.05}Fe_3S_2O_{14}$	7.30293	7.30293	17.2043	794.624	
Jarosite	$K_{0.87}H_{6.13}Fe_{2.79}S_2O_{14}$	7.3063	7.3063	17.0341	787.49	
Jarosite	$K_{0.02}H_7Fe_3S_2O_{14}$	7.3478	7.3478	17.028	796.176	
Jarosite	$K_{0.84}H_{6.16}Fe_{2.73}S_2O_{14}$	7.3128	7.3128	17.1973	796.45	
Jarosite	$(K_{0.76}Na_{0.24})Fe_3S_2O_{14}H_6$	7.3045	7.3045	17.0875	789.569	

This is a preprint, the final version is subject to change, of the American Mineralogist (MSA)
Cite as Authors (Year) Title. American Mineralogist, in press.
DOI: http://dx.doi.org/10.2138/am-2018-6123

Jarosite	$(K_{0.6}Na_{0.4})Fe_3S_2O_{14}H_6$	7.3052	7.3052	16.9706	784.318
Jarosite	$K_{0.52}Na_{0.46}Fe_3S_2O_{14}H_6$	7.3079	7.3079	16.9028	781.762
Jarosite	$K(Fe_{2.79}Al_{0.21})S_2O_{14}H_6$	7.2913	7.2913	17.1744	790.719
Jarosite	$K_{0.81}H_{5.83}Fe_{2.88}S_2O_{13.64}$	7.311	7.311	17.175	795.025
Jarosite	$KFe_3(SO_4)_2(OH)_6$	7.304	7.304	17.268	797.8
Jarosite	$KFe_3(SO_4)_2(OH)_6$	7.315	7.315	17.224	798.166
Natrojarosite	$(Na_{0.99}K_{0.01})Fe^{3+}{}_3(S_1O_4)_2(OH)_6$	7.3156	7.3156	16.6097	769.826
Natrojarosite	$Na_{0.69}K_{0.29}Fe_3S_2O_{14}H_6$	7.3101	7.3101	16.7658	775.892
Natrojarosite	$Na_{0.85}K_{0.11}Fe_3S_2O_{14}H_6$	7.3144	7.3144	16.6491	771.399
Natrojarosite	$NaFe_3(SO_4)_2(OH)_6$	7.31525	7.31525	16.5868	768.691
Natrojarosite	$Na_{0.87}H_{6.13}Fe_3S_2O_{14}$	7.31984	7.31984	16.6474	772.468
Natrojarosite	$Na_{0.67}H_{6.33}Fe_3S_2O_{14}$	7.3254	7.3254	16.7209	777.057
Natrojarosite	$NaFe_3(SO_4)_2(OH)_6$	7.317	7.317	16.5955	769.462
Hydroniumjarosite	$[(NH_4)_{0.32}(H_3O)_{0.68}]Fe_{3.04}(SO_4)_2(OH)_6$	7.3431	7.3431	17.1595	801.30
Hydroniumjarosite	$H_{6.92}Fe_3S_2O_{14}$	7.3552	7.3552	16.9945	796.211
Hydroniumjarosite	$K_{0.1}H_{6.86}Fe_3S_2O_{14}$	7.3521	7.3521	17.0108	796.303
Hydroniumjarosite	$K_{0.2}H_{6.81}Fe_3S_2O_{14}$	7.3428	7.3428	17.0316	795.261
Hydroniumjarosite	$K_{0.35}H_{6.65}Fe_3S_2O_{14}$	7.3373	7.3373	17.103	797.399
Hydroniumjarosite	$Na_{0.49}H_{6.51}Fe_3S_2O_{14}$	7.33876	7.33876	16.8105	784.073
Hydroniumjarosite	$Na_{0.35}H_{6.65}Fe_3S_2O_{14}$	7.342	7.342	16.8574	786.955
Hydroniumjarosite	$Na_{0.24}H_{6.76}Fe_3S_2O_{14}$	7.34742	7.34742	16.9253	791.292
Hydroniumjarosite	$S_2Fe_{2.919}O_{14.905}H_6$	7.3559	7.3559	17.0186	797.492
Hydroniumjarosite	$S_2Fe_3O_{15}$	7.3499	7.3499	17.0104	795.807
Hydroniumjarosite	$H_{14.31}O_{14.77}Na_{0.2}K_{0.02}Fe_{2.949}Al_{0.03}(S_{1.97}Si_{0.03})$	7.3408	7.3408	17.0451	795.457
Ammoniojarosite	$[(NH_4)_{0.59}(H_3O)_{0.39}]Fe_{3.03}(SO_4)_2(OH)_6$	7.3293	7.3293	17.3584	807.54
Ammoniojarosite	$[(NH_4)_{0.93}(H_3O)_{0.07}]Fe_{3.05}(SO_4)_2(OH)_6$	7.3226	7.3226	17.499	812.60
Ammoniojarosite	$NFe_3S_2O_{14}H_{10}$	7.3177	7.3177	17.534	813.132

1139 [1] Basciano L C, Peterson R C (2007) Jarosite - hydronium jarosite solid solution series
1140 with full iron occupancy: Mineralogy and crystal chemistry. American Mineralogist, 92,
1141 1464-1473.
1142 [2] Basciano L C, Peterson R C (2007) The crystal structure of ammoniojarosite,
1143 (NH4)Fe3(SO4)2(OH)6 and the crystal chemistry of the ammoniojarosite-hydronium
1144 jarosite solid-solution series. Mineralogical Magazine, 71, 427-441.
1145 [3] Basciano L C, Peterson R C (2008) Crystal chemistry of the natrojarosite-jarosite
1146 and natrojarosite-hydronium jarosite solid-solution: A synthetic study with full Fe site
1147 occupancy. American Mineralogist, 93, 853-862.
1148 [4] Becker U, Gasharova B (2001) AFM observations and simulations of jarosite growth
1149 at the molecular scale:
1150 probing the basis for the incorporation of foreign ions into jarosite as a storage mineral.
1151 Physics and Chemistry of Minerals, 28, 545-556.
1152 [5] Kato T, Miura Y (1977) The crystal structure of jarosite and svanbergite.
1153 Mineralogical Journal, 8, 419-430.
1154 [6] Majzlan J, Stevens R, Boerio-Goates J, Woodfield B F, Navrotsky A, Burns P C,
1155 Crawford M K, Amos T G (2004) Thermodynamic properties, low-temperature heat-
1156 capacity anomalies, and single-crystal X-ray refinement of hydronium jarosite,
1157 (H3O)Fe3(SO4)2(OH)6. Physics and Chemistry of Minerals, 31, 518-531.

[7] Majzlan, J., Speziale, S., Duffy, T.S., Burns, P.C. (2006) Single-crystal elastic properties of alunite, KAl3(SO4)2(OH)6. Physics and Chemistry of Minerals, 33, 567-573.
[8] Menchetti S, Sabelli C (1976) Crystal chemistry of the alunite series: crystal structure refinement of alunite and synthetic jarosite. Neues Jahrbuch fur Mineralogie, Monatshefte, 1976, 406-417.
[9] Mills S J, Nestola F, Kahlenberg V, Christy A G, Hejny C, Redhammer G J (2013) Looking for jarosite on Mars: The low-temperature crystal structure of jarosite. American Mineralogist, 98, 1966-1971.
[10] Nestola F, Mills S J, Periotto B, Scandolo L (2013) The alunite supergroup under high pressure: the case of natrojarosite, NaFe3(SO4)2(OH)6. Mineralogical Magazine, 77, 3007-3017.
[11] Plasil J, Skoda R, Fejfarova K, Cejka J, Kasatkin A V, Dusek M, Talla D, Lapcak L, Machovic V, Dini M (2014) Hydroniumjarosite, (H3O)+Fe3(SO4)2(OH)6, from Cerros Pintados, Chile: Single-crystal X-ray diffraction and vibrational spectroscopic study. Mineralogical Magazine, 78, 535-547.
[12] RRUFF.info

This is a preprint, the final version is subject to change, of the American Mineralogist (MSA)
Cite as Authors (Year) Title. American Mineralogist, in press.
DOI: http://dx.doi.org/10.2138/am-2018-6123

Appendix 2 - Error analysis

The uncertainties associated with *y*, estimated composition, are computed as follows:

$$\sigma_y^2 = \sigma_{SE}^2 + \sigma_{y\,uc}^2$$

Where:

$$\sigma_{SE}^2 = \frac{1}{n}\sum_{i=1}^{n}(y_i - \hat{y}_i)^2$$

Where *n* is the number of datasets in the regression; y_i and $\hat{y}_i$ are the observed and calculated *y* values of the regression data, respectively.

and

$$\sigma_{y\,uc}^2 = \frac{1}{m}\sum_{j=1}^{m}(\hat{y}_j - \hat{y}_{j\,\sigma_{uc}})^2$$

Where m is the number of unit-cell parameters in the function (e.g., five in plagioclase), $\hat{y}_j$ is the composition calculated with your input unit-cell parameters, $\hat{y}_{j\,\sigma_{uc}}$ is the calculated composition calculated with the error associated with your unit-cell parameter added to the unit-cell parameter [e.g., $a_{\sigma_{uc}} = (a+\sigma_a)$].

Errors associated with arithmetical equations were computed with the following formula:

$$\sigma_{y_i}^2 = \sum_{i}^{n}\sigma_{x_i}^2$$

Where σ_{x_i} is the uncertainty associated with each coefficient in the equation.

Root-Mean-Square Error (RMSE) = $\sqrt{\frac{\sum_{i=1}^{n}(y_i-\hat{y}_i)^2}{n}}$

Where *n* is the number of datasets in the regression; y_i and $\hat{y}_i$ are the observed and calculated *y* values of the equation, respectively.

This is a preprint, the final version is subject to change, of the American Mineralogist (MSA)
Cite as Authors (Year) Title. American Mineralogist, in press.
DOI: http://dx.doi.org/10.2138/am-2018-6123

Appendix 3 - plots of unit-cell parameters versus composition

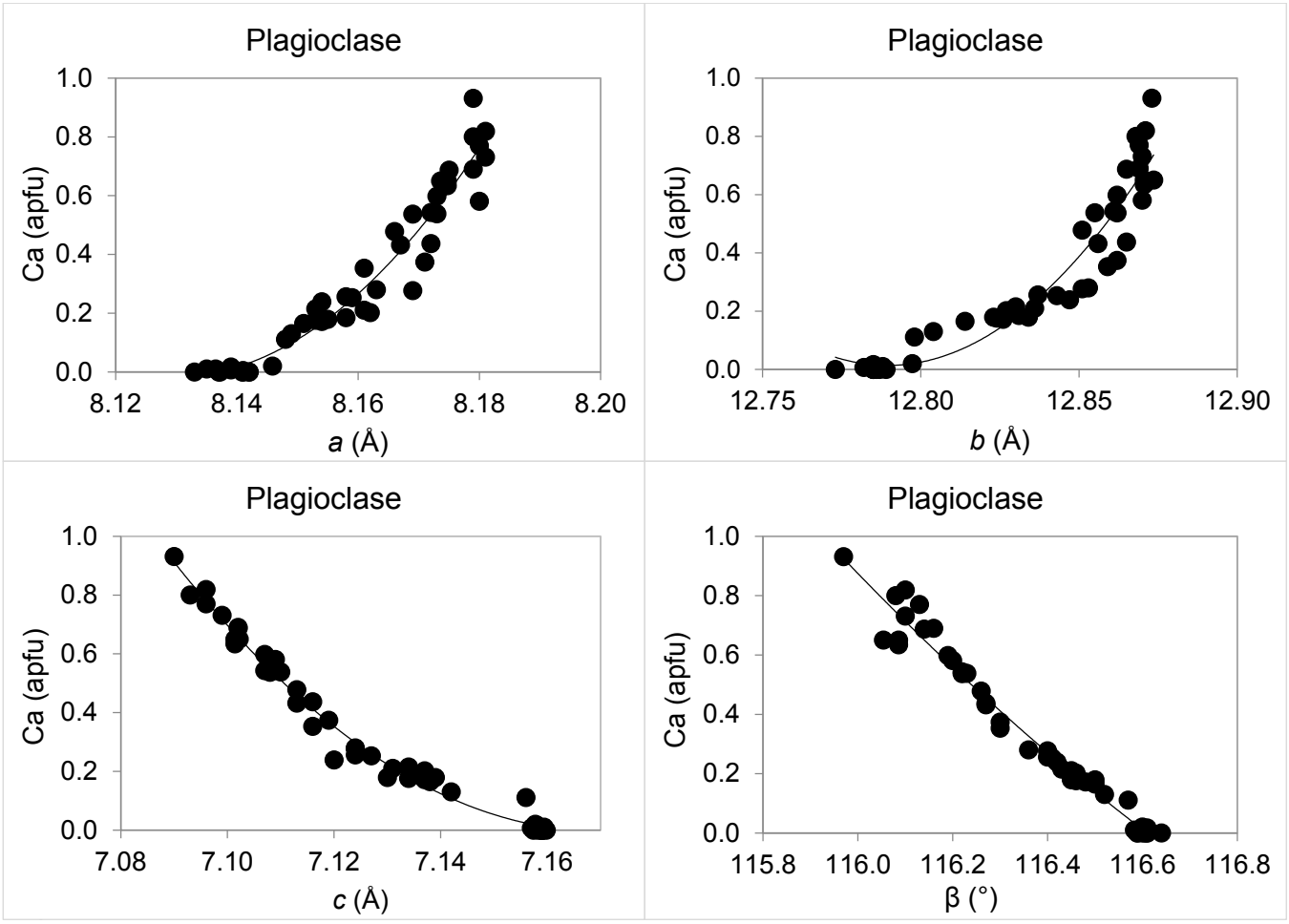

Figures A3a-d. Ca-content of plagioclase as a function of unit-cell parameters. Dataset from literature and RRUFF Project data (Table A1a).

This is a preprint, the final version is subject to change, of the American Mineralogist (MSA)
Cite as Authors (Year) Title. American Mineralogist, in press.
DOI: http://dx.doi.org/10.2138/am-2018-6123

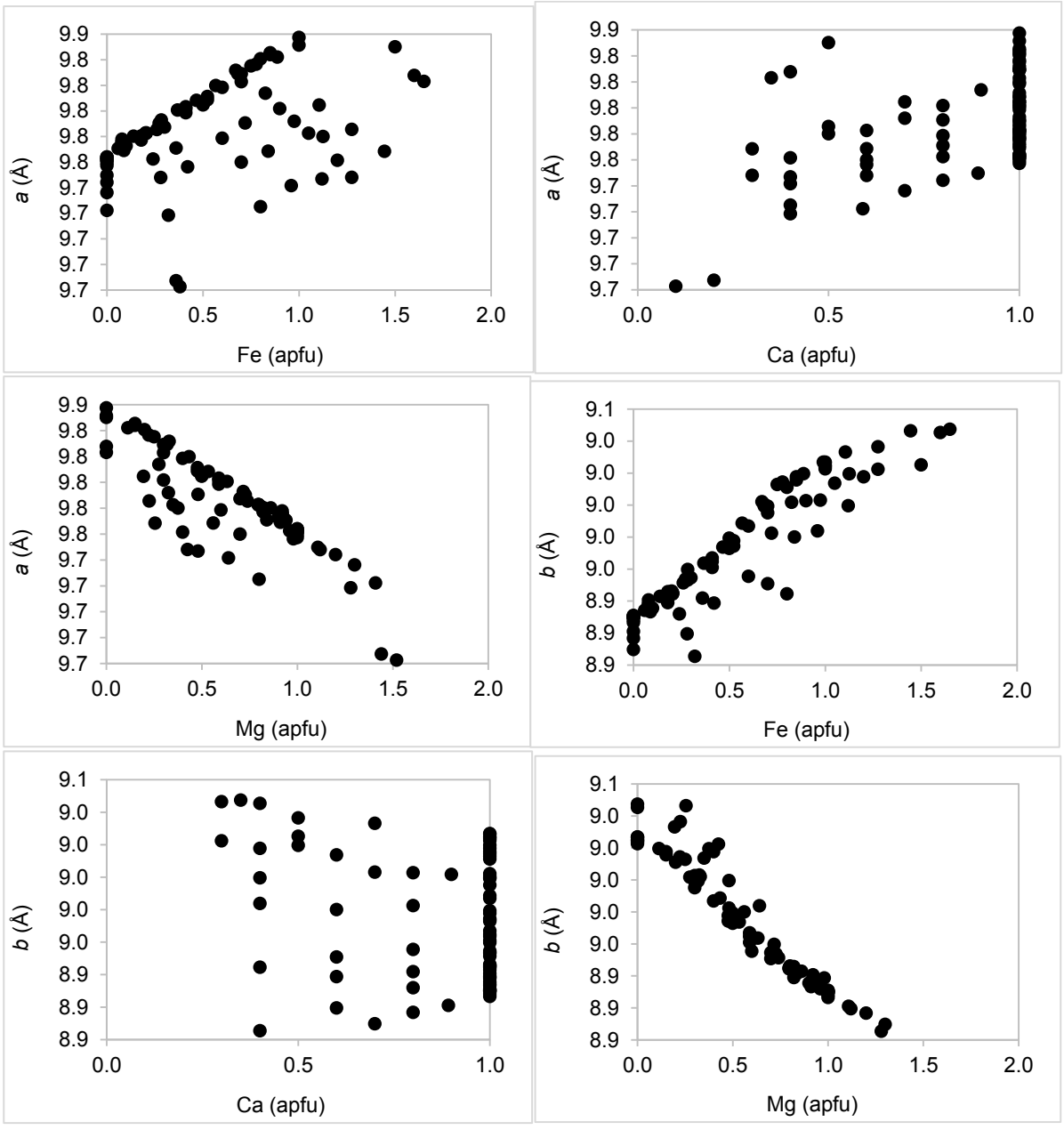

This is a preprint, the final version is subject to change, of the American Mineralogist (MSA)
Cite as Authors (Year) Title. American Mineralogist, in press.
DOI: http://dx.doi.org/10.2138/am-2018-6123

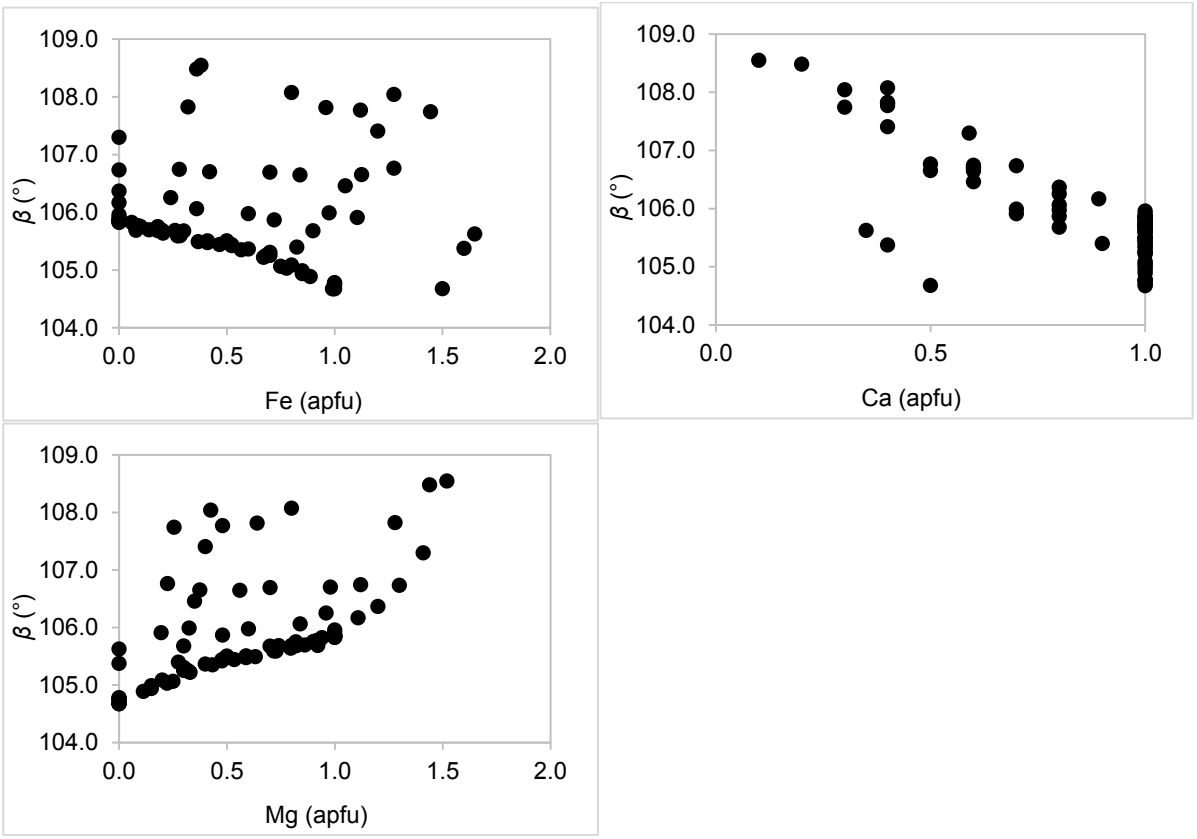

Figures A3e-m. Fe, Ca, and Mg-content of augite as a function of *a, b,* and β, respectively. Dataset from literature and RRUFF Project data (Table A1c).

This is a preprint, the final version is subject to change, of the American Mineralogist (MSA)
Cite as Authors (Year) Title. American Mineralogist, in press.
DOI: http://dx.doi.org/10.2138/am-2018-6123

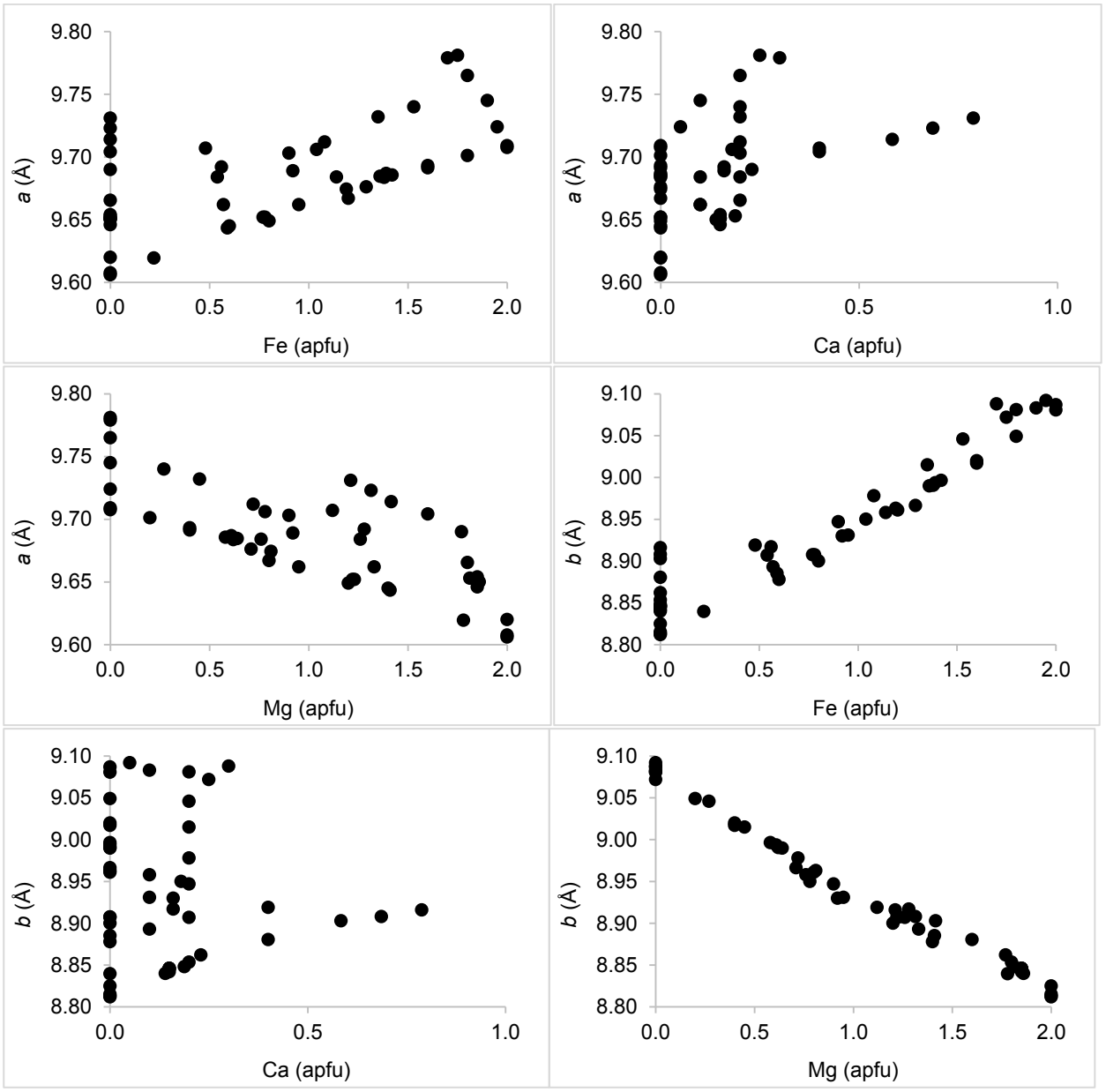

This is a preprint, the final version is subject to change, of the American Mineralogist (MSA)
Cite as Authors (Year) Title. American Mineralogist, in press.
DOI: http://dx.doi.org/10.2138/am-2018-6123

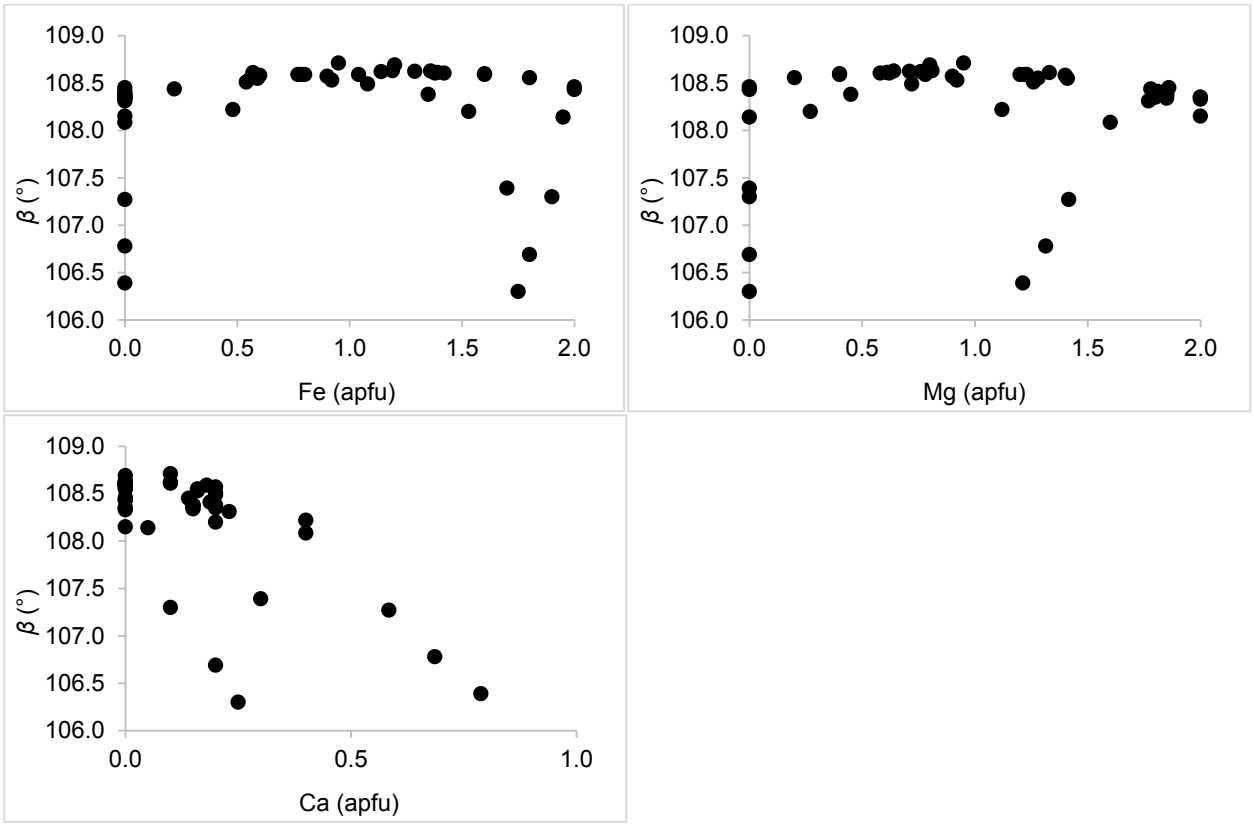

Figures A3n-v. Fe, Ca, and Mg-content of pigeonite as a function of *a, b,* and β, respectively. Dataset from literature and RRUFF Project data (Table A1b).

This is a preprint, the final version is subject to change, of the American Mineralogist (MSA)
Cite as Authors (Year) Title. American Mineralogist, in press.
DOI: http://dx.doi.org/10.2138/am-2018-6123

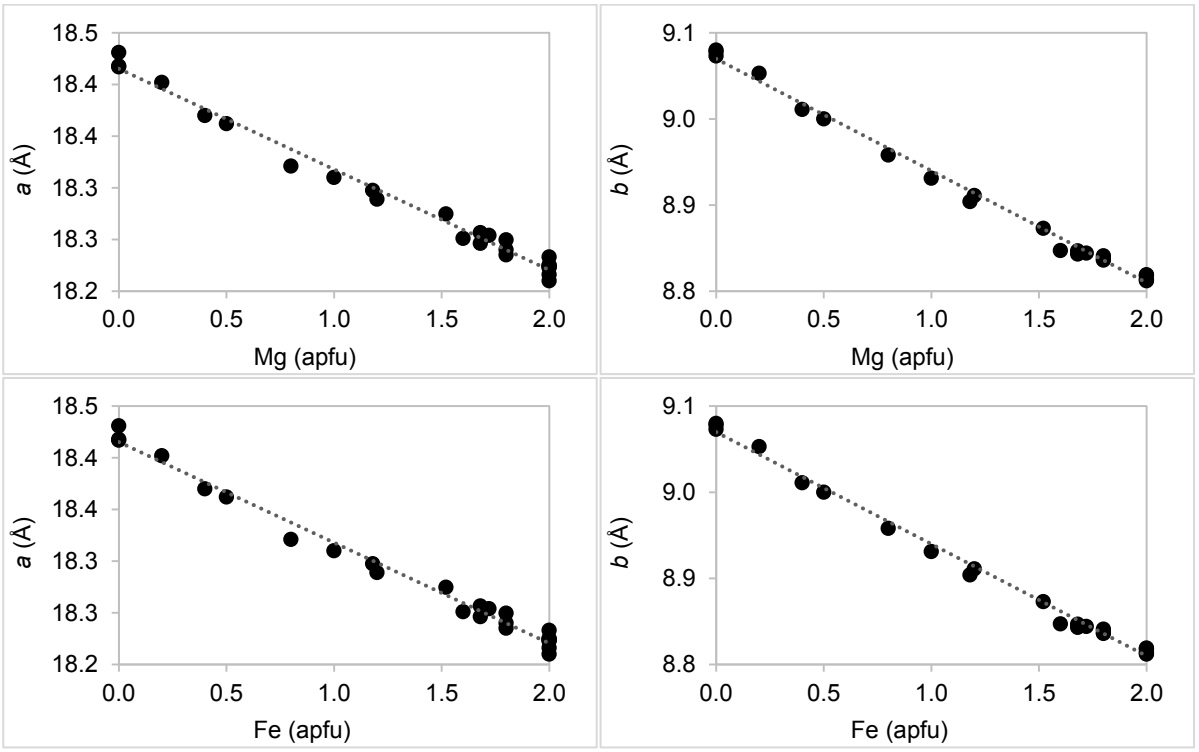

Figures A3w-z. Mg-and Fe-content of orthopyroxene as a function of *a* and *b* unit-cell parameters. Dataset from literature and RRUFF Project data (Table A1d).

This is a preprint, the final version is subject to change, of the American Mineralogist (MSA)
Cite as Authors (Year) Title. American Mineralogist, in press.
DOI: http://dx.doi.org/10.2138/am-2018-6123

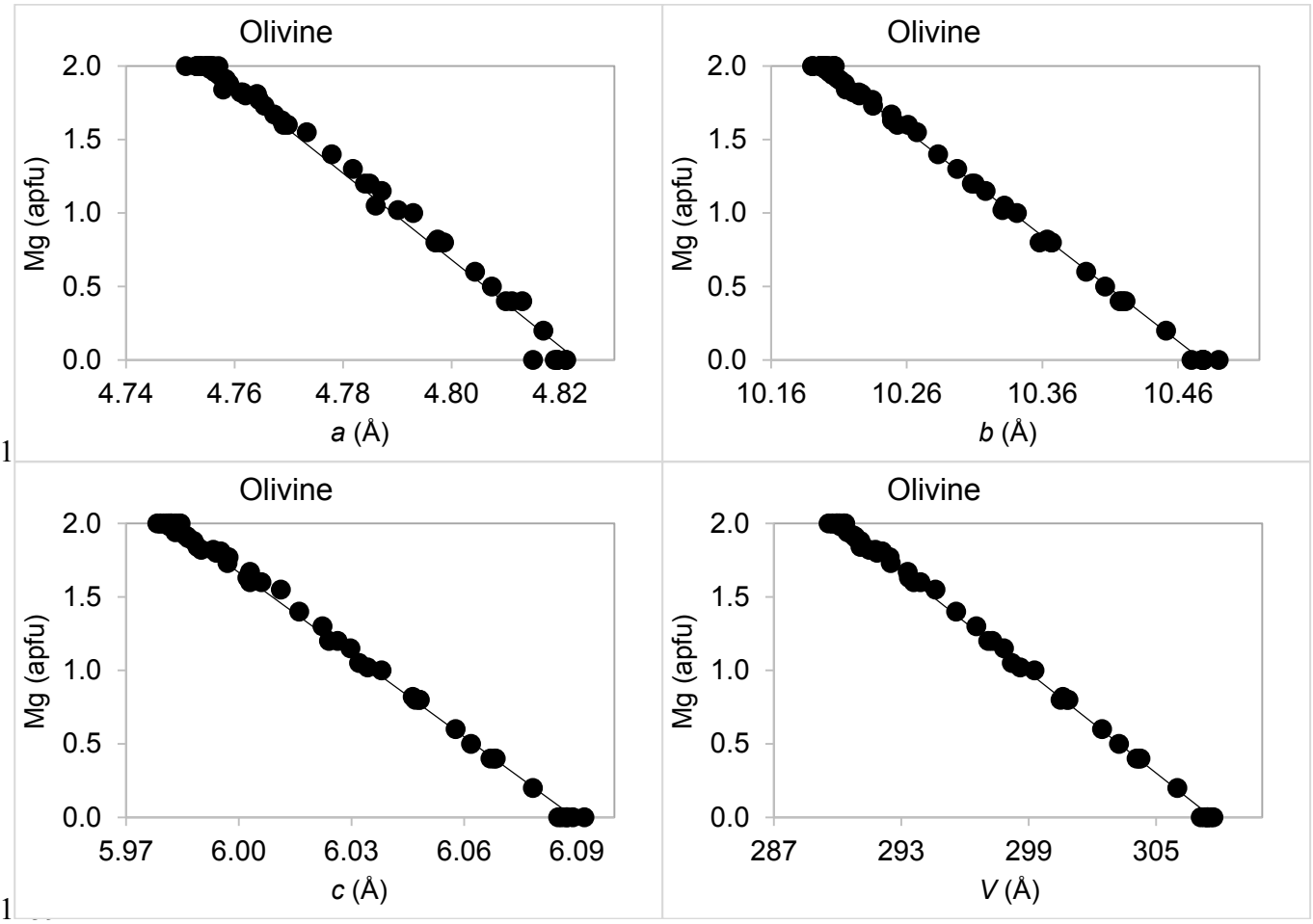

Figures A3ac-ad. Mg-content of Fa-Fo olivine as a function of *a, b, c* cell edges and unit-cell volume, *V*. Dataset from literature and RRUFF Project data (Table A1e).

This is a preprint, the final version is subject to change, of the American Mineralogist (MSA)
Cite as Authors (Year) Title. American Mineralogist, in press.
DOI: http://dx.doi.org/10.2138/am-2018-6123

Appendix 4 – magnetite/chromite martian meteorite references

1. Aoudjehane, H.C., Avice, G., Barrat, J.A., Boudouma, O., Chen, G., Duke, M.J.M., Franchi, I.A., Gattacceca, J., Grady, M.M., Greenwood, R.C., and Herd, C.D.K. (2012) Tissint martian meteorite: A fresh look at the interior, surface, and atmosphere of Mars. Science, 338(6108), 785-788.
2. Balta, J.B., Sanborn, M., McSween, H.Y., and Wadhwa, M. (2013) Magmatic history and parental melt composition of olivine-phyric shergottite LAR 06319: Importance of magmatic degassing and olivine antecrysts in Martian magmatism. Meteoritics & Planetary Science, 48(8), 1359-1382.
3. Balta, J.B., Sanborn, M.E., Udry, A., Wadhwa, M., and McSween, H.Y. (2015) Petrology and trace element geochemistry of Tissint, the newest shergottite fall. Meteoritics & Planetary Science, 50(1), 63-85.
4. Barrat, J.A., Jambon, A., Bohn, M., Gillet, P., Sautter, V., Göpel, C., Lesourd, M., and Keller, F. (2002) Petrology and chemistry of the picritic shergottite North West Africa 1068 (NWA 1068). Geochimica et Cosmochimica Acta, 66(19), 3505-3518.
5. Basu Sarbadhikari, A., Babu, E.V.S.S.K., Vijaya Kumar, T., and Chennaoui Aoudjehane, H. (2016) Martian meteorite Tissint records unique petrogenesis among the depleted shergottites. Meteoritics & Planetary Science, 51(9), 1588-1610.
6. Beck, P., Barrat, J.A., Gillet, P., Wadhwa, M., Franchi, I.A., Greenwood, R.C., Bohn, M., Cotten, J., Van de Moortèle, B., and Reynard, B. (2006) Petrography and geochemistry of the chassignite Northwest Africa 2737 (NWA 2737). Geochimica et Cosmochimica Acta, 70(8), 2127-2139.
7. Bunch, T.E., and Reid, A.M. (1975) The nakhlites Part I: Petrography and mineral chemistry. Meteoritics & Planetary Science, 10(4), 303-315.
8. Day, J., Taylor, L.A., Floss, C., and McSween, H.Y. (2006) Petrology and chemistry of MIL 03346 and its significance in understanding the petrogenesis of nakhlites on Mars. Meteoritics & Planetary Science, 41(4), 581-606.
9. Floran, R.J., Prinz, M., Hlava, P.F., Keil, K., Nehru, C.E., and Hinthorne, J.R. (1978) The Chassigny meteorite: A cumulate dunite with hydrous amphibole-bearing melt inclusions. Geochimica et Cosmochimica Acta, 42(8), 1213-1229.
10. Folco, L., Franchi, I.A., D'orazio, M., Rocchi, S., and Schultz, L. (2000) A new martian meteorite from the Sahara: The shergottite Dar al Gani 489. Meteoritics & Planetary Science, 35(4), 827-839.
11. Gattacceca, J., Rochette, P., Scorzelli, R.B., Munayco, P., Agee, C., Quesnel, Y., Cournède, C., and Geissman, J. (2014) Martian meteorites and Martian magnetic anomalies: A new perspective from NWA 7034. Geophysical Research Letters, 41(14), 4859-4864.
12. Gillet, P., Barrat, J.A., Beck, P., Marty, B., Greenwood, R.C., Franchi, I.A., Bohn, M., and Cotten, J. (2005) Petrology, geochemistry, and cosmic-ray exposure age of Iherzolitic shergottite Northwest Africa 1950. Meteoritics & Planetary Science, 40(8), 1175-1184.
13. Gleason, J.D., Kring, D.A., Hill, D.H., and Boynton, W.V. (1997) Petrography and bulk chemistry of Martian lherzolite LEW88516. Geochimica et Cosmochimica Acta, 61(18), 4007-4014.

14. Gnos, E., Hofmann, B., Franchi, I.A., Al-Kathiri, A., Huser, M., and Moser, L. (2002) Sayh al Uhaymir 094: A new martian meteorite from the Oman desert. Meteoritics & Planetary Science, 37(6), 835-854.
15. Goodrich, C.A. (2003) Petrogenesis of olivine-phyric shergottites Sayh al Uhaymir 005 and Elephant Moraine A79001 lithology A. Geochimica et Cosmochimica Acta, 67(19), 3735-3772.
16. Goodrich, C.A., Herd, C.D., and Taylor, L.A. (2003) Spinels and oxygen fugacity in olivine-phyric and lherzolitic shergottites. Meteoritics & Planetary Science, 38(12), 1773-1792.
17. Greshake, A., Fritz, J., and Stöffler, D. (2004) Petrology and shock metamorphism of the olivine-phyric shergottite Yamato 980459: Evidence for a two-stage cooling and a single-stage ejection history1 1Associate editor: C. Koeberl. Geochimica et Cosmochimica Acta, 68(10), 2359-2377.
18. Gross, J., Filiberto, J., Herd, C.D., Daswani, M.M., Schwenzer, S.P., and Treiman, A.H. (2013) Petrography, mineral chemistry, and crystallization history of olivine-phyric shergottite NWA 6234: A new melt composition. Meteoritics & Planetary Science, 48(5), 854-871.
19. Gross, J., Treiman, A.H., Filiberto, J., and Herd, C.D. (2011) Primitive olivine-phyric shergottite NWA 5789: Petrography, mineral chemistry, and cooling history imply a magma similar to Yamato-980459. Meteoritics & Planetary Science, 46(1), 116-133.
20. Hale V. S. (1998) A Re-evaluation of cumulus pyroxene estimates and oxidation state for the Shergotty meteorite. M.S. Thesis, University of Tennessee, Knoxville, 105.
21. Harvey, R.P., Wadhwa, M., McSween, H.Y., and Crozaz, G. (1993) Petrography, mineral chemistry, and petrogenesis of Antarctic shergottite LEW88516. Geochimica et Cosmochimica Acta, 57(19), 4769-4783.
22. Herd, C.D., Papike, J.J., and Brearley, A.J. (2001) Oxygen fugacity of martian basalts from electron microprobe oxygen and TEM-EELS analyses of Fe-Ti oxides. American Mineralogist, 86(9), 1015-1024.
23. Hewins, R.H., Zanda, B., Humayun, M., Nemchin, A., Lorand, J.P., Pont, S., Deldicque, D., Bellucci, J.J., Beck, P., Leroux, H., and Marinova, M. (2017) Regolith breccia Northwest Africa 7533: Mineralogy and petrology with implications for early Mars. Meteoritics & Planetary Science, 52(1), 89-124.
24. Howarth, G.H., and Udry, A. (2017) Trace elements in olivine and the petrogenesis of the intermediate, olivine-phyric shergottite NWA 10170. Meteoritics & Planetary Science, 52(2), 391-409.
25. Howarth, G.H., Pernet-Fisher, J.F., Bodnar, R.J., and Taylor, L.A. (2015) Evidence for the exsolution of Cl-rich fluids in Martian magmas: Apatite petrogenesis in the enriched lherzolitic shergottite Northwest Africa 7755. Geochimica et Cosmochimica Acta, 166, 234-248.
26. Howarth, G.H., Pernet-Fisher, J.F., Balta, J.B., Barry, P.H., Bodnar, R.J., and Taylor, L.A. (2014) Two-stage polybaric formation of the new enriched, pyroxene-oikocrystic, lherzolitic shergottite, NWA 7397. Meteoritics & Planetary Science, 49(10), 1812-1830.

27. Hu, S., Feng, L., and Lin, Y. (2011) Petrography, mineral chemistry and shock metamorphism of Yamato 984028 lherzolitic shergottite. Chinese Science Bulletin, 56(15), 1579-1587.
28. Ikeda, Y. (1997) Petrology and mineralogy of the Y-793605 Martian meteorite. Antarctic Meteorite Research, 10, 1340
29. Ikeda, Y. (1998) Petrology of magmatic silicate inclusions in the Allan Hills 77005 lherzolitic shergottite. Meteoritics & Planetary Science, 33(4), 803-812.
30. Ikeda, Y. (2004) Petrology of the Yamato 980459 shergottite. Antarctic meteorite research, 17, 35-54
31. Imae, N., and Ikeda, Y. (2007) Petrology of the Miller Range 03346 nakhlite in comparison with the Yamato-000593 nakhlite. Meteoritics & Planetary Science
32. Jambon, A., Barrat, J.A., Sautter, V., Gillet, P., Göpel, C., Javoy, M., Joron, J.L., and Lesourd, M. (2002) The basaltic shergottite Northwest Africa 856: Petrology and chemistry. Meteoritics & Planetary Science, 37(9), 1147-1164.
33. Jiang, Y., and Hsu, W. (2012) Petrogenesis of Grove Mountains 020090: An enriched "lherzolitic" shergottite. Meteoritics & Planetary Science, 47(9), 1419-1435.
34. Johnson, M.C., Rutherford, M.J., and Hess, P.C. (1991) Chassigny petrogenesis: Melt compositions, intensive parameters and water contents of Martian (?) magmas. Geochimica et Cosmochimica Acta, 55(1), 349-366.
35. Kring, D.A., Gleason, J.D., Swindle, T.D., Nishiizumi, K., Caffee, M.W., Hill, D.H., Jull, A.J., and Boynton, W.V. (2003) Composition of the first bulk melt sample from a volcanic region of Mars: Queen Alexandra Range 94201. Meteoritics & Planetary Science, 38(12), 1833-1848.
36. Lin, Y., Guan, Y., Wang, D., Kimura, M., and Leshin, L.A. (2005) Petrogenesis of the new lherzolitic shergottite Grove Mountains 99027: Constraints of petrography, mineral chemistry, and rare earth elements. Meteoritics & Planetary Science, 40(11), 1599-1619.
37. Lin, Y., Hu, S., Miao, B., Xu, L., Liu, Y., Xie, L., Feng, L., and Yang, J. (2013) Grove Mountains 020090 enriched lherzolitic shergottite: A two-stage formation model. Meteoritics & Planetary Science, 48(9), 1572-1589.
38. McCoy, T.J., Wadhwa, M., and Keil, K. (1999) New lithologies in the Zagami meteorite: Evidence for fractional crystallization of a single magma unit on Mars. Geochimica et Cosmochimica Acta, 63(7), 1249-1262.
39. McSween, H.Y., and Jarosewich, E. (1983) Petrogenesis of the Elephant Moraine A79001 meteorite: Multiple magma pulses on the shergottite parent body. Geochimica et Cosmochimica Acta, 47(8), 1501-1513.
40. McSween, H.Y., and Treiman, A.H. (1998) Martian meteorites. Reviews in Mineralogy and Geochemistry, 36(1), 6-1.
41. Mcsween, H.Y., Eisenhour, D.D., Taylor, L.A., Wadhwa, M., and Crozaz, G. (1996) QUE94201 shergottite: Crystallization of a Martian basaltic magma. Geochimica et Cosmochimica Acta, 60(22), 4563-4569.
42. Mikouchi, T., and Miyamoto, M. (2002) Mineralogy and olivine cooling rate of the Dhofar 019 shergottite. Antarctic meteorite research, 15, 122-142.

43. Mikouchi, T. (2001) Mineralogical similarities and differences between the Los Angeles basaltic shergottite and the Asuka-881757 lunar mare meteorite. Antarctic meteorite research, 14, 1-20.
44. Mikouchi, T. (2005) Northwest Africa 1950: Mineralogy and comparison with Antarctic lherzolitic shergottites. Meteoritics & Planetary Science, 40(11), 1621-1634.
45. MIKOUCHI, T., MIYAMOTO, M., and McKAY, G.A. (1998) Mineralogy of Antarctic basaltic shergottite Queen Alexandra Range 94201: similarities to Elephant Moraine A79001 (lithology B) martian meteorite. Meteoritics & Planetary Science, 33(2), 181-189.
46. Mittlefehldt, D.W. (1994) ALH84001, a cumulate orthopyroxenite member of the Martian meteorite clan. Meteoritics & Planetary Science, 29(2), 214-221.
47. Nagao, K., Nakamura, T., Miura, Y.N., and Takaoka, N. (1997) Noble gases and mineralogy of primary igneous materials of the Yamato-793605 shergottite. Antarctic meteorite research, 10, 125-142.
48. Peslier, A.H., Hnatyshin, D., Herd, C.D.K., Walton, E.L., Brandon, A.D., Lapen, T.J., and Shafer, J.T. (2010) Crystallization, melt inclusion, and redox history of a Martian meteorite: Olivine-phyric shergottite Larkman Nunatak 06319. Geochimica et Cosmochimica Acta, 74(15), 4543-4576.
49. Santos, A.R., Agee, C.B., McCubbin, F.M., Shearer, C.K., Burger, P.V., Tartese, R., and Anand, M. (2015) Petrology of igneous clasts in Northwest Africa 7034: Implications for the petrologic diversity of the Martian crust. Geochimica et Cosmochimica Acta, 157, 56-85.
50. Sarbadhikari, A.B., Day, J.M., Liu, Y., Rumble, D., and Taylor, L.A. (2009) Petrogenesis of olivine-phyric shergottite Larkman Nunatak 06319: Implications for enriched components in Martian basalts. Geochimica et Cosmochimica Acta, 73(7), 2190-2214.
51. Sautter, V., Barrat, J.A., Jambon, A., Lorand, J.P., Gillet, P., Javoy, M., Joron, J.L., and Lesourd, M. (2002) A new Martian meteorite from Morocco: the nakhlite North West Africa 817. Earth and Planetary Science Letters (195(3), 223-238.
52. Shearer, C.K., Leshin, L.A., and Adcock, C.T. (1999) Olivine in Martian meteorite Allan Hills 84001: Evidence for a high-temperature origin and implications for signs of life. Meteoritics & Planetary Science, 34(3), 331-339.
53. Steele, Ian M., and Joseph V. Smith. (1982) Petrography and mineralogy of two basalts and olivine-pyroxene-spinel fragments in achondrite EETA79001. Journal of Geophysical Research: Solid Earth 87, A375-A384.
54. Szymanski, A., Brenker, F.E., Palme, H., and El Goresy, A. (2010) High oxidation state during formation of Martian nakhlites. Meteoritics & Planetary Science, 45(1), 21-31.
55. Taylor, L.A., Nazarov, M.A., Shearer, C.K., McSween, H.Y., Cahill, J., Neal, C.R., Ivanova, M.A., Barsukova, L.D., Lentz, R.C., Clayton, R.N., and Mayeda, T.K. (2002) Martian meteorite Dhofar 019: A new shergottite. Meteoritics & Planetary Science, 37(8), 1107-1128.
56. Treiman, A.H., Dyar, M.D., McCanta, M., Noble, S.K., and Pieters, C.M. (2007) Martian Dunite NWA 2737: Petrographic constraints on geological history, shock events, and olivine color. Journal of Geophysical Research: Planets, 112(E4).
57. Treiman, A.H., McKay, G.A., Bogard, D.D., Mittlefehldt, D.W., Wang, M.S., Keller, L., Lipschutz, M.E., Lindstrom, M.M., and Garrison, D. (1994) Comparison of the LEW88516

and ALHA77005 martian meteorites: Similar but distinct. Meteoritics & Planetary Science, 29(5), 581-592.

58. Udry, A., McSWEEN Jr, H.Y., LECUMBERRI-SANCHEZ, P., and Bodnar, R.J. (2012) Paired nakhlites MIL 090030, 090032, 090136, and 03346: Insights into the Miller Range parent meteorite. Meteoritics & Planetary Science, 47(10), 1575-1589.
59. Usui, T., McSween, H.Y., and Floss, C. (2008) Petrogenesis of olivine-phyric shergottite Yamato 980459, revisited. Geochimica et Cosmochimica Acta, 72(6), 1711-1730.
60. Wadhwa, M., Lentz, R.C.F., McSween, H.Y., and Crozaz, G. (2001) A petrologic and trace element study of Dar al Gani 476 and Dar al Gani 489: Twin meteorites with affinities to basaltic and lherzolitic shergottites. Meteoritics & Planetary Science, 36(2), 195-208.
61. Warren, P.H., Greenwood, J.P., and Rubin, A.E. (2004) Los Angeles: A tale of two stones. Meteoritics & Planetary Science, 39(1), 137-156.
62. Wittmann, A., Korotev, R.L., Jolliff, B.L., Irving, A.J., Moser, D.E., Barker, I., and Rumble, D. (2015) Petrography and composition of Martian regolith breccia meteorite Northwest Africa 7475. Meteoritics & Planetary Science, 50(2), 326-352.
63. Yukio, I., Makoto, K., Hiroshi, T., Gen, S., Kita, N., Yuichi, M., Akio, S., Emil, J., and Gerlind, D. (2006) Petrology of a new basaltic shergottite: Dhofar 378. Antarctic Meteorite Research, 19 (20-44.
64. Zipfel, J., Scherer, P., Spettel, B., Dreibus, G., and Schultz, L. (2000) Petrology and chemistry of the new shergottite Dar al Gani 476. Meteoritics & Planetary Science, 35(1), 95-106.